UNIVERSITY OF OKLAHOMA

GRADUATE COLLEGE

DESIGN OF SOLID ACID CATALYSTS FOR BIOMASS UPGRADING VIA C-C COUPLING AND DEHYDRATION REACTIONS

A DISSERTATION

SUBMITTED TO THE GRADUATE FACULTY

in partial fulfillment of the requirements for the

Degree of

DOCTOR OF PHILOSOPHY

By

TUONG VINH BUI
Norman, Oklahoma
2018

DESIGN OF SOLID ACID CATALYSTS FOR BIOMASS UPGRADING VIA C-C COUPLING AND DEHYDRATION REACTIONS

A DISSERTATION APPROVED FOR THE
SCHOOL OF CHEMICAL, BIOLOGICAL AND MATERIALS ENGINEERING

BY

Dr. Daniel E. Resasco, Chair

Dr. Steven P. Crossley

Dr. Bin Wang

Dr. Lance L. Lobban

Dr. David A. Sabatini

To my beloved family, especially to my father, my mother and my younger brother

Acknowledgements

First of all, I would like to express my deepest gratitude to my advisor, Professor Daniel E. Resasco for his unwavering support, his ingenious guidance and professionalism in gearing the planning and development of this research work from the very beginning.

My special thanks are also extended to Dr. Bin Wang, Dr. Steven Crossley, Dr. Lance Lobban, and Dr. Tawan Sooknoi for their constructive discussions and valuable suggestions. I also highly appreciate Dr. David A. Sabatini for his willingness to be my committee member.

I extend my most sincere thanks to the department staffs: Wanda, Terry, Donna, and Ginger for their assistance with purchasing and paperwork to ensure the smooth progress of my research. I also acknowledge the significant financial support of the Department of Energy.

I would always appreciate all the current and past group members: Santiago, Valeria, Gap, anh The Anh, Yen, Nhung, Tania, Cristian, Xiang, Ismaeel, Gengnan, Galveston, Tong, Reda, Lu, Duong, Taiwo, Camila, Diken, Anvit, Rejiv, Santhanaraj, Abhishek, Miguel, Felipe, Zheng, Nick, Feifei, Lawrence, Qiaohua for their warm collaboration and enjoyable friendship. My sincere thanks also go to my wonderful friends anh Ngoc, chi Huyen, Tuan, Tram, Thuc, Thanh, Kien, Hung, Han, chi Vi, Vy, Oanh, anh Minh, anh Cuong, anh Quoc, Khoi, anh Tuan-chi Anh and family, chi Tuoc

and family, Phuong for having become my second family here and for our unforgettable shared memories.

Finally, I am thankful to my parents and my younger brother for their unconditional love and continued support in what I have been pursuing.

Table of Contents

List of Tables

List of Figures and Schemes

ABSTRACT

Furanics fraction has been a major obstacle that impedes the feasibility of practical upgrading of bio-oil. The high reactivity of species existing in the mixture favors humins formation via polymerization. This leads to rapid catalyst deactivation and carbon loss. Via the Piancatelli ring rearrangement, furfural, one of the most abundant species found in the second-stage of biomass torrefraction, can be stabilized into cyclopentanone (CPO) which can be used as a potential building block for C-C coupling reaction.

This work covers two main sections. In the first part, different propitious upgrading strategies, focusing on using CPO as the building block for C-C coupling reactions (hydroxylalkylation, aldol condensation and alkylation) with other available oxygenates existing in a bio-oil mixture have been investigated. For example, via aldol condensation/hydroxyalkylation pathway and a following hydrodeoxygenation step, a mixture of C_7-C_{16} saturated hydrocarbons, which are in the gasoline/diesel range can be effectively produced. Over 90% efficiency of the whole catalytic upgrading process starting from CPO has been demonstrated, which highlights the potential of this strategy for future biofuel applications. Along with the practical investigations, fundamental studies have also been conducted to give some extensive insights into the reaction mechanisms, active site requirements as well as the effects of water, a commonly found impurity in biomass conversion, to the catalytic activity and the stability of the catalysts.

The second section mainly focuses on designing suitable solid acid catalysts that could be applied for the bio-oil upgrading processes. The catalysts have to satisfy several

requirements including high activity, stability and resistance against deactivation in harsh chemical environments (high temperature, high water content, polar solvent, etc.). The results have shown that zeolites and mesoporous silica are susceptible to the water/polar species attack, caused by the presence of surface silanols. This results in rapid deactivation and structure collapse. The effective way to improve hydrothermal stability of the catalysts is to reduce the density of surface silanols via functionalization with organic-functional groups which could increases the surface hydrophobicity and protect the surface from water

Chapter 1 - Introduction and Research Direction

1.1 Bio-oil Upgrading to Alternative Transportation Fuels

Recently, the separated upgrading of vapors and liquids obtained from fractionation of bio-oil via step-wise condensation of pyrolysis vapors [1, 2] as well as multistage pyrolysis process [3-6] have been investigated by our group. The core of this approach is to carry out the sequence of thermal treatments by heating the biomass at increasing temperatures so that the bio-oil is fractionated into different segments containing light oxygenates, sugar-derived, and phenolics-derived components [3-6]. Accordingly, by segregating each specific group of functional molecules into each fraction, a combined catalyst development and upgrading strategy could be developed more selectively and effectively to be able to exploit the different chemistries of each fraction and optimize the upgrading instead of a single hydro-treating step for the full bio-oil [7-9].

The fraction of light-oxygenates is rich in acetic acid, acetol, and acetaldehyde. We have previously proposed [8] that they could undergo ketonization to produce acetone, which in turn could be coupled with furfural, an abundant component in the sugar-derived stream, to produce C_8-C_{13} oxygenates over basic catalysts [10, 11]. Alternatively, instead of directly condensing with acetone, furfural can also be pre-stabilized into key intermediates to diminish carbon losses and humins formation, a major cause of catalyst deactivation. The intermediate products are still functional, so they can be further upgraded (C-C bond-chain enlarged) to a wide range of desirable products. The phenolics fraction can also be used to effectively incorporate into the fuel range those oxygenates,

which are too small to be directly hydrotreated. That is, converting C_2-C_4 oxygenates to alcohols greatly facilitates their incorporation via alkylation. For example, iso-propanol, obtained from the hydrogenation of acetone, can produce hydrocarbons in a molecular weight range suitable for the gasoline/diesel pool

Hydrogenation-decarbonylation of furfural to furan compounds (i.e., methyl furan, dimethyl furan) [12, 13], or oxidation of furfural to carboxylic acids [14, 15] are outstanding examples of furfural conversion into more stable forms, which have been recently reported in the literature. In the so-called Sylvan process, methyl furan is condensed with different types of carbonyl compounds, such as acetone, butanal, or furfural [16, 17] to elongate the carbon chain and bring the products to the fuel range. Dimethyl furan can also be coupled with ethylene via Diels-Alder reaction to produce valuable aromatics such as p-xylene [18]. Specific strategies for upgrading biomass-derived furanics via C-C coupling reaction have been analyzed in our recent review [19].

Hronec et al. [20, 21] have shown that the Piancatelli ring rearrangement in reducing condition is also a promising route to stabilize furfural into cyclopentanone. This is a remarkable pathway, because the O heteroatom is removed from the ring, producing CPO, a useful chemical and potential building block for C-C coupling reactions [20]. Although the Piancatelli ring rearrangement of furfuryl alcohol readily occurs in hot liquid water without the need of an additional catalyst, hydrogenation is required to first hydrogenate the CO group in furfural, as well as the resulting C=C double bond after the ring closure to obtain CPO. For this reaction, noble metal catalysts such as Pt, Pd, Ru, Ir as well as inexpensive metals such as Ni, Cu have been used in the conversion of furfural in the aqueous phase under H_2 pressure [22, 23]. For example, over 75% yield of CPO

has been reported over Pt/C or Ni-CNTs [24, 25]. High selectivity toward cyclopentanone is a definite techno-economic advantage of this approach compared to other upgrading strategies. For the Piancatelli rearrangement, the presence of liquid water plays a crucial role in the reaction [21, 24, 26]. Moreover, the presence of acetic acid in the reaction mixture provides a positive effect on the yield of the desired products [20]. That is, components that are naturally present in biomass-derived streams, i.e., aqueous solutions with high acidity, favor the occurrence of this reaction. CPO is not only a very convenient building block for carbon retention in the liquid fuel range, but reaching high conversions of furanics to this single molecule greatly reduces catalyst deactivation by avoiding the typical resinification of furfurals to humins. From all of this, we propose that the path of furanics to cyclopentanone is a very effective strategy for upgrading furfural-rich streams [19].

In this work, we explore the different C-C bond forming reactions that can be utilized to optimize the upgrading process, maximizing the yield in the desirable molecular weight range, for the specific production of gasoline, diesel, or chemicals. These C-C coupling reactions include aldol condensation, hydroxyalkylation and alkylation (**Figure 1.1**). The ultimate goal is to critically evaluate the different ideas about the feasibility for each of these reactions. Not least important, reaction mechanisms, structure/function relationships as well as catalytic materials design were also investigated with focus on the topological, chemical requirements of the active sites (acid, base, acid base pairs, both of Brønsted and Lewis types) and their stability when exposed to harsh chemical environments normally found in the upgrading processes.

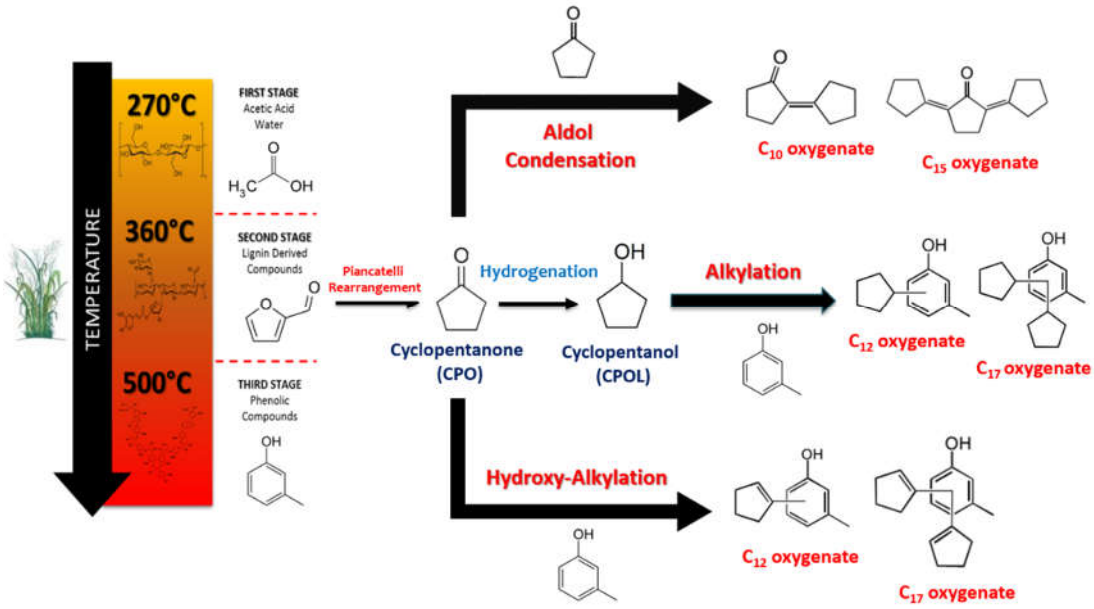

Figure 1.1 Upgrading strategy based on using cyclopentanone (CPO) as the building block for C-C coupling reactions

1.2 Research Direction

The thesis will cover five main parts, focusing on evaluating the feasibility of the upgrading strategies with different chemistries and designing active/stable catalysts for the upgrading processes:

(i) Conversion of furfural to cyclopentanone via Piancatelli ring rearrangement over Pd-Fe/SiO_2 catalysts;

(ii) Aldol condensation/hydroxyalkylation of cyclopentanone and m-cresol over solid acid catalysts. The effects of catalyst acidity and topology to catalytic activity and selectivity were investigated;

(iii) Alkylation of cyclopentanol, a hydrogenation product of cyclopentanone, with m-cresol over functionalized mesoporous silicas (MCM-41 and SBA-15). The catalysts stability and the nature of the leaching phenomenon on functionalized

mesoporous silicas catalysts were also investigated. A functionalization method has been proposed to produce active and stable solid acid catalysts (zeolites, mesoporous silica) for the upgrading process in harsh chemical environments (high temperature, high water content, polar solvent, etc.);

(iv) Self- and cross-aldol condensation of cyclopentanone and acetone over ZSM-5 zeolites. Mechanistic and kinetic studies were carried out to understand reaction mechanisms, the active sites and the factors that govern the catalytic activity and selectivity of cross- and self- aldol condensation;

(v) The effects of water on the catalyst stability and activity. Water has shown to yield both negative and positive effects on the catalytic performance. Each case will be carefully examined.

Chapter 2 - Conversion of Furfural to Cyclopentanone in Condensed Aqueous Phase

2.1 Introduction and Literature Review

2.1.1 Introduction

The fast polymerization of furfural, one of the abundant species in the second stage of torrefraction, to humins results in a rapid deactivation of heterogeneous catalysts and low carbon balance of the upgrading process. Since the humins formation occurs spontaneously even at low temperature and in the absence of catalysts, pre-stabilization of furfural to other stable molecules seems to be more economically and technologically feasible. Piancatelli *et al.* [26] and later Hronec *et al.* [27] have shown that furfural could be effectively converted to cyclopentanone (CPO), a compound that is stable even in the presence of hot water. Additionally, the carbonyl functionality of CPO allows various C-C coupling chemistries with other oxygenates that exist in other streams of torrefraction. The proposed strategy is promising enough that encourages us to carry out further investigation.

2.1.2 Literature review - Reaction Mechanism and Active Site Requirements

The ring rearrangement reaction transforms furanic species to more stable C_5 ketones through the creation of a C-C bond. This reaction was initially reported by Piancatelli *et al.* upon observing the ring rearrangement of 2-furylcarbinol into a 4-hydroxycyclopent-2-enone in an acidic aqueous system [26], and has subsequently been referred to as a Piancatelli rearrangement. This rearrangement has been the subject of numerous

additional studies with 2-furylcarbinol [28-32], furfuryl alcohol [27, 33] and a variety of substituted furanic compounds [34].

The ring rearrangement of furfural requires an initial hydrogenation step to form furfuryl alcohol. Therefore, the reaction pathway for the ring rearrangement of furfural includes two steps: hydrogenation of furfural to furfuryl alcohol, which is typically approached through the use of H_2 over metal catalysts [21, 24], and the acid catalyzed ring rearrangement of the alcohol to cyclopentanone in the presence of water [26, 28-31, 35, 36]. The protonation of the OH group on furfuryl alcohol to form a carbocation has been firstly proposed by Piancatelli as the initiation step for the ring rearrangement reaction [26, 31], resulting in the formation of species A. The unstable nature of protonated H_2O promotes the decomposition of A to B, followed by the nucleophilic attack of water onto the ring to form intermediate C shown in **Scheme 2.1** [26]. Intermediate C consecutively undergoes ring opening to generate species D, which can undergo 4π-conrotatory cyclization to facilitate the ring closure. This 4π-conrotatory cyclization is commonly referred to as Nazarov cyclization [26, 37-40]. The successive deprotonation of this species yields 4-hydroxy-2-cyclopentenone (4-HCP). In the presence of a metal catalysts and H_2, the intermediate 4-HCP could undergo hydrogenation to form 2-cyclopentene (2-PEN) and sequential cyclopentanone (CPO) or cyclopentanol (CPOL) **(Scheme 2.1)**.

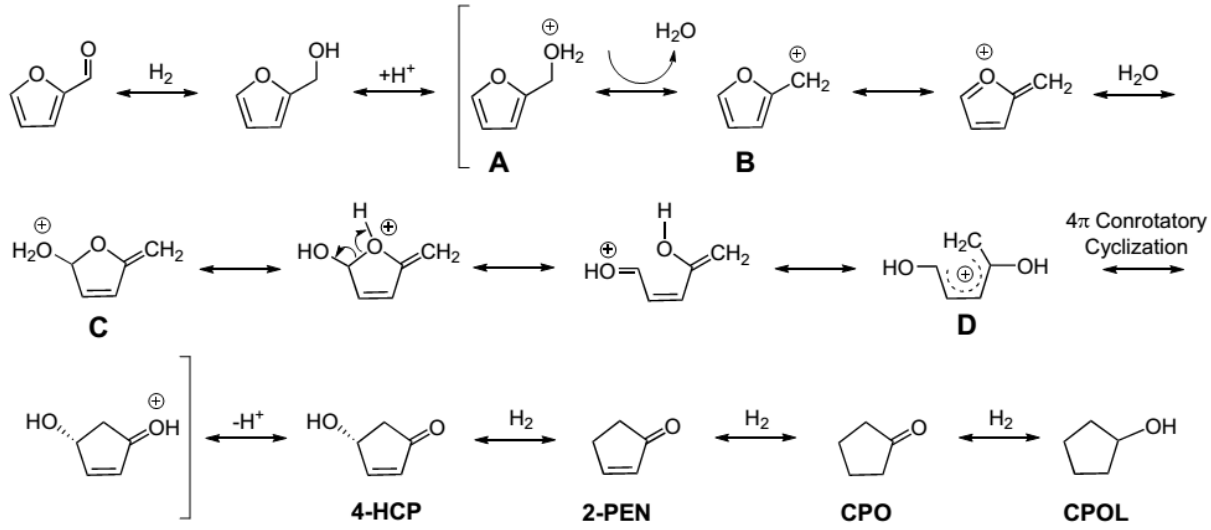

Scheme 2. 1. Mechanism of the furfural conversion to cyclopentanone. Adopted from Ref [26]

It is generally accepted that water plays an essential role in the formation of CPO since several literature sources report the necessity of aqueous media as a prerequisite for the ring rearrangement reaction [21, 24, 41]. In the presence of organic solvents, typical hydrogenation products such as tetrahydrofurfuryl alcohol (THFA), 2-methyl tetrahydrofuran (MTHF), etc. were obtained [21, 24, 41, 42]. It was proposed that water was responsible for initiating the opening and closure of the furan ring via nucleophile attack by H_2O in the 5-position of the furan ring [27] as well as affecting the adsorption of reactants and intermediate species on the metal surface [24]. By using 97% ^{18}O abundant water as a solvent, Jie Xu *et al.* observed that 95% of ^{18}O existing in CPO which indicates the incorporation of oxygen from water into the keton group of CPO [21].

As can be seen from **Scheme 2.1**, the proposed mechanism is related to the formation of 4-hydroxy-2-cyclopentenone (4-HCP) as the intermediate. The 4-HCP and its isomers have been synthesized from the rearrangement of furfuryl alcohol and furan compounds

under acidic conditions [43-47]. However, it is interesting to note that in the aqueous medium, furfuryl alcohol can spontaneously convert to 4-HCP at temperatures above 110^{o}C in the absence of H_2 pressure or catalysts [21, 24, 27]. It is believed that the ring rearrangement reaction is catalyzed by the hydronium ions generated from the auto-dissociation of water [48]. The two steps in the furfural to CPO pathway require different types of catalysts including the metal catalysts for the typical hydrogenation and acid catalysts or hydronium ions formed from the dissociation of water for the ring rearrangement of furfuryl alcohol. Though chemists proposed many effective Brønsted and Lewis acid catalysts for the Piancatelli rearrangement [28-30] as early as 1978, the recent discovery of spontaneous ring rearrangement of furfuryl alcohol to CPO in water attracts more engineering attention due to the simplicity of the process.

The concentration of hydronium ions in water depends on the temperature and the pH. An appropriate addition of weak acids such as acetic acid has a positive effect on the conversion of furfuryl alcohol to CPO over a Ni-based catalyst while the addition of basic sodium hydroxide shows the opposite trend [27]. Similarly, results over Pt and Pd-C catalysts showed a similar correlation [21] in which the addition of weak acids such as acetic acid, NaH_2PO_4 preferred the CPO formation while the addition of Na_2CO_3, Na_2HPO_4 favored the tetrahydrofurfuryl alcohol formation as depicted in **Scheme 2.2**. It has been typically believed that the role of acidic medium is to enhance the ratio between the rate of ring rearrangement and that of typical hydrogenation. However, the addition of strong inorganic acids such as H_3PO_4, H_2SO_4 over Pt, Pd-C have been reported to not favor the formation of CPO, but instead lead to rapid polymerization and consequently losses in the carbon balance [24].

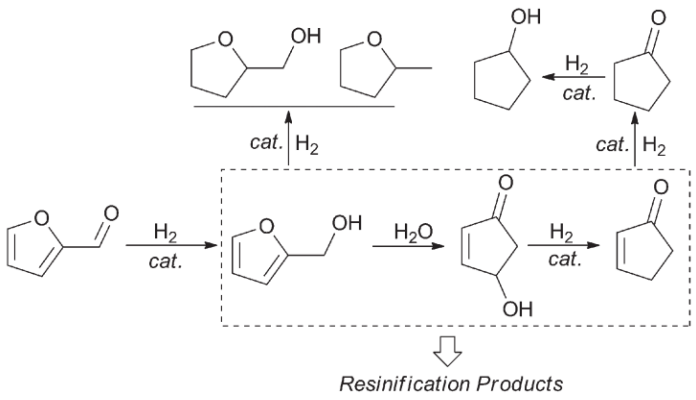

Scheme 2. 2. Reaction pathway of furfural hydrogenation. Reproduced with permission from Ref [21]

The catalysts for hydrogenation have been well developed, ranging from noble metals such as Pt, Pd, Ru, Ir, to non-noble ones such as Ni, Cu, etc, from mono to bimetallic and alloy systems [22, 23, 49, 50]. The evolution of typical hydrogenation reactions competes with the ring arrangement reaction, which has a significant impact on the overall product distribution. This will obviously also change with the selectivity of a particular metal catalyst for hydrogentation of the aldehyde C=O vs. the selectivity for hydrogenation of the ring, as well as the rate of C-O hydrogenolysis. Hronec *et al.* [27] demonstrated this balance in competing rates by using partial pressures of hydrogen in the range of 0.8MPa-2.5MPa over commercial nickel basedcatalyst at 160^{o}C, demonstrating high selectivity to CPO with the yields higher than 90 mol% while the yield of THFA was below 7%. The nature of the interaction of the C=O bond with the metal surface plays an important role in this selectivity as well. For example, the adsorption of furfural on Cu favors a η^1-(O) aldehyde species [51, 52] due to the interaction between the electron lone pair of oxygen. In the case of noble metals such as Pd, Pt, however, the adsorbed furfural molecule lays flat on catalyst surface and the π electron of the furan ring, and the lone

pair electron of the carbonyl oxygen interacts strongly with the surface [53-56]. This will inherently influence the rates of THFA formation and the resulting product distribution. Therefore, the catalysts and reaction conditions should be chosen appropriately to maximize the yield and selectivity of ring rearrangement products.

The acidity of support also influences the selectivity of ring rearrangement products (CPO+CPOL). For instance, the Pt over acidic alumina is less favorable for CPO+CPOL formation than that of neutral active carbon while in the case of basic MgO, the furfural alcohol was the dominant product [24]. Additionally, it was stated that the acid–base properties of the support enhanced the chemisorption of furfural on the support, which favored undesired reactions such as condensation and oligomerization of furfural and furfuryl alcohol, resulting in low mass balance. The summary of the catalysts for the conversion of furfural to CPO is presented in **Table 2.1**.

Based on the literature review, it could be seen that the control of hydrogenation activity plays an essential role in the selective production of CPO. The competition between ring rearrangement and normal hydrogenation determines the overall product distribution. Our previous study has demonstrated that when acetone and m-cresol were co-fed into a single reactor, bimetallic Pd-Fe catalysts exhibited enhanced selectivity for acetone hydrogenation while leaving m-cresol unreacted [8]. That is, by a suitable combination of metals, it is possible to enhance hydrogenation of the carbonyl groups (the initial step of the ring rearrangement mechanism) rather than saturation of the aromatic rings (normal hydrogenation). In other words, the hydrogenation activity of Pd could be regulated by incorporating Fe. This promising result has pointed us to use

bimetallic catalysts (Pd-Fe) to selectively produce cyclopentanone from sugar-rich streams.

Table 2. 1 Catalytic conversion of furfural to cyclopentanone on solid catalysts * [23]

Catalyst (g)	Reaction conditions	Conv., %	Yield, %			Ref
			CPO	CPO +CPOL	TH[a]	
1.4% Pt-C (0.18)	160°C, 80 bar H_2, 0.5 h	99.6	43.9	60.2	7.9	[24]
1% Pt-Al_2O_3 (0.25)	160oC, 80 bar H_2, 0.5 h	97.7	44.7	48.3	5.8	[24]
1.4%Pt + 1.4%Ru-C (0.09)	160°C, 80 bar H_2, 0.5h	100	3.7	46.4	19.6	[24]
1% Pt-MgO (0.25)	160°C, 80 bar H_2, 0.5h	97.9	9.1	10	3.2	[24]
5%Pt-C (0.05)	160°C, 30 bar H_2, 0.5h	100	76. 5	81.3	3.8	[24]
5%Pt-C (0.1)	175°C, 80 bar H_2, 0.5h	100	40.2	76.4	14.7	[24]
5%Pd-C (0.1)	160°C, 30 bar H_2, 1h	97.8	67	68.4	10.5	[27]
5%Ru-C (0.1)	175°C, 80 bar H_2, 0.5h	98.7	56.7	66.3	12.9	[24]
NiSAT® 320 RS (0.1)	175°C, 80 bar H_2, 0.5 h	98.3	61.0	78.3	15.7	[24]
G-134 A (0.1)	175°C, 80 bar H_2, 0.5 h	100	57.3	64.2	14.2	[24]
G-134 A (0.04)[b]	160°C, 8 bar H_2, 1h	100	88.5	90.1	2.13	[27]
5%Ru-C (0.1)	160°C, 30 bar H_2, 0.5h	60.1	12.7	13.3	1.69	[41]
5%Ru-C (0.1)	175°C, 80 bar H_2, 1h	100	57.3	66.8	12.6	[41]
CoMnCr (0.15)	175°C, 80 bar H_2, 0.5 h	100	7.6	24	17.3	[41]
Raney Ni Actimet C (0.2)	160°C, 30 bar H_2, 1 h	100	17.5	57.5	34.7	[41]
5%Ru-C (0.4)	165°C, 25 bar H_2, 5h	100	10.6	27	44.7	[42]
5%Ru-C (0.4)	165°C, 25 bar H_2, 5h [c]	100	1.1	48.3	23.7	[42]
NiCu-50-SBA-15 (0.2)	160°C, 40 bar H_2, 4 h	~100	~62	65	17	[21]
10 wt% Ni-CNTs (1.5)	140°C, 50 bar H_2, 10h	94	77	79	-	[25]
30 wt% Ni-CNTs (1.5)	140°C, 50 bar H_2, 10h	95	5	88.6	-	[25]
Cu-Ni-Al hydrotalcite (1.5)	140°C, 40 bar H_2, 8h Cu-Ni-Al -1 : 14 : 5	100	95.8	98.8	-	[57]
Cu-SBA-15 (0.2)	150°C, 40 bar H_2, 6h	89.6	10.5	24.2	0.2	[58]
Cu-SiO_2 (0.2)	150°C, 40 bar H_2, 6h	71.9	7.31	0	0.3	[58]
CuZnAl (0.2)	150°C, 40 bar H_2, 6h	97.9	60.3	62.8	0	[58]
Au-Nb_2O_5[d] (0.01)	140°C, 80 bar H_2, 12h	>99	86[e]	-	-	[59]
Au-Al_2O_3[d] (0.01)	140°C, 80 bar H_2, 12h	>99	72[e]	-	-	[59]
Pt, Pd, Ru-Nb_2O_5[d] (0.01)	140°C, 80 bar H_2, 12h	>99	28-66[e]	-	-	[59]

[a]Yield of typical hydrogenation products including THFAL, 2-MeF, 2-MeTHF, etc; [b]feed furfuryl alcohol, 0.05g acetic acid as additive *: water solvent in most cases except [c]MTHF-water solvent [d]Feed 5-hydroxymethyl furfural [e]Yield of 3-hydroxymethylcyclopentanone

2.2 Experimental Methods

2.2.1 Catalyst synthesis

Pd-Fe bimetallic catalysts were prepared by conventional incipient wetness impregnation of a solution of $Pd(NO_3).xH_2O$ (Sigma Aldrich) and $FeCl_3.xH_2O$ (Sigma

Aldrich) in HCl onto SiO_2 support (HI-SI 915) at room temperature. The loading of Pd-Fe were chosen to be 1% and 2% with an equivalent molar ratio of Pd and Fe. The volume of the solution was chosen as liquid/solid ratio of 1 ml/g. After impregnation, the catalyst was dried overnight in a vacuum oven at 100°C (12 h). The dry catalyst was calcinated at 500°C under air flow 100 ml/min for 5 h.

2.2.2 Catalyst characterization

The metal catalysts were examined by transmission electron microscopy (TEM) in a JEOL JEM-2100 Scanning Transmission Electron Microscope, operating at 200 kV with the images recorded on a CCD camera. The samples were prepared by suspending 2-5 mg of sample in 10 mL of 2-propanol, followed by deposition over a Cu grid coated with carbon and dried at 80°C. The catalysts were pre-reduced in 5%H_2/He flow at 150ºC before taking TEM images.

2.2.3 Catalytic reaction measurements

The liquid-phase catalytic conversion of furfural (99%-Sigma Aldrich) was studied in a 300-mL batch reactor. The reaction conditions were at 150°C and 200-600 psi of H_2 pressure. In a typical experiment, 150 mg of catalyst was mixed with 90 ml of water in a stainless steel vessel. 2ml of furfural in 28ml of water was mixed in a vial and placed inside a feed cylinder. Before reaction, the reactor was purged several times with N_2 and H_2 to remove air in the system. The reduction process was conducted at 250°C, 300pisa of H_2 for 6 h to activate the metal catalysts. Afterward, the sytem was cooled down to room temperature and the pressure was released. The furfural conversion reaction was started by heating the reactor to 150ºC. The feed was injected into the reactor after the

temperature reached 147ºC. The reaction time began being counted after 5 mins for temperature stabilization.

The product mixture was analyzed by Shimadzu QP2010S gas chromatograph/mass spectrometer (GC-MS) and quantified by GC-FID Agilent 6890 equipped with a flame ionization detector for quantification. Both GC's were equipped with a Zebron ZB-1701 column with dimensions of 60m x 0.25 mm x 0.25 μm.

The conversion (X), yield (Y_i) and selectivity (S_i) were calculated as:

$$X_{FA} = \frac{C_{FA-in} - C_{FA-out}}{C_{FA-in}}; Y_i = \frac{C_i}{C_{FA-in}}; S_i = \frac{C_i}{\sum C_i}$$

The carbon balance for the furfural conversion (C_{bl}) was calculated as:

$$C_{bl} = \frac{C_{FA-out} + \sum C_i}{C_{FA-in}}$$

where $C_{FA(in, out)}$: Concentration of furfural before and after reaction; mM
C_i: Concentration of each product; mM

2.3 Results and Discussions

2.3.1 TEM images of Pd-Fe catalysts

The TEM images of 1%Pd, 1%Pd-Fe and 2%Pd-Fe are shown in **Figure 2.1**. As illustrated, the metal species could be well-distributed over the silica support. High dispersion of metal species could be detected in all of the studied samples (**Table 2.2**). The average particle sizes of 1%Pd, 1%Pd-Fe and 2%Pd-Fe are 2.67, 1.38, 1.63nm, respectively. The bimetallic catalysts have lower particle sizes, indicating that the

addition of Fe assists to reduce the particle size. Accordingly, the dispersion of the catalysts followed the order: %1Pd-Fe (77%) > 2%Pd-Fe (65%) >1%Pd (40%). It could be seen that the higher loading of metal yielded a larger particle size and the lower dispersion (1%Pd-Fe and 2%Pd-Fe).

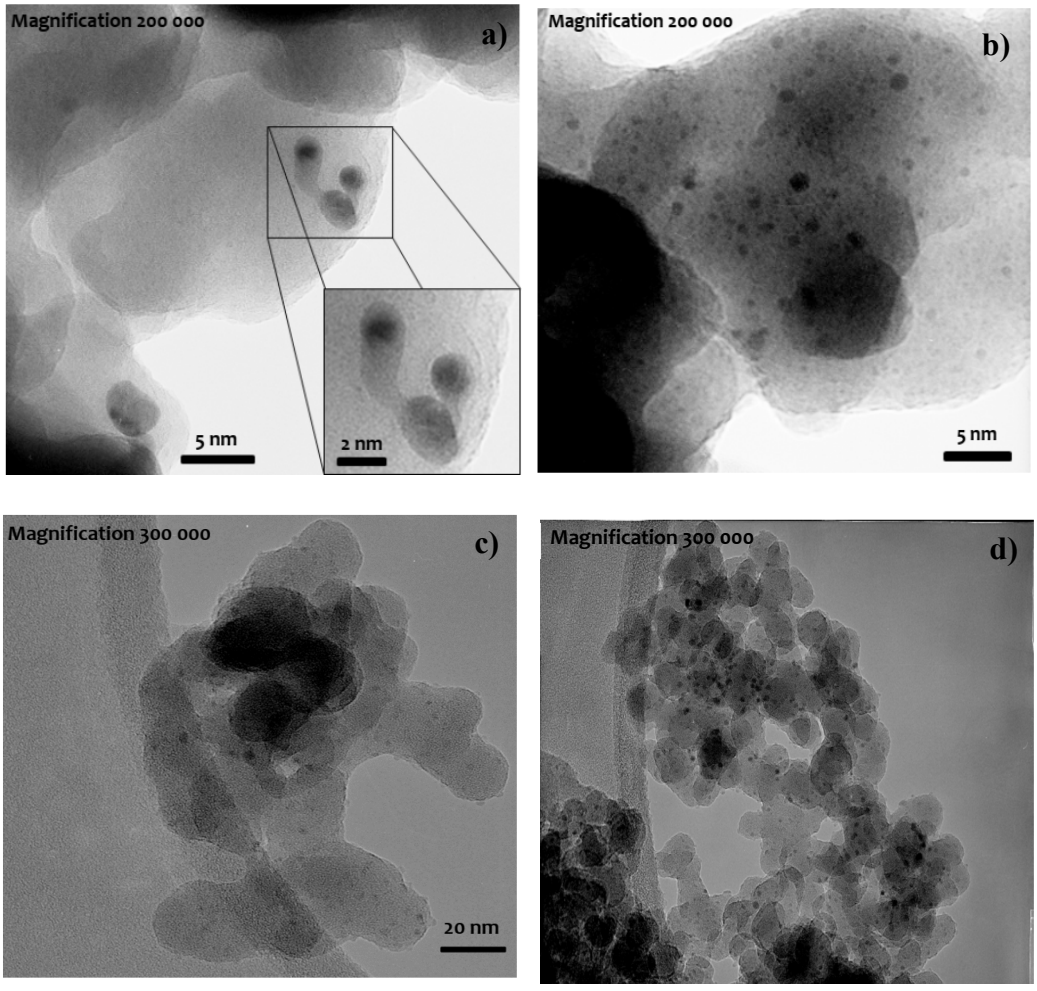

Figure 2. 1 TEM images of a-b) 1%Pd/SiO_2 c) 1%Pd-Fe d) 2%Pd-Fe/SiO_2. All of the catalysts were pre-reduced in 5%H_2/He flow at 150^oC

Table 2. 2 Average particle sizes and dispersion of Pd and Pd-Fe catalysts

Samples	Particle size, nm	Dispersion, %
1%Pd	2.67	40
1%Pd-Fe	1.38	77
2%Pd-Fe	1.63	65

2.3.2 Catalytic activity of Pd-Fe catalysts

The activity and selectivity of the mono- and bi- metallic catalysts are shown in **Figure 2.2**. There are two main products: ring-rearrangement (Cyclopentanone-CPO) and normal hydrogenated products (Furfuryl Alcohol-FOL, Tetrahydrofurfuryl Alcohol-THFOL and Tetrahydrofurfural-THFA). High conversion of Furfural (FA) and selectivity to CPO could be obtained on 1%Pd catalyst (71% and 71%, respectively) (**Figure 2.2**). Pd-Fe/SiO_2 catalysts exhibit significantly higher selectivity of CPO, reaching up to over 90%. It is obvious that the incorporation of Fe assists to control the hydrogenation activity of Pd that would drive the reaction toward the ring rearrangement reaction. As can be seen from **Table 2.3**, a higher H_2 pressure favors the formation of the normal hydrogenated products (THFOL and THFAL), resulting in a decrease of CPO selectivity.

Table 2. 3 Furfural hydrogenation at different H_2 pressures. Reaction condition: 2%Pd-Fe/SiO_2 catalyst, 150^{o}C, 6 h, 200-600 psia H_2 pressure, 0.2M furfural in water solvent. FOL, THFOL and THFA are furfuryl alcohol, tetrahydrofurfuryl alcohol and tetrahydro furfural, respectively.

H_2 Pressure (psia)	**Conversion**	**Selectivity**			
		FOL	THFOL	Cyclopentanone	THFAL
200	49%	3%	2%	**95%**	0%
300	79%	4%	2%	**93%**	0%
600	93%	2%	8%	**88%**	2%

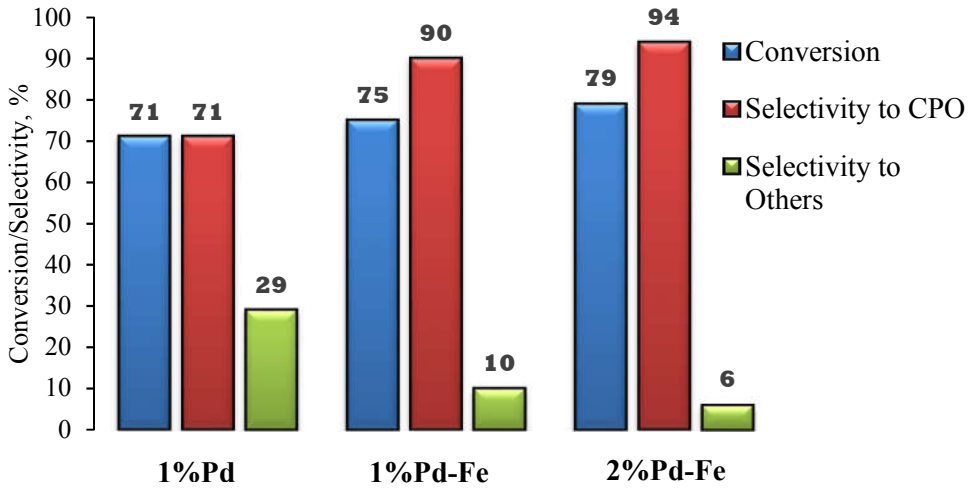

Figure 2. 2 Conversion of furfural (FA) and Yields of CPO and other hydrogenated products including furfuryl alcohol (FOL), tetrahydrofurfuryl alcohol (THFOL) and tetrahydrofurfural (THFA). Reaction conditions: 2%Pd-Fe/SiO_2 (1:1 molar ratio), 150^oC, 6 h, 300 psia H_2 pressure, 0.2M furfural in water solvent.

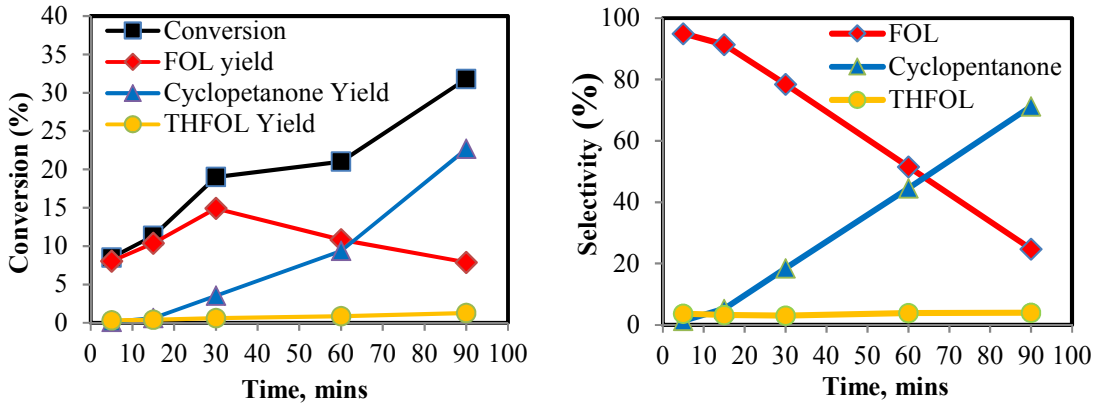

Figure 2. 3 The conversion of FA and the yields of different hydrogenated products over time

As the reaction proceeded over time, the yield of FOL increased then decreased while the CPO yield kept increasing after 30 mins of reaction (**Figure 2.3**). Similar trend could be observed in the selectivity of those products. The results indicate that FOL is the

intermediate product of the FA ring rearrangement to CPO, which agrees well with reported studies in the literature [26] (**Scheme 2.1**). The furfuryl alcohol then undergoes the ring rearrangement to produce 4-Hydroxy-2-Cyclopentanone (4-HCP) as an intermediate. This intermediate is later dehydrated/ hydrogenated to yield CPO.

In the absence of a catalyst, under either H_2 or N_2 pressure, 4-HCP could also be formed (**Table 2.4)**. Another intermediate product detected was 2-Cyclohexene (2-CP) which possibly is the dehydrated and partially hydrogenated product of 4-HCP. This finding agrees with the literature which states that the ring rearrangement reaction is catalyzed by the hydronium ions generated from the auto-dissociation of water at the temperature above 110^{o}C [21, 24, 27, 48]. Besides temperature, the concentration of hydronium ions in water also depends on the pH of the solution. It has been reported that an acidic solution facilitates the formation of hydronium ions. As shown in **Table 2.4**, the use of increasing acidic solid catalysts enhanced the total yield of the ring rearrangement products (2-CP + 4-HCP). An increase of 4-HCP selectivity with increasing acidity of the solution suggests that perhaps, the pre-hydrogenation of 4-HCP to 3-Hydroxy-cyclopantanone is required prior to the dehydration which could be a slow step in the absence of H_2 pressure. When a metal catalyst with H_2 pressure is applied, the total formation rate of the ring rearrangement intermediates (2-CP+4-HCP) controls the overall rate of CPO formation.

Table 2. 4 The conversion of furfuryl alcohol to the intermediate products over different catalysts. Reaction condition: 150°C, 6 h, 300 psia N_2 pressure, 0.2M furfuryl alcohol in water solvent.

Catalysts	pH of water	Surface area (m2/g)	Conc., mM		
			2-CP	4-HCP	Sum
SiO_2	7	215	39.5	73.9	113.4
Activated Carbon	6-8	600	12.9	106.0	118.9
Al_2O_3	4.2-4.6	200	8.9	111.6	120.5
No catalyst- 300 psia H_2 pressure	-	-	2.6	101.2	103.8
No catalyst- 300 psia N_2 pressure	-	-	0.9	103.6	104.5

2.4 Conclusion

Since the typical hydrogenation always occurs in parallel with the Piancatelli rearrangement, the reaction condition that favors the hydrogenation of C=C-C=O or hydrogenolysis such as the utilization of highly active metal catalysts and high H_2 pressure would strongly enhance the formation of the byproducts such as tetrahydrofurfuryl alcohol (THFA) or 2-methyl tetrahydrofuran (MTHF), methyl furan (2-MF) etc., leading to the decrease of ring rearrangement selectivity. Therefore, it is desirable to optimize the reaction condition as well as the catalysts so that it is sufficient for effectively converting furfural to CPO while harnessing excess hydrogenation acitivty which could drive the reaction toward typical hydrogenation.

An excellent yield and high selectivity toward CPO could be achieved over 2%Pd-Fe/SiO_2 catalysts, reaching 93 % furfural conversion and 88% selectivity to

cyclopentanone at 600 psia H_2 and 150ºC. The rapid conversion of furfurals into cyclopentanone shows several benefits for the upgrading of biomass processes. For instance, a) It is favored by the presence of water and acids prevalent in high content in real bio-oil streams; b) It results in excellent yields to cyclopentanone, reducing the concentration of other contaminants and thus lowering separation costs; c) Cyclopentanone is a very convenient building block for carbon retention in the liquid fuel range; d) It lessens catalyst deactivation by mitigating carbon losses caused by the rapid resinification of furfurals to humins.

Chapter 3 - Simultaneous Upgrading of Furanics and Phenolics via Hydroxyalkylation/Aldol condensation Reactions

ABSTRACT

The simultaneous conversion of cyclopentanone and m-cresol has been investigated on a series of solid acid catalysts. Both compounds are representative of biomass-derived streams. Cyclopentanone can be readily obtained from sugar-derived furfurals via Piancatelli rearrangement under reducing conditions. Cresol represents the family of phenolics, typically obtained from the depolymerization of lignin. In the first biomass conversion strategy proposed here, furfural is converted in high yields and selectivity to cyclopentanone (CPO) over metal catalysts such as Pd-Fe/SiO_2 catalyst at 600 psia H_2 and 150^{o}C. Subsequently, CPO and cresol are further converted via acid-catalyzed hydroxyalkylation. This C-C coupling reaction may be used to generate products in the molecular weight range that is appropriate for transportation fuels. Since molecules beyond this range may be undesirable for fuel production, a catalyst with suitable porous structure may be advantageous for controlling the product distribution in the desirable range. In fact, when Amberlyst resins were used as a catalyst, C_{12}-C_{24} products were obtained, whereas when zeolites with smaller pore sizes were used, they selectively produced C_{10} products. Alternatively, CPO can undergo the acid-catalyzed self-aldol condensation to form C10 bicyclic adducts. As an illustration of the potential of practical implementation of this strategy for biofuel production, the long chain oxygenates

obtained from hydroxyalkylation/aldol condensation were successfully upgraded via hydrodeoxygenation to a mixture of linear alkanes and saturated cyclic hydrocarbons, which in practice would be direct drop-in components for transportation fuels. Aqueous acidic environments, typically encountered during the liquid-phase upgrading of bio-oils would inhibit the efficiency of base-catalyzed process. Therefore, the proposed acid-catalyzed upgrading strategy is advantageous in terms of process simplicity for biomass conversion.

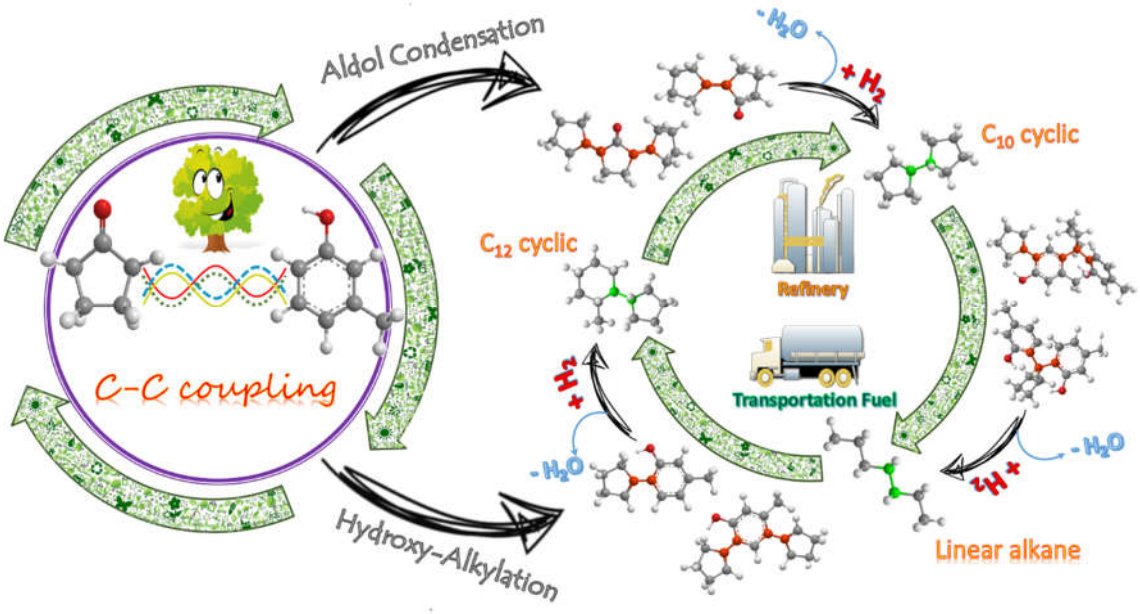

3.1 Introduction and Literature Review

3.1.1 Introduction

Fossil sources exhibit undoubted technological and economical advantages for production of chemicals and transportation fuels. However, emission of greenhouse gases (CO_2 and CH_4) is an issue of critical concern regarding global warming and climate change. This concern has led to increased research efforts with the goal of commercializing fuels and chemicals from biomass sources that would greatly reduce the carbon footprint. However, techno-economic evaluations indicate that immediate implementation is not possible. The great variety of oxygenated compounds with incompatible chemistries makes a single-stage upgrading practically impossible. Therefore, greater efforts are needed to help in the development of more efficient biomass upgrading technologies with a number of unit operations that make the process economically feasible. Although several strategies have been investigated to process vapors and liquids derived from biomass pyrolysis, finding efficient processes that can be techno-economically attractive has been challenging [60]. The direct catalytic hydrotreating of condensed bio-oil faces major problems [61, 62], including low yields of liquids in the fuel range and high hydrogen pressures, which complicates their integration with a pyrolysis system [63]. Incorporation of pre-hydrogenated bio-oils into conventional petroleum feedstocks in refinery operations, such as the fluidized catalytic cracking (FCC) and hydrotreating units [64, 65] have also shown technical impediments that may obstruct their implementation in commercial processes. Some important advances have been made in the upgrading of pyrolysis vapors that leads to enhanced

stability of the condensed liquid by forming C-C bonds before adjusting the oxygen content [66, 67].

The utilization of torrefraction allows us to selectively fractionate a complex mixture of bio-oil into diffrent streams with a specific group of functionalities enriched in each stream [3, 4]. The stabilization of the furanics fraction via Piancatelli ring rearrangement (**Chapter 2**) has opened up many potential possibilities for incorporating this new chemistry with the upgrading of other fractions such as phenolics.

Corma *et al.* [16, 68, 69] have pointed out the feasibility of forming C-C bonds between carbonyl compounds with other organic molecules whenever their electron-density is high enough to promote the electrophilic-attack of the oxonium ion generated by the protonation of the carbonyl group. Phenolics compounds such as m-cresol and guaiacol, abundant species in biomass pyrolysis vapors, are suitable candidates as hydroxyalkylation aromatic substrates. In fact, several studies have reported successful examples of hydroxyalkylation in systems comprising acetaldehyde/p-cresol [70], acetaldehyde /phenol [71], formaldehyde/guaiacol [72], acetaldehyde/o-xylene [73], aldehyde/benzene derivatives [74, 75], acetone / phenol [76], benzaldehyde/benzene derivatives [77], paraformaldehyde /anisole [78], formaldehyde/benzene [79], formaldehyde / phenol [80] over acid-functionalized solids, such as Amberlyst acidic resin and acidic zeolites to produce crucial platforms for the chemical industry. For example, Rode et al. [81] have reported 80-95% yields of coupling products from the reaction of acetaldehyde/p-cresol over Hβ and bentonite clay catalysts impregnated with dodecatungstophosphoric acid.

In this contribution, we propose a novel approach for the simultaneous upgrading of furfural and m-cresol, two model compounds that represent two streams of sequential biomass thermal treatment at moderate and high temperatures. In this strategy, furfural is first pre-stabilized as cyclopentanone via the Piancatelli rearrangement/hydrogenation process [24, 82]. This intermediate product is then used to hydroxyalkylate m-cresol and generate C_{10}-C_{24} oxygenates, a suitable range for transportation fuel precursors.

3.1.2 Literature review: Reaction mechanism and active site requirements

Several catalyst systems have been studied for the hydroxy-alkylation reaction including homogeneous Brønsted acids: HCOOH, CH_3COOH, H_3PO_4, H_2SO_4 [83], para-toluene sulfonic acid (PTA) [84]; heterogeneous Brønsted solid acids: Amberlyst 15, Nafion 212 [84], acidic resin [85]; homogeneous Lewis acids such as: BF_3, $BeCl_2$, $TiCl_4$, $SbCl_5$, $SnCl_4$; super acid $HF{\cdot}SbF_5$ and $HSO_3F{\cdot}SbF_5$ [86-88]; solid Lewis acids: Al-MCM-41[89], Sn/Si-MCM41[90]; Brønsted and Lewis solid catalysts including: USY [77], HY[77, 78], HZSM-5 [77, 78, 89], HBEA [77, 78, 89, 91], Al-MCM-41[89], heteropolyacids deposited on solid supports [76, 92, 93], montmorillonite clay, $NbOPO_4$ [94], MOF [95]

Brønsted acid-catalyzed mechanism:

An example of a proposed Brønsted acid-catalyzed mechanism for the hydroxyl-alkylation of ketone/aldehyde with aromatics on a solid surface [96-98] is shown in **Scheme 3.1**. In the first step, formaldehyde (1) is protonated to form a hydroxymethyl carbocation (2), which then undergoes electrophilic substitution toward the ortho/para carbon atom of phenol molecule. This C-C coupling step includes several elementary

steps regarding the rearrangement of C-C, C-H and C-O bonds inside the aromatic ring to form a hydroxyl oxygen cation (3). This unstable species then returns the proton to the surface to form (4-hydroxy benzyl alcohol) (4). The alcohol product could be re-protonated to generate a carbocation intermediate (5), which continues to react with another phenol molecule to yield a trimer intermediate and water as a by-product (6). Afterward, the intermediate species (6) is deprotonated to produce bisphenol F [99-102]. The hydroxy-alkylation mechanism in homogeneous Brønsted acids would be very similar. The only difference is that the proton transfer process occurs between the reactants and the solubilized H^+ with its conjugate base in the reaction solution rather than the ones on the surface. Accordingly, it should be noticed that the electron density of a substrate plays an essential role. Barthel et. al [103] has shown that the consumption rate of substituted benzenes (phenol, anisole and toluene) for the hydroxy-alkylation with chloral on zeolites follows the order of anisole ($X=OCH_3$) > phenol (X= OH) >toluene ($X=CH_3$). This order matches with the corresponding σ_{p+} substituent constant which demonstrates the strength of the electron donation effect of a substituent to the aromatic ring. In this study, it is likely that the kinetically relevant step is C-C bond formation since a higher electron density in the aromatic ring results in a higher condensation rate. Other mechanisms have also been proposed for the reaction such as Lewis acid-catalyzed mechanism on BF_3, $BeCl_2$, $AlBr_3$, $TiCl_4$, $SbCl_5$, $SnCl_4$ [86-88, 104-110] or super-electrophiles [86, 111-118]. Lewis acids activate the carbonyl compounds by polarizing the C=O bond of the carbonyl group via the interaction with the oxygen lone pair, making the C-carbonyl more susceptible to a nucleophilic attack [87, 104-110].

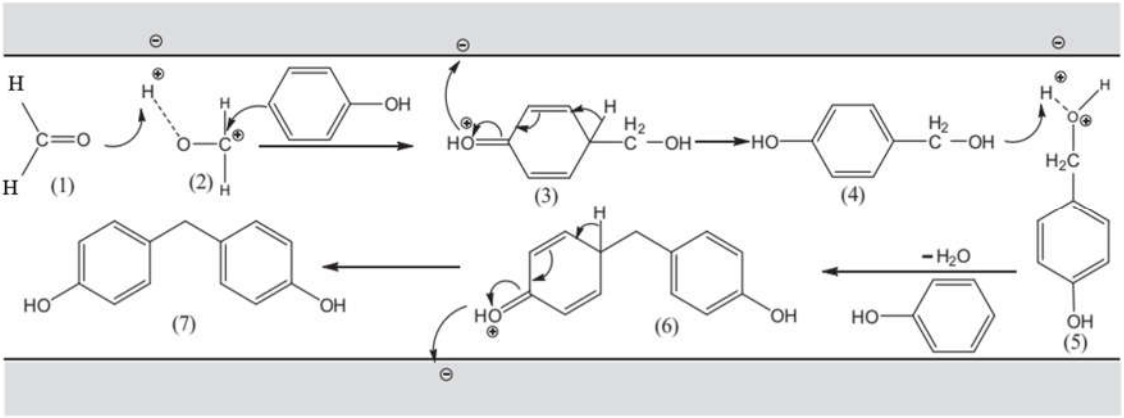

Scheme 3. 1 Mechanism of the hydroxyalkylation of formaldehyde/phenol. Reproduced with permission from Refs [99]

Site requirements:

Brønsted and Lewis acids both activate the carbonyl compounds by rendering the C-carbonyl electrophilicity. In heterogeneous systems, there is lack of a comprehensive study related to the mechanism of Lewis acid-catalyzed hydroxy-alkylation on a solid surface. This is essentially important, especially when one has to deal with a complex catalyst system that might contain both type of acid sites (Brønsted and Lewis). Several studies on different solid catalysts have not clearly differentiated the contribution of each site type to the observed activity [93, 99, 119]. For example, Garade et al. [101] have investigated the production of bisphenol F from the hydroxyalkylation of phenol and formaldehyde on dodecatungstophosphoric acid (DTP) impregnated on fumed silica. They have shown that pure SiO_2 showed negligible activity due to the presence of only weak Lewis acid sites. The deposition of DTP on SiO_2 significantly increased the density of strong sites as well as the total acid density (both Brønsted and Lewis sites), resulting

in an increase in product yields. However, no further explanation about the role of each site type or their contribution have been reported.

Garade *et al.* [71] have shown that the conversion of formaldehyde as well as the trimer selectivity on DTP/montmorillonite K10 catalyst increased with increasing Brønsted/Lewis ratio, suggesting that the Brønsted sites are more crucial in the formaldehyde activation [71, 81, 120, 121]. On the other hand, Bai et al. [122] have reported that zeolites modified with oxalic acid exhibited a significant increase in Lewis acid site and a decrease in Brønsted acid site density (as confirmed by Pyridine-IR). This resulted in an enhancement of catalytic performance/stability for the hydroxy-alkylation of anisole and chloral. They attributed the improvement of the turnover number to the higher Lewis site density, which suggests that the Lewis sites are more effective for this reaction. Study on p-cresol/formaldehyde system has demonstrated that 70% coupling product yield could be achieved on Sn/Si-MCM41 catalyst at 90ºC for 2 h. The Lewis acid site was originated from the presence of Sn^{4+} in tetrahedral coordination in silica framework [90].

Xia et al. [123] have proposed the synergy effect of both type of acid sites in their study, using mesoporous Al-incorporated silica-pillared clay interlayer catalysts for the production of bisphenol F from phenol/formaldehyde. The weak and moderate acid sites were proposed to be originated from OH groups bonded to the pillars'Al ion (Al-OH) while the strong acid sites were associated with the OH groups bonded to the tetrahedrally coordinated Al ions. The band at 1447 cm^{-1}, 1544 cm^{-1} and 1490 cm^{-1} in FTIR-pyridine spectra corresponded to the pyridine adsorbed on Lewis, Brønsted acid site and the one

associated with both Lewis and Brønsted acid site, respectively [124-126]. They have proposed that while the Brønsted site activates the formaldehyde by donating a proton (H^+) to the O-carbonyl, the Lewis cite (Al^{3+}) abstracts a H^- from the carbonyl C atom [127]. The increase of Al content leads to an increase in Lewis/Brønsted sites ratio as well as the activity enhancement. The activation of formaldehyde by Lewis acid site has been reported to require higher activation energy than that by Brønsted acid site. Therefore, the higher condensation rate observed at high Lewis/Brønsted ratio suggests that the reaction might be catalyzed by the combination (synergy effect) of both type of sites rather than by just a single one [123]. However, the nature of this synergy effect is not fully addressed.

The type of active sites also influences the selectivity of desired products. While the Brønsted acid site promotes the trimer production, the Lewis ones with weaker strength favors the dimer generation. For instance, high selectivity of trimer bisphenol F was obtained with high density of strong acid sites [71, 92]. Lewis acid sites with moderate activity (low TPD desorption temperature range) was responsible for the highest selectivity toward the dimer of p-cresol/formaldehyde hydroxy-alkylation on MFI structured molecular sieves of SnO_2/Al_2O_3 [128]. Increasing Al contents led to the increase of Brønsted acid density, resulting in an enhancing formaldehyde conversion as well as trimer yield. Tan et al. [80] have reported that the Brønsted acid site favors the formation of 4,4'-substituted whereas Lewis one favors the production of 2,4' and 2,2'-isomers on formaldehyde/phenol system [80]

3.2 Experimental Methods

3.2.1 Chemical and materials:

Amberlyst 15, Amberlyst 36, p-TSA and SiO_2-Al_2O_3 were purchased from Sigma Aldrich and used as provided. Zeolite NH_4-β (Zeolyst) was calcined at 600^oC for 5 h in 150ml/min air flow to produce H-β. 2% Pd-Fe/SiO_2 catalyst was synthesized by impregnation method as reported previously in Chapter 2. Cyclopentanone and m-cresol were obtained from Sigma Aldrich. Cyclopentanone was distilled to remove impurities before used for the reaction while m-cresol was used as provided.

3.2.2 Catalytic reaction measurements:

The conversion of furfural to cyclopentanone was carried out in a Parr reactor at 150^oC, 14-40 bar for 6 h in water solvent over 0.15 g 2% Pd-Fe/SiO_2 catalyst, at an initial concentration of furfural of 200 mM. The hydroxyalkylation of m-cresol with cyclopentanone was conducted at atmospheric pressure in a glass reactor at atmospheric pressure in the temperature range 65-140^oC, for 2 h in the presence of Amberlyst 15, Amberlyst 36, or p-TSA (Sigma Aldrich) catalysts. Alternatively, the reaction was conducted in a Parr reactor at 100-250^oC, under 300 psia N_2 for 2 h in the presence of Zeolite Hβ (Zeolyst) or SiO_2-Al_2O_3 (Sigma Aldrich). In all cases, the amount of catalyst used was 0.15 g and the feed was either pure CPO or m-cresol/CPO mixtures. The effect of m-cresol/CPO ratio (2:1, 5:1, and 7:1) on the product distribution was examined in the Parr reactor at 120^oC, 300 psia N_2 for 2 h in the presence of 1 g Amberlyst 15 in decalin solvent. The aldol condensation of cyclopentanone was examined in Parr reactor at 100^oC and 300 psia N_2 for 2 and 6 h. 0.5M of CPO in decalin solvent over 1 g Amberlyst 15.

The product mixture was analyzed by Shimadzu QP2010S gas chromatograph/mass spectrometer (GC-MS) and quantified by GC-FID Agilent 6890 equipped with a flame ionization detector for quantification. Both GC's were equipped with a Zebron ZB-1701 column with dimensions of 60m x 0.25 mm x 0.25 μm.

The conversion (X), yield and selectivity were calculated as:

$$X = \frac{C_{CPO-in} - C_{CPO-out}}{C_{CPO-in}} \quad ; \qquad Y_i = \frac{C_i \times n}{C_{CPO-in}} \quad ; \qquad S_i = \frac{C_i}{\sum C_i}$$

The carbon balance for the HAA reaction was calculated as:

$$Carbon\ \ balance = \frac{C_{CPO \rightarrow products} + C_{CPO-out}}{C_{CPO-in}}$$

The carbon balance for the HDO step was calculated as:

$$Carbon\ \ balance = \frac{\sum C_i \times n_{Ci}\big|_{product}}{\sum C_i \times n_{Ci}\big|_{feed}}$$

where $C_{CPO(in,\ out)}$: Concentration of cyclopentanone before and after reaction;
C_i: Concentration of each product;
n: Number of cyclopentanone molecule in molecular structure of products;
n_{Ci}: Number of carbons in molecular structure

3.3 Results and Discussions

3.3.1 Hydroxyalkylation of m-cresol/cyclopentanone

a/Product distribution over solid acid Amberlyst 15:

The hydroxyalkylation of m-cresol and CPO yields various cyclopentyl-substituted cresol compounds including (3), (4), (5) and (6) (HAA products) as shown in path B **Scheme 3.2**. Two products from self-aldol condensation of cyclopentanone including (1) and (2) (AC products) were also observed, as shown in path A. In most cases, the formation of product (2) is negligible compared to that of the other products; therefore, in most runs, product (1) is the only representative of the self-aldol condensation reaction.

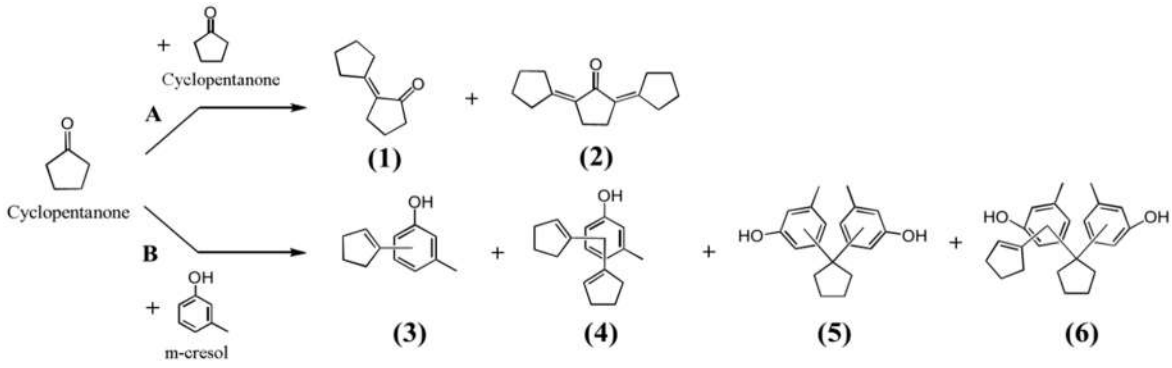

Scheme 3. 2 Products from hydroxyalkylation of m-cresol and cyclopentanone

Figure 3.1 shows the reaction data obtained after 2 h in a batch reactor on Amberlyst 15 in the temperature range 65-145^{o}C at a 2:1 m-cresol/CPO molar feed ratio. The results demonstrate that the acid resin displays an acceptable activity, with conversion increasing from 8 to 38% as the temperature increases, keeping a good carbon balance. For instance, 13% CPO conversion was obtained at 100^{o}C, with 40% selectivity to AC products, 60% selectivity to HAA products and a carbon balance of 98%. Higher temperatures favor the formation of monomer and dimer coupling products (1, 3, 4, and 5). Above 120^{o}C, the decomposition of the trimer (6) becomes evident and undesired reactions start to occur. For example, at 145^{o}C, the carbon balance dropped from almost 100 to 83 %, most probably due to polymerization as indicated by the change in color of the solution. One

problem associated with the use of a resin catalyst like Amberlyst 15 is the decomposition of the polymeric matrix that may become significant as temperature increases.

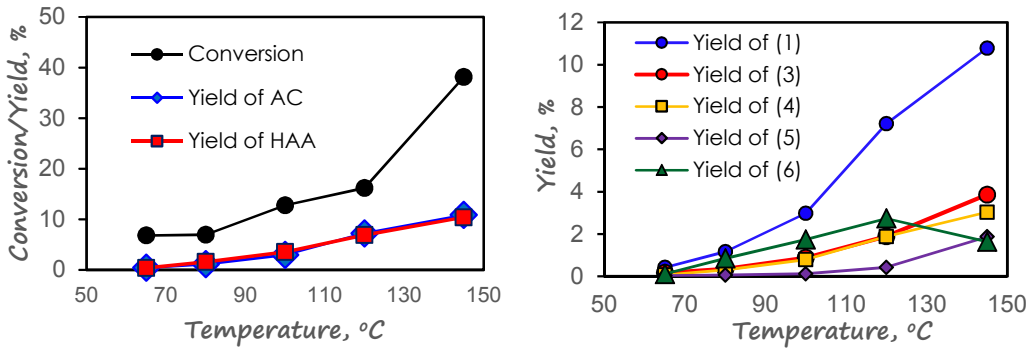

Figure 3. 1 Catalytic performance of Amberlyst 15 at different temperatures. Product (1) – (6) are presented in **Scheme 3.2**

The acid-catalyzed formation of AC products is in itself an interesting outcome of the study since the aldol condensation of cyclopentanone has been typically reported over basic catalysts, such as MgO, KF/Al_2O_3, $CaO\text{-}CeO_2$, CaO, magnesium–aluminum hydrotalcites (MgAl-HT) and lithium–aluminum hydrotalcites (LiAl-HT) [82], or even in NaOH solutions [21]. While it is widely known that the aldol condensation can be catalyzed by both bases and acids, the latter has seldom been reported for cyclopentanone. Zou et al. [129] reported the self-aldol condensation of cyclopentanone and cyclohexanone in glass reactor over MOF-encapsulating phosphotungstic, Amberlyst 15 and HZSM-5 materials. The reaction was conducted at 130°C in pure cyclic ketone for 48 h and moderate conversion of the ketones could be obtained. However, no information related to carbon balance was reported.

In this work, the experiments were conducted in a Parr reactor in more controlled and quantitative ways than previous studies with shorter reaction times and direct

measurement of the carbon balance. The results summarized in **Figure 3.2** confirm that solid acids such as Amberlyst 15 are capable of producing acceptable yields of AC products (1+2). The yield of the monomer (1) increases over time, reaching 16% after 6 h of reaction. The amount of dimer product (2) is very small, reaching only about 1% yield. Excellent carbon balances of 94-97% were observed in both cases. Although the reaction conditions and catalyst formulations will need to be optimized to enhance the yield to coupling compounds, these preliminary results are promising enough to be considered an interesting approach for biomass conversion, particularly since the acidic environment is commonly found in bio-oil upgrading. The high content of water in real pyrolysis mixtures would require to operate in biphasic system [130].

Implementation of the concepts derived from model compound studies in the separation and conversion of bio-oil to fuel may demonstrate the advantage of using solid emulsifier materials such as hydrophobized zeolites [131, 132] nanotubes, and other amphiphilic catalysts that stabilize emulsions [133] to achieve maximized adducts yields for the reaction.

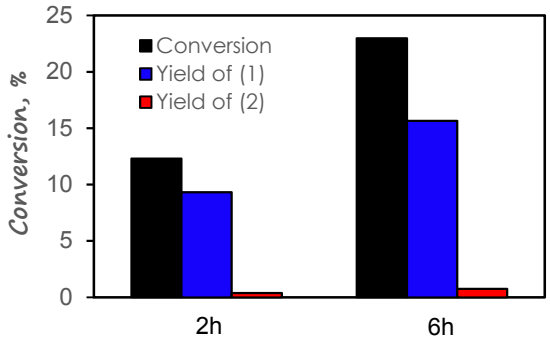

Figure 3. 2 The acid-catalyzed aldol condensation of cyclopentanone over Amberlyst 15 (Parr reactor at 100°C and 300 psia N_2 for 2 and 6 h in decalin solvent over 1 g Amberlyst 15)

Comparison of different solid acid catalysts:

Based on these observations, several solid catalysts with different characteristics, including a resin with higher acid density (Amberlyst 36), a microporous zeolite (Hβ), and a mesoporous acid catalyst (SiO_2-Al_2O_3) were investigated and compared to a homogeneous catalyst, para-toluene sulfuric acid (p-TSA) to explore the effect of catalyst topology and acidity. To make a proper comparison of selectivity, we adjusted the reaction temperature to reach an overall CPO conversion of about 15 %. Specifically, the activity comparison was made at 100°C for Amberlyst and p-TSA, and at 250°C for Hβ, SiO_2-Al_2O_3. The results are summarized in **Table 3.1** and **Figure 3.3**. Amberlyst 36 shows an analogous behavior to Amberlyst 15, reaching 15% CPO conversion with selectivities of 38% and 62% for AC and HAA products, respectively. Interestingly, while (at 100°C) Amberlyst resins catalyzed the generation of both AC and HAA, the zeolite Hβ and amorphous SiO_2-Al_2O_3 yielded only AC products (at 250°C).

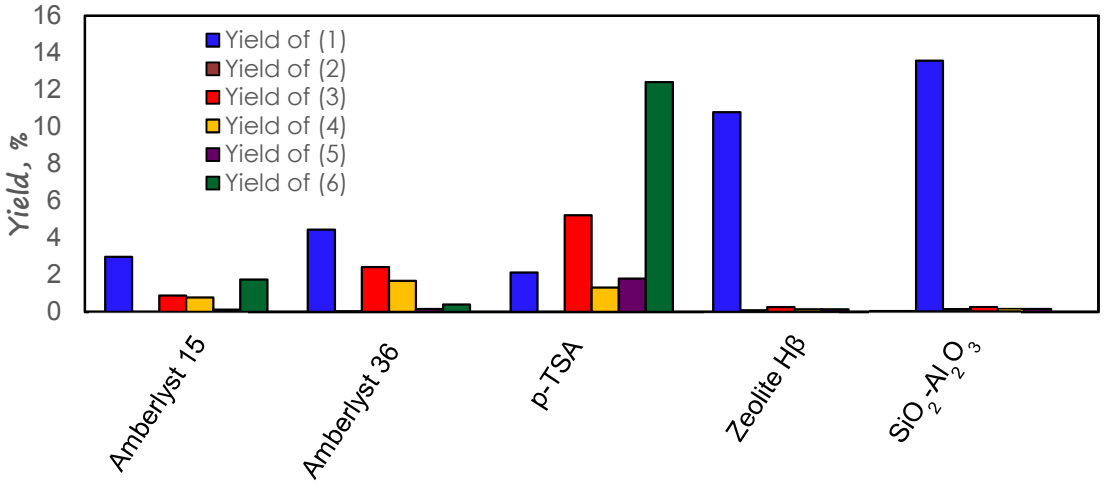

Figure 3. 3 Yield of coupling products from different catalysts at comparable CPO conversion

It is possible that the drop in HAA selectivity might be due to different steric constrain in the catalysts. For instance, Amberlyst resins have large cavities that may allow the formation and desorption of the relatively large HAA products (see example of products 3, 4, 5 and 6 in **Scheme 3.2**). By contrast, the more constrained Zeolite Hβ may only allow the smaller AC products (93% selectivity) leave the zeolite, while the HAA, if formed will remain trapped inside the microporous structure. It is suggestive that the homogenous p-TSA exhibits a higher selectivity to large HAA products (3 + 4 + 5 + 6) (**Figure 3.3**) in comparison to the behavior of solid catalysts. More specifically, at comparable CPO conversion (15-20%) the yields of 3, 4, 5 and 6 were 2.4%, 1.7%, 0.16% and 0.4% on Amberlyst 36 while they are much higher, reaching 5.2%, 1.3%, 1.8% and 12.4%, respectively with the homogeneous catalyst p-TSA.

To check the effect of reaction temperature to the product distribution, reaction runs were conducted on zeolite Hβ at different temperatures (100-250°C). As shown in the **Table 3.1**, the selectivity on this zeolite did vary with temperature. Higher selectivity toward HAA is favorable as the temperature deceases. This observation agrees with those obtained from homogeneous catalysts in which low temperature favors the formation of HAA products rather than AC products.

However, at this point, it can be concluded that although the temperature can change product distribution, the porous characteristic of solid acid catalysts is the dominant factor that makes AC products dominant (i.e., over 70% sel. at 120ºC). At 100ºC, no adducts were observed. In the case of SiO_2-Al_2O_3, the same analysis was conducted with temperature range from 100 to 280ºC. Interestingly, high selectivity towards AC is

observed in all cases. With a large pore size, (average 4.8 nm) and rather slow reactions, one would not expect internal mass transfer limitations on this mesoporous material.

Table 3. 1 Activity and Average pore size of sceened catalysts

Catalyst	T, °C	Conversion, %	Selectivity, %		Yield, %		Acid density, mmol/g_{cat}	Conversion per site (mol.L^{-1}.$mmol_{acid}^{-1}$)	Carbon balance, %	Average pore size, nm
			AC	HAA	AC	HAA				
p-TSAa	100	20	9.3	90.7	2.9	27.5	5.8[c]	1.3	97	-
Amberlyst 15[a]	100	12.8	39.6	60.4	3	3.5	4.7[c]	0.6	94	29[c]
Amberlyst 36[a]	100	15.3	38	62	4.5	4.6	4.9[c]	0.7	94	24[c]
Zeolite Hβ[b]	100	6.8	-	-	-	-	0.75[d]	2.02	90	0.6[f]
	120	11	71.1	28.9	0.2	0.045		3.38	93	
	200	11.7	85	15	2.9	0.2		3.48	92	
	250	16.3	93	7	11	0.5		4.86	94	
SiO_2-Al_2O_3[b]	100	0.76	-	-	-	-	0.53[e]	0.32	98	4.8[g]
	150	1.14	-	-	-	-		0.48	99	
	200	5.42	99	1	0.9	0.004		2.29	95	
	250	17	98	2	10.4	0.1		7.26	96	
	280	33.8	95	5	21.6	0.7		14.3	85	

[a]Glass reactor; [b]Parr reactor; [c]reported by manufacturer; [d]measured by TPD-isopropyl amine [e]ref [134] [f]ref. [135], [g]measured by BET-N_2 ads./des.

As shown in **Figure 3.4a**, the variation of overall CPO conversion as a function of temperature indicates an apparent activation energy of about 50 kJ/mol, while on the Hβ zeolite, which is clearly affected by mass transfer limitations, the apparent activation energy is only 4.5kJ/mol. Moreover, when the product yields are used for the Arrhenius plot (**Figure 3.4b**), apparent activation energy values of about 90 and 140 kJ/mol are obtained for AC and HAA formation, respectively. The lower activation energy calculated from CPO conversion (or disappearance) is due to the lower activation energy for the polimerization or coke formation that might be more favorable at higher temperatures. This results in a faster rate of carbon loss compared to C-C coupling product formation rate as the temperature increased.

The low activity exhibited by the amorphous silica-alumina catalyst towards formation of HAA products could be due to the relatively weak acid strength of this material. Indeed, calorimetry measurements of ammonia adsorption on SiO_2-Al_2O_3 give evidence of much lower density of strong acid sites than Amberlyst or any zeolite [136, 137]. Therefore, the acid strength of the mesoporous silica-alumina might not be high enough for catalyzing HAA reaction. That is, only materials with strong acidity and large pore structure could be effective catalysts for the HAA reaction.

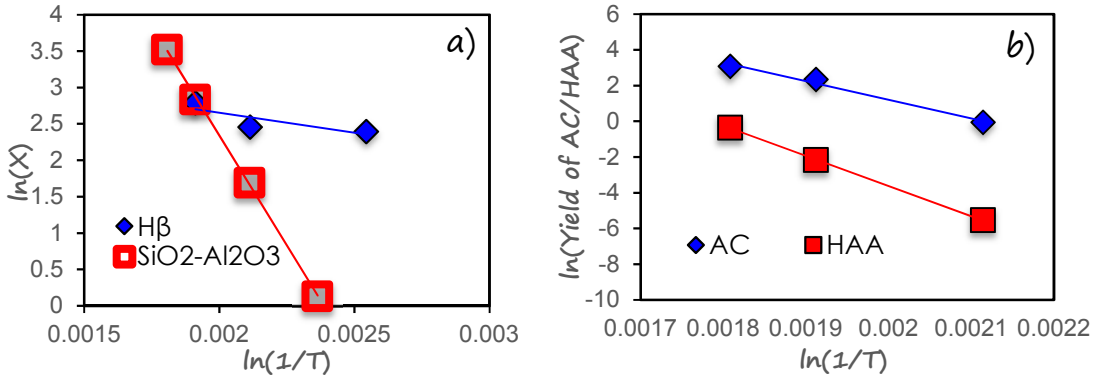

Figure 3. 4 Arrhenius plots for a) overall CPO conversion over Hβ and SiO_2-Al_2O_3; and b) Yield of AC and HAA products over SiO_2-Al_2O_3.

To gain a deeper understanding of the pathway for HAA product formation on zeolite Hβ, several separate runs were conducted at 250°C with varying amounts of catalyst. As seen in **Figure 3.5a, b** the yields of HAA and AC products uniformly increase with the amount of catalyst, as expected. At the same time, it is observed that while the selectivity to product (3) dominates at low yields (at the lowest catalyst mass) the selectivity to products (4) and (5) increased with overall conversion which demonstrates the expected series/parallel sequence for this reaction, i.e., CPO → (3); followed by (3) → (4) or (3) → (5). In this case, no traces of product (6) were observed.

Another series of independent runs was conducted, keeping the catalyst mass constant while varying temperatures. As shown in **Figure 3.5c**, contrary to the behavior of Amberlyst 15 and 36, which were able to achieve measureable yields (7-9%) at low temperatures (100-120^{o}C), the Hβ catalyst only generated small amounts of condensation products at these temperatures (traces of AC and HAA products were detected). It is conceivable that the diffusion of these large products out of the micro-porous structure is greatly hindered at low temperatures in this zeolite, leading to some disappearance of CPO, but without the formation of any noticeable coupling products. **Figure 3.5d** shows the distribution of HAA products from zeolite Hβ as a function of reaction temperature. At low temperatures (100-120^{o}C), the major product is (5), which is necessarily produced from product (3). By contrast, at higher temperatures, the selectivity towards product (5) decreases while that to (3) increases. Clearly, at high enough temperatures, product (5) begins to decompose via C-C cleavage yielding back product (3). The low selectivity towards product (4) might be due to the higher abundance of m-cresol with respect to CPO (m-cresol/CP feed ratio = 2:1).

In fact, as shown in **Table 3.1**, the carbon balance is over 90% for all cases. That is, by using a less reactive intermediate such as cyclopentanone, not only the carbon losses can be minimized, but valuable condensation products can be obtained with less humins formation.

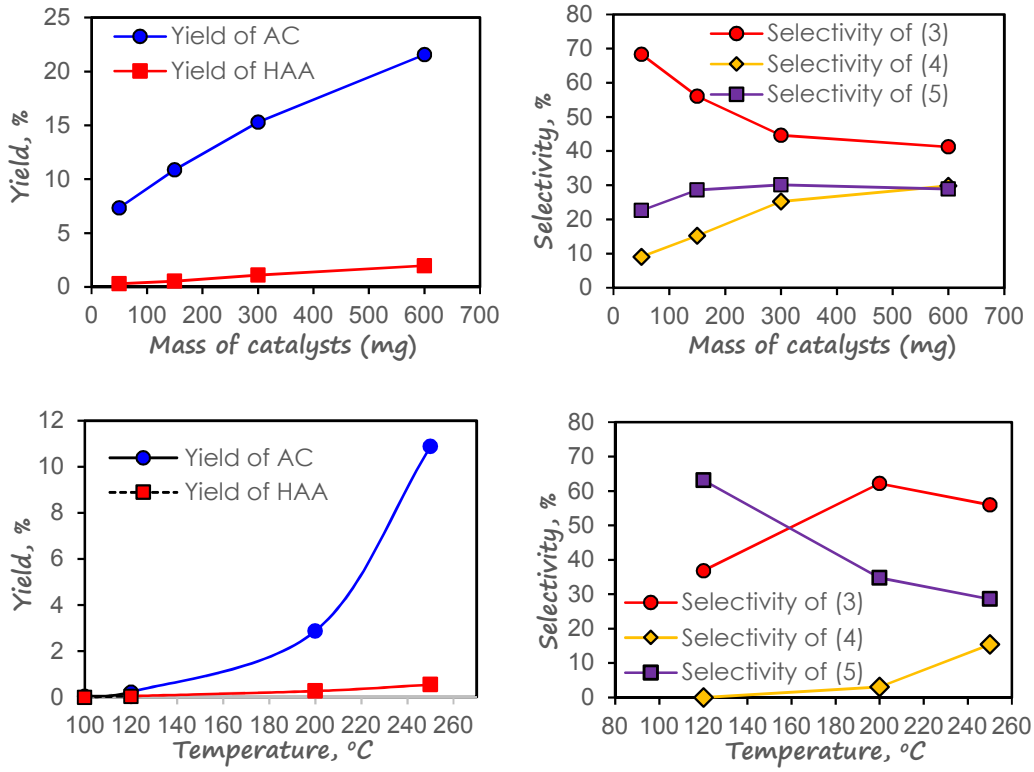

Figure 3. 5 a) Yield of AC, HAA products and **b)** Distribution of HAA products at different mass of catalysts **c)** Yield of AC and HAA products and **d)** Distribution of HAA products at different temperatures over zeolite Hβ

Effect of temperature on the competition between self-aldol condensation (AC) and hydroxyalkylation (HAA):

The investigated reaction, in fact, is complicated since two possible parallel reactions are taking place at the same time. The relative rate between two pathways depends on factors such as feed ratio, temperature, etc. Moreover, the porous characteristic of each solid catalyst places different influence in the diffusion of formed products and so on the obtained product distribution. A series of experiments was conducted with a homogeneous catalyst (para-toluene sulfuric acid) to get an insight into the nature of this reaction. In this case, there is no possible role of porous cavities affecting the product distribution as in solid acid catalysts. As shown in **Figure 3.6a**, at low temperatures (e.g.,

60°C), hydroxyalkylation products (HAA) dominate, with selectivity above 90%. As temperature increases, the selectivity toward aldol condensation products (AC) slowly increases (up to 150°C) but beyond this temperature, it jumps dramatically from 20% at 200°C to 60% at 250°C. The change of product distribution with increasing temperature in this case might be due to the low stability of the HAA C-C coupling products (the alcohol) that makes it easily decomposed back to CPO and m-cresol at high temperature (250°C) before dehydration. This results in more abundant AC products at 250°C.

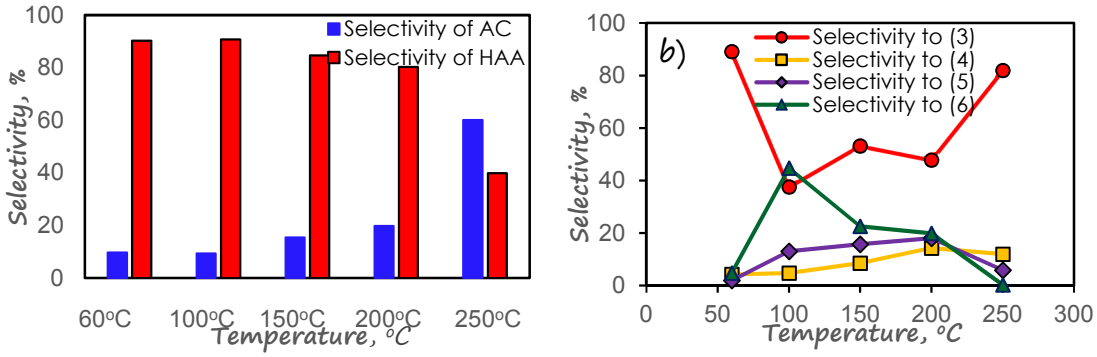

Figure 3. 6. **a)** Selectivity of aldol condensation and hydroxylalklyation products (AC and HAA) at different temperatures (Reaction condition: m-cresol/cyclopentanone=2/1, Parr reaction, reaction volume 120ml, the conversions at 60°C, 100°C, 150°C, 200°C, 250°C are 20%, 20%, 23%, 21%, 20%, respectively) **b)** Selectivity of hydroxyalkylation products at different temperatures

At the lowest temperature, only the C-C coupling monomer (3) is observed in the products. However, at 100°C, the trimer (6) is formed easily, becoming one of the most abundant products and reaching 45% selectivity. As the temperature is further increased, the selectivity to (6) greatly decreases with the other products increasing, even when the reactant conversion remained unchanged. It is clear that (6) starts decomposing back to monomer (3). Indeed, negligible amounts of the trimer (6) are detected at 250°C.

Likewise, as shown previously (**Figure 3.1**), similar decomposition of the trimer (6) is observed over the solid acid Amberlyst 15 at temperatures above 120^{o}C. **Figure 3.6b** also shows similar trends for the trimers (4) and (5), which initially increase with temperature, but then decrease, reaching a maximum selectivity at 200^{o}C (~20%).

The possible reaction mechanism includes four primary steps: (a) protonation of cyclopentanone on acid sites to form an enolate, (b) C-C coupling of the activated CPO with another CPO or m-cresol to form condensation products (ACol and HAAol), (c) deprotonation, and (d) dehydration of the resulting alcohols to generate the AC and HAA products. It is possible that the rate limiting step for each reaction could be one of those. However, in the presence of acid catalysts the dehydration step is relatively fast. It should be noted that the relative activation energy between each step could be shifted, depending on catalysts with different acid strength. More detailed kinetic and theoretical studies are required on each individual reaction to obtain a more comprehensive understanding of the system.

Effect of feed ratio:

Both AC and HAA can yield products with longer carbon chains, which can subsequently be hydrodeoxygenated to molecules that directly fall in the gasoline/diesel range. In some applications, in may be desirable to produce a narrow molecular weight distribution. In this case, our results show that a narrower molecular weight distribution can indeed be obtained by adjusting the m-cresol/CPO feed ratio. As illustrated in **Figure 3.7**, as the m-cresol/CPO increases from 2:1 to 5:1, the yield of AC products drops from 4.5% to 1.4% while that of HAA products increases from 3.7 to 5.4%. Interestingly, when

the m-cresol/CPO ratio increases to 7:1, only HAA products are obtained with no traces of AC products.

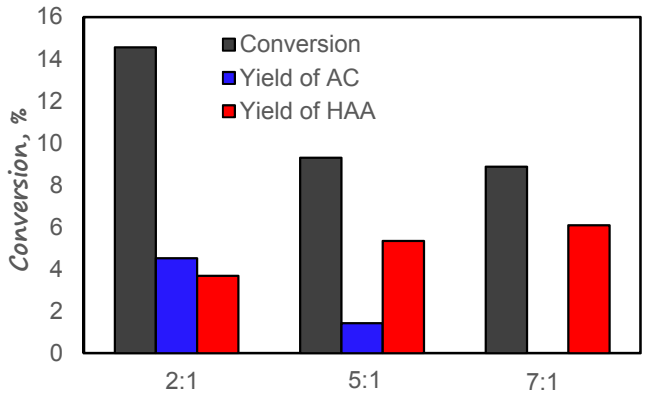

Figure 3. 7 The distribution of AC and HAA products at different m-cresol/CPO ratios over Amberlyst 15 (Parr reactor at 120°C, 300 psia N_2 for 2 h in the presence of 1 g Amberlyst 15 in decalin solvent)

3.3.2 Hydrodeoxygenation of coupling products obtained in the first step

Hydrodeoxygenation is the final step after accomplishing the desired molecular weight via C-C coupling. For practical implementation as fuels, the coupling compounds generated from hydroxyalkylation would need to be saturated and deoxygenated to produce alkanes with properties similar to those derived from petroleum energy sources. To demonstrate the sequence, first, the C-C coupling step was carried via HAA reaction on a 3g Amberlyst 36 sample in a Parr reactor (150°C, m-cresol/CPO=2:1, 12h). In this step, the goal is to obtain a reasonable yield of coupling products, which can be used later as feedstock for the HDO upgrading. In this case, 51% CPO conversion with a wide range of long-chain oxygenates was obtained, as shown in **Figure 3.8**, with (1) and (3) as major products, accounting for 18% and 14% yield, respectively.

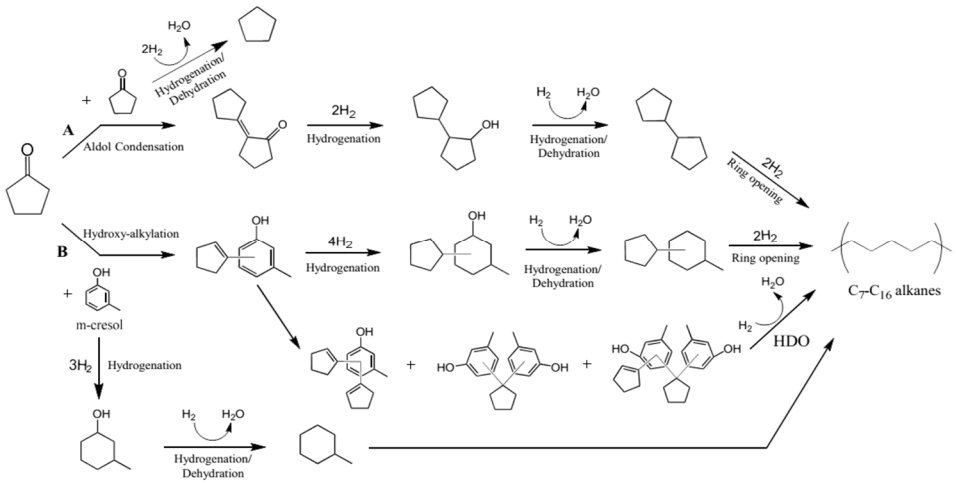

Scheme 3. 3 Biofuel production scheme starting from cyclopentanone

To carry out the HDO upgrading step, 2 ml of the liquid product of the previous step was diluted in 118 ml of undecane solvent together with 500 mg of 2% Pd/Al_2O_3 catalysts. The catalyst was reduced at 150^oC for 3 h under 400 psia of H_2. The HDO run was conducted at 250^oC in the batch reactor for 12 h. The most abundant products were cyclopentane and methyl cyclohexane, which come from the hydrogenation/dehydration of CPO and m-cresol. Long-chain hydrocarbon products include fully saturated C_{10} alkanes, C_{12} cyclic and C_{12} alkane products which are generated from the ring opening of the saturated species (1) and hydrogenation of (3), followed by the ring opening, respectively (**Scheme 3.3** and **Figure 3.9**). Trace amount of carbon chain longer than 12 was observed, which is probably due to the decomposition of dimer/trimer at the high temperatures and long reaction time used in this experiment. The observed alkanes represent over 39% selectivity of the upgraded liquid. In fact, hydrogenated products derived from m-cresol, such as methylcyclohexane or methylcyclohexanol, also fall into gasoline range (C_7-C_{12}). Therefore, the whole applicable products in the fuel range would

account for 90% of the upgraded liquid. More interestingly, the carbon balance for the HAA and HDO steps are 96% and 95%, respectively, resulting in over 90% efficiency for the whole catalytic upgrading process, which starts from CPO and results in with drop-in liquid fuel products. This promising result illustrates the great potential of this strategy for biomass-derived liquid fuel production.

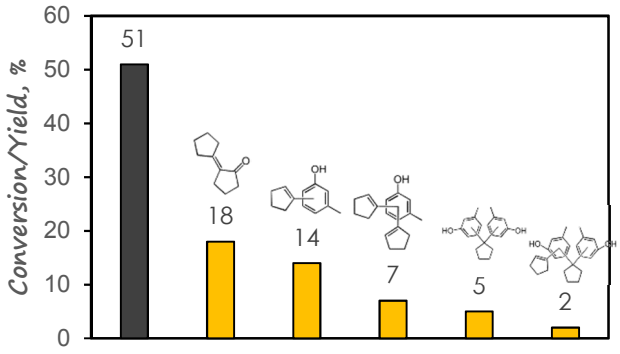

Figure 3. 8 Conversion/Yield of HAA reaction between CPO and m-cresol (dash-black bar is the conversion of CPO, yellow bars are the yield of each product)

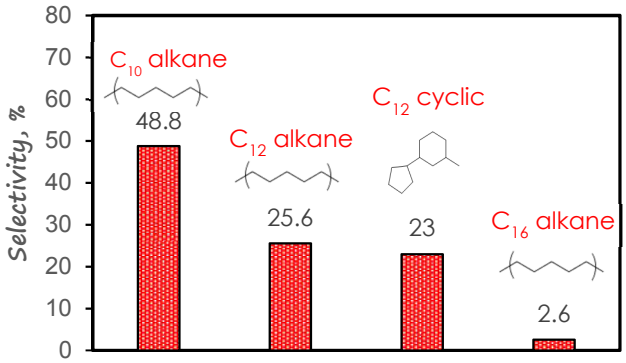

Figure 3. 9 Selectivity of each saturated products in HDO upgraded liquid

3.4 Conclusion

The Piancatelli rearrangement of furanic compounds to CPO represents a very attractive biomass upgrading strategy that pre- stabilizes reactive molecules such as

furfural into a useful and less reactive ketone. Compared to conventional hydrogenation/hydrogenolysis strategies, this approach demands less energy and less H_2 consumption. In addition, the high water and acid content of bio-oil are in fact favorable for this conversion, which makes the process more appealing in terms of practical implementation. The production of this stable intermediate can be followed by C-C bond formation reactions, such as self-aldol condensation or hydroxyalkylation with phenolics-derived fractions. When the C-C bond forming process is followed by a hydrodeoxygenation step a mixture of C_{10}-C_{16} hydrocarbons, which are in the gasoline/diesel range can be effectively obtained. For example, when the product stream from the AC/HAA reaction of CPO and m-cresol was followed by HDO on a bifunctional catalyst over 90% efficiency of the whole catalytic upgrading process starting from CPO was demonstrated, which highlights the potential of this strategy for future biofuel applications.

The major obstacle of this approach is that the large organic molecules produced by the HAA reaction are trapped in microporous catalysts, particularly at low temperatures. Thermally stable zeolites that can be operated at higher temperatures show a lower degree of trapping, but the problem still subsists. Further research on acidic materials with hierarchical structures with a proper mesoporous/microporous balance that minimizes the diffusion path of large adducts out of the catalyst cavities would be desirable.

Chapter 4 - High-Temperature Grafting Silylation for Minimizing Leaching of Acid Functionality from Hydrophobic Mesoporous Silicas

ABSTRACT

Ordered-hexagonal silica materials such as MCM41 and SBA15 have important applications in heterogeneous catalysis and biomass conversion due to their chemical stability and mesoporous structure. Conventional grafting (CG) is one of the most common functionalization methods to modify the silica surface with acidic/basic or hydrophobic/hydrophilic moieties. However, the materials prepared by this method are prone to the leaching of functional groups into the reaction medium. The exact nature of the leaching phenomenon has not been fully addressed in the literature. In this contribution, we have investigated this process at the molecular level by combining well-controlled reaction experiments and several characterization techniques (FT-IR, ^{1}H-^{29}Si CPMAS NMR, XRD, TGA and BET). We have found that leaching is originated by the presence of terminal surface silanols, which render the catalysts susceptible to the attack of water and polar compounds. Hence, leaching can be better described as a partial dissolution of the surface layers of the silica, thus removing the functional groups during this process. Therefore, an effective strategy to minimize leaching is to reduce the density of free silanols via full functionalization of the surface. We propose a novel silylation method, high-temperature grafting, which allows the grafting process to be conducted at high temperatures (180^{o}C) under solvent-free conditions. By this method, a more

complete silylation of surface silanols is obtained. Consequently, the samples prepared by this high-temperature grafting (HG) method are highly stable during acid-catalyzed alkylation reaction, conducted under severe conditions (high temperature and in the presence of polar solvents).

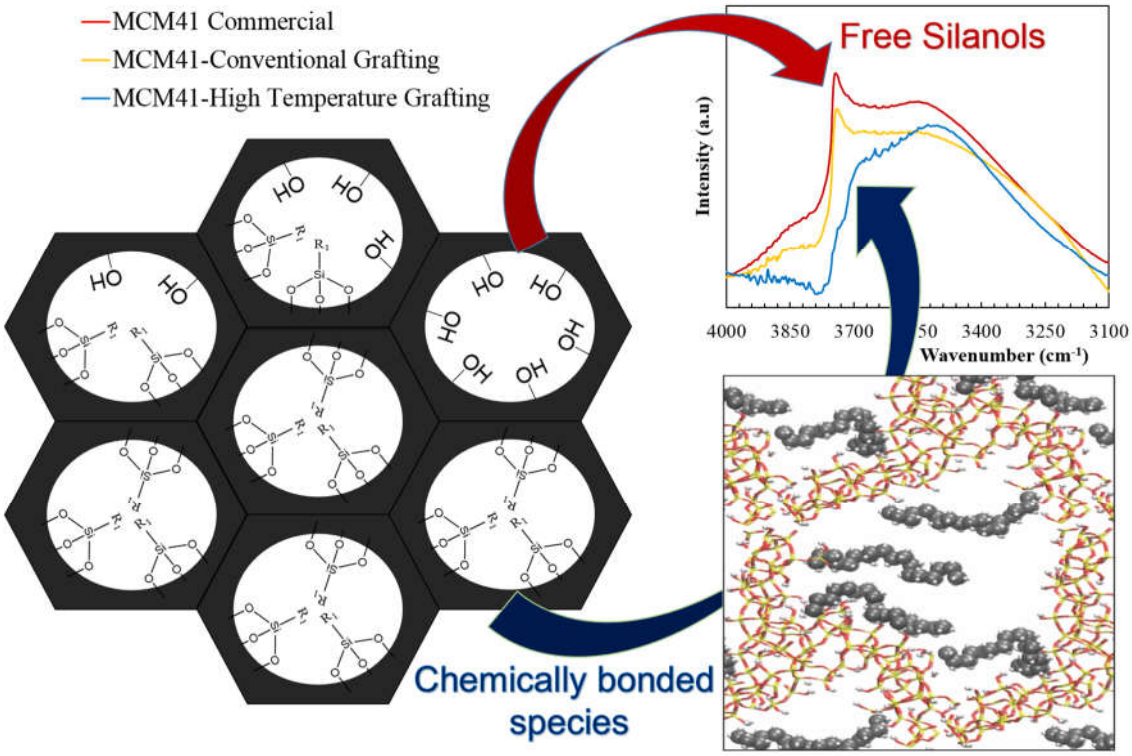

4.1 Introduction and Literature Review

Significant efforts have been dedicated in recent years to the development of catalytic processes for the production of biomass-derived chemicals and transportation fuels [138-142]. One of the major challenges in these developments is the selection of catalytic materials with enough activity, selectivity, and stability to operate under the severely deactivating aqueous environments required by the biomass upgrading processes [143].

Among the family of siliceous mesoporous materials, MCM41 and SBA15 are the two promising candidates for the upgrading of large molecules due to their relatively large pores [144-155]. The ordered mesoporous structure allows for the accommodation and rapid diffusion of intermediates and products within the catalyst cavities, reducing mass transfer limitations, which are pervasive in microporous catalysts [156]. In addition, the high density of surface free silanols of these siliceous materials provides the capability of modifying their surface properties via silylation with acid/base moieties or hydrophobic/hydrophilic linkers [157-160], which may improve the chemical stability of these materials in aqueous media. Two major techniques to synthesize this type of hybrid inorganic-organic mesoporous materials that have been reported in the literature are co-condensation and grafting [146, 155, 161-164].

Unfortunately, both methods exhibit a serious drawback for catalysis applications; that is, the attached functional groups tend to leach out from the surface, causing loss of surface activity, replaced by homogeneous reactions catalyzed by the leached species. Obviously, this is undesirable, not only for applications in continuous flow processes, but also for research studies involving measurement of specific catalytic activity of the

heterogeneous sites. Leaching of active moieties into the reaction liquid medium has been observed in many cases. For example, significant leaching of sulfonic groups has been observed from SBA15 functionalized with propane-sulfonic acid during the vapor-phase dehydration of fructose at 403K[165]. It has been proposed that the in-situ generated water hydrolyzes the Si-O bond between the attached functional groups and the solid surface to 3-(trihydroxysilyl)-1-propanesulfonic acid and surface silanols. Other studies have also indicated that the Si-O bond breaking is responsible for the observed leaching [146, 166], according to the expression:

$$(\equiv SiO)_3Si(CH_2)_3SO_3H + 3H_2O \rightarrow 3 \equiv SiOH + (HO)_3Si(CH_2)_3SO_3H$$

In contrast, the cleavage of other bonds such as Si-C, C-S or C-C of the functionalized species on the surface have been identified as directly responsible for the observed leaching. For example, some reports of $-SO_3H$ leaching from ion-exchange poly(styrene-divinylbenzene-sulfonicacid) resins [167] and Amberlyst 15 [168], caused by hydrolysis in the presence of water ascribe the functionality losses to cleavage of Si-C bonds. Alternatively, reports of leaching from carbon substrates functionalized with sulfonated polycyclic aromatics suggest the cleavage of C-C or C-S bonds [169].

$$RSO_3H + H_2O \rightarrow RH + H_2SO_4 \text{ (R= resin matrix)}$$

Despite a wide diversity of opinion proposed in the literature for the origin of leaching, a common observation is that increasing temperature or polarity of the surrounding medium intensifies the leaching phenomenon [166, 168, 170]. That is, as illustrated in **Table S1 Supplementary Information,** leaching is typically not observed

below 150°C, a temperature range used in many studies with functionalized mesoporous silicas. However, even at low temperatures (e.g., 100°C) leaching of sulfonic groups from silica has been observed in highly polar media, such as a mixture of sunflower oil and methanol [166]. Several other reports have shown leaching in non-polar [171-173] or polar solvents [174] under various conditions.

These observations strongly suggest that leaching is somehow related to a chemical attack initiated by polar compounds, which is intensified at higher temperatures and with increasing solvent polarity. In this paper, we analyze the environment of the oxygen-containing polar groups in the silica support, which may play a crucial role in rendering the catalysts more or less vulnerable to the severe attack caused by the polar liquid medium at high temperatures. The attack could be caused by either the cleavage of the Si-O bond associated with the functional group or unzipping the Si-O-Si bonds of the silica surface, resulting in losses of surface moieties into the solution[165, 175]. The analysis requires a comprehensive examination of the crucial factors involved in this attack that determine the leaching propensity of a given functionalized catalyst, as well as potential effective solutions to minimize this undesirable effect.

The present study attempts to investigate the origin of leaching at the molecular level by using a series of surface characterization techniques. At the same time, a novel functionalization method, which we call “high-temperature grafting (HG)”, is proposed as a simple approach for preparing highly stable catalysts for acid-catalyzed reactions to be employed under severe conditions (polar solvents and high temperatures), typically encountered in the liquid-phase upgrading of biomass-derived products. The alkylation

of m-cresol with cyclopentanol has been used as a probe reaction to investigate the stability of the functionalized catalysts in polar and non-polar environments at high temperatures (250ºC). This reaction is relevant to the conversion of biomass-derived oxygenated compounds into lower-oxygen-content products with enhanced C-C chain length, potentially applicable in the production of gasoline and diesel fuel components.

4.2 Experimental Methods

4.2.1 Chemicals and Materials

As-received mesoporous MCM41-Type A was dried at 120°C for 12 h under N_2 flow (99.999%, Airgas) prior to further treatment or use. The functional organosilanes (3-Mercaptopropyl)-trimethoxysilane (95% purity, from Aldrich, MPTS), Ethyl-(trichloro)silane (99%, from Sigma-Aldrich, ETS), Trimethoxy(octyl)silane (90% purity, from Aldrich, OTS) were used as provided. Anhydrous toluene (99.8%, from Sigma-Aldrich) and anhydrous methanol (99.8%, from Sigma-Aldrich) were purified on silica-alumina molecular sieves (Zeochem) heat-treated overnight in air at 300°C. A hydrogen peroxide aqueous solution (30 wt. %, from EMD Millipore) was utilized as an oxidized agent to convert the thiol (-SH) of MPTS to sulfonic groups ($-SO_3H$). Cyclopentanol (99%), m-cresol (99%), and decahydronaphthalene, mixture cis + trans (99%) (Sigma-Aldrich) were used as provided.

4.2.2 Conventional grafting of mesostructured silica MCM41 (CG method)

The grafting methods using solvent (e.g. toluene) at low temperature (<120ºC) (Conventional grafting – CG) have been widely reported in the literature [146, 171, 176-

186]. In this work, a typical synthesis was used, following a previously reported procedure [186]. First, the pretreated MCM41 was dispersed in toluene (25 mL of Toluene/g of MCM41) and heated up to 40 or 110°C with constant stirring in a reflux system. Once the temperature remained stable, the trialkoxy-organosilanes (MPTS) was injected into the dispersion and then stirred at a constant temperature for 12 h. After this period, the solid was separated in a vacuum filtration system (filter 0.22 μm) and washed several times with ethanol at room temperature to remove any organosilane residue. The resulting solid product (MCM41-SH) was dried at 80°C overnight. The thiol (-SH) groups was converted to active sulfonic groups (-SO_3H) via oxidation in a solution of 30% H_2O_2 (25 mL per gram of MCM41-SH) at room temperature for 12 h. After being separated from solution by filtration and washed with an excess amount of ethanol at room temperature, the catalyst was dried overnight in a vacuum oven at 80°C. The functionalization of MCM41 with ethyl-(trichloro)silane and trimethoxy(octyl)silane were carried out similarly, but without the oxidation step since the functional groups only include hydrocarbon linkers.

4.2.3 High-temperature grafting of mesostructured silica MCM41 (HG method)

A novel functionalization method is proposed here to synthesize active and stable functionalized catalysts. In this case, dry MCM41 was impregnated with a solution of trialkoxy-organosilanes (MPTS) in methanol (0.6 mL of methanol per gram of MCM41) at incipient wetness. The obtained solid was placed in an autoclave and heated to 180°C for 14 h. After thermal treatment, the resulting solid was washed several times with ethanol at room temperature and dried at 80°C overnight. The essential differences of HG

from CG method is high-temperature grafting under solvent-free condition. It should be noted that in this procedure, methanol was used with a little amount to reduce the viscosity of the pure MPTS precursor and to make sure the MPTS liquid was evenly dispersed over the solid sample (at incipient wetness point). Oxidation of the thiol groups was carried out with a solution of 30% H_2O_2 (25 mL per gram of MCM41-SH) at room temperature for 12 h. The final catalyst was washed several times with ethanol at room temperature and dried overnight at 80ºC.

4.2.4 One-step co-condensation of SBA15-SO_3H

The co-condensation procedure was conducted following a published procedure [187]. Pluronic 123 (Aldrich, P123) was dissolved in a solution of 1.9 M of HCl at room temperature. The temperature of the solution was stabilized to 40°C. Tetraethyl orthosilicate (>99.0%, Aldrich) was added to the mixture for pre-hydrolysis for 45 mins, followed by addition of the trialkoxy-organosilane (MPTS). The mixture was stirred at 40°C for 20 h and aged at 100°C for 24 h (without stirring). The solid (SBA15-SH) was recovered by filtration and washed with ethanol in reflux at room temperature to remove the template (400 mL of Methanol/1.5 g SBA15-SH). The product was recovered by filtration and dried overnight at 80ºC, followed by the oxidation in a solution of 30% H_2O_2 (25 mL per gram of solid) at room temperature to convert (-SH) groups into (-SO_3H) groups. The solid was then washed several times with ethanol at room temperature and dried overnight at 80ºC.

4.2.5 Characterization of the mesostructured silicas

The surface area, pore size, and pore volume were evaluated by N_2 physisorption at -198°C in a micromeritics ASAP 2020. Prior to adsorption, the samples were degassed for 6 h under vacuum at 250°C. A Perkin–Elmer Spectrum 100 FTIR equipped with a high-temperature DRIFT (Diffuse Reflectance Infrared Fourier Transformation) CaF2 cell (HVC, Harrick) to study the surface chemistry of the functionalized silica. The samples were pretreated in-situ at 250°C for 1 h under He flow (30 mL/min) to remove water physically adsorbed on the catalyst surface. The cell was then cooled down to 50°C and then 64 DRIFT spectra were collected at a resolution of 1 cm^{-1} [131].

Solid-state ^{1}H-^{29}Si CPMAS NMR was used to evaluate the silica structure and the functionalization modes present on the surface. The ^{1}H-^{29}Si CPMAS NMR spectra were obtained on a Bruker AVIII HD NMR spectrometer operating at a magnetic field strength of 11.74T, equipped with a 4 mm Bruker MAS probe. The spinning rate of 12kHz and a recycle delay of 25s were used. Spectra were averaged over 4096 scans and referenced to the TMS signal at -10.2 ppm.

The structural characterization was conducted on an XRD unit, D8 Series II X-ray diffractometer BRUKER AXS, in reflection geometry using CuKα radiation generated at 40 kV and 35 mA in the 2θ = 2-60° diffraction angle range. The topology of the catalysts was examined by transmission electron microscopy (TEM) in a JEOL JEM-2100 Scanning Transmission Electron Microscope, operating at 200 kV with the images recorded on a CCD camera. The samples were prepared by suspending 2-5 mg of sample in 10 mL of 2-propanol, followed by deposition over a Cu grid coated with carbon and dried at 80°C.

The organic content of the catalysts was evaluated via thermogravimetric analysis coupled with temperature program oxidation (TGA-TPO) using a Netzsch STA-449 F1 Jupiter. In a typical experiment, the functionalized material (30 mg) was placed on a crucible with a constant flow of Ar (40 mL/min) and air (10 mL/min). The cell was preheated to 40°C then increased to 700°C with a ramping rate of 3°C/min. The outlet gases (CO_2, SO_2) were analyzed on an on-line mass chromatography Aeolos QMS 403C.

4.2.6 Catalytic reaction measurements

The liquid phase alkylation was carried out at 250°C and 850 psi of N_2 in a 160 mL Mini Bench Top Parr high-pressure reactor (Model Parr 4564) equipped with a Parr 4848 Reactor Controller. Reactant concentrations of 1.0 M m-cresol and 0.5 M cyclopentanol (CPOL) were used in decalin solvent or as a pure m-cresol/CPOL mixture of 2:1 molar ratio. The collected liquid was analyzed with a GC-FID and GC-MS equipped with a Phenomenex capillary column (ZB-1701, 15 m x 0.25 mm x 0.25 μm).

A specific test was designed to investigate the leaching of active moieties from different samples under reaction conditions. The experiments included two steps. First, the alkylation reaction was carried out at 250°C, 2 h, 850 psi under either decalin solvent (non-polar medium) or pure m-cresol/CPOL mixture (polar medium) (Step 1). After reaction, the catalyst was separated from the reaction mixture. A small fraction of the obtained liquid was collected for GC analysis while the remaining liquid product was placed back in a clean reactor and re-run at 250°C for 14 h, 850 N2 psi, without the presence of a solid catalyst (Step 2). Therefore, any enhancement in the yield of alkylated

products in the second step should be due to the presence of solubilized functional groups that further catalyze the alkylation reaction (homogeneous catalysis). The extent of leaching was evaluated with the calculated ratio of the homogeneous (r_{homo}) to heterogeneous rates (r_{hetero}). First, the heterogeneous rate of formation of a coupling product (i) was defined as the product concentration obtained during the first run divided by the reaction time (2 h). Likewise, the homogeneous rate was defined as the increase in concentration from the first to the second run, divided by the reaction time of this run (14 h), as shown below. The higher the value of the r_{homo}/r_{hetero} ratio is, the higher is the extent of leaching is.

$$\frac{r_{homo}}{r_{hetero}} = \frac{(C_{i-run2} - C_{i-run1})/14}{C_{i-run1}/2}$$

In all runs, the conversion of CPOL (X), yield of a product (Y_i), and carbon balance ($C_{balance}$) were calculated as follows:

$$X = \frac{C_{CPOL-in} - C_{CPOL-out}}{C_{CPOL-in}} \qquad Y_{CPOL \to Pi} = \frac{C_i \times n}{C_{CPOL-in}} \qquad C_{balance} = \frac{C_{CPOL-out} + C_{CPOL \to P}}{C_{CPOL-in}}$$

$C_{CPOL\text{-}in}$ and $C_{CPOL\text{-}out}$: Initial and remaining concentration of CPOL (mM)

C_i and n_i : Concentration of the product i (mM) and the corresponding stoichiometric number

C_{in} and C_{out}: Initial and remaining amount of carbon existing in the system (mM)

$C_{i\text{-}run1}$ and $C_{i\text{-}run2}$: Concentration of the coupling product (i) in the first and second run (mM)

r_{homo} and r_{hetero}: the homogeneous and heterogeneous rate of formation of a coupling product (i), respectively; 2 h and 14 h were the reaction time of the first and second run,

respectively. Assuming that the homogeneous activity in the first run was negligible compared to the heterogeneous one.

4.2.7 Computational simulations

Ab initio molecular dynamics (AIMD) simulations were performed using Vienna ab initio simulation package (VASP)[188]. The ion–electron interaction was described through the projector-augmented wave (PAW) approach[189, 190]. For the structural optimization, the exchange and correlation energy was represented using the Perdew-Burke-Ernzerhof (PBE) functional of the generalized gradient approximation (GGA)[191]. The van der Waals interaction has been taken into account through the Grimme's DFT-D3 semi-empirical method[192]. The Brillouin zone was sampled using a single k-point at Γ. A 300 eV cutoff for the plane-wave basis set was adopted in the AIMD simulations. The simulations were performed at 320 K in canonical ensembles. The time step was set to 1 fs. The velocities were scaled each step to the temperature. The MCM41 unit cell was taken from a previous report[193]; the wall thickness of this structure is a bit less than 1 nm and the pore diameter is about 3 nm. Both T1 and T2 adsorption modes for OTS have been tested, and the results were similar in terms of the configuration of the OTS grafted to the MCM41 framework.

4.3 Results and Discussions

4.3.1 Structure, morphology and porosity analysis of the functionalized MCM41

A. X-ray Diffraction and Surface Area Measurements

The XRD profile for the bare MCM41 sample displays the typical diffraction peaks at 2.16°, 3.76° and 4.34° corresponding to (100), (110) and (200) planes, respectively, which are characteristic of the hexagonal arrangement of the mesostructured silica [194] (**Figure 4.1**). The decreased intensities observed on the functionalized catalysts indicate different extents of crystallinity loss during the functionalization step [195-198]. The almost negligible difference in crystallinity of the MCM41-SO_3H-CG sample prepared by conventional grafting compared to the parent MCM41 correlates with the low extent of grafting resulting from this functionalization method. In contrast, a more significant decline in crystallinity is observed for the MCM41-ETS-CG, MCM41-OTS-HG and MCM41-SO_3H-HG samples. That is, the extent of functionalization parallels the reduced crystallinity and porosity. Interestingly, it should be noticed that the (100) peak of MCM41-SO_3H-HG sample gets broadened and shifted to higher angle.

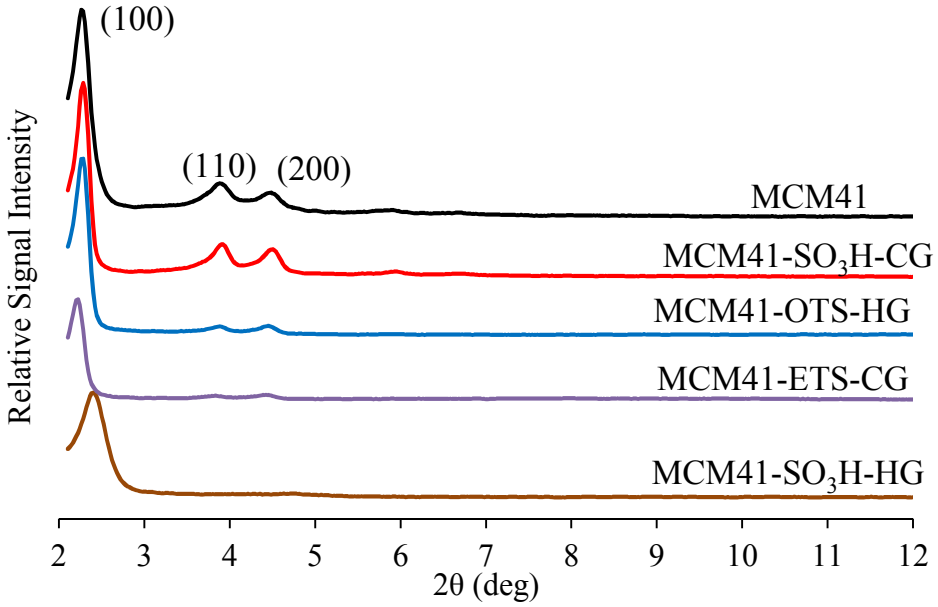

Figure 4. 1 XRD spectra for the functionalized and parent MCM41.

Nevertheless, despite the reduction in XRD intensity, the N_2 adsorption-desorption isotherms for the functionalized MCM41 and SBA15 materials (See Figure **S2-Supplementary Information**) are of type IV, which is characteristic of the mesoporous materials. Similarly, the hexagonal structure typical of MCM41 can still be observed in the TEM images for all the functionalized samples, including MCM41-SO_3H-CG and MCM41-SO_3H-HG (**Figure S1. Supplementary Information**). As summarized in **Table 4.1**, it is clearly observed that the surface area, pore diameter, and pore volume consistently decrease after functionalization, according to the following order: MCM41 > MCM41-ETS-CG ~ MCM41-OTS-HG > MCM41-SO_3H-HG. However, even the samples exhibiting significant decreases in surface area and pore volume still retain a high surface area (about 400 m^2/g or more), which is high enough for catalysis applications. The decrease in the porosity with increasing degree of functionalization can be attributed to the deposition of the alkyl and alkyl-sulfonic functional groups on the inner surface of the mesoporous silica as well on the mouth of the pores, near the external surface.

Table 4. 1 Porosity properties of parent and functionalized mesostructured silica. The surface area and pore diameter were calculated using BET method. The pore volume was obtained by BJH method

Sample	Surface Area (m^2/g)	Average Diameter (Å)	Pore Volume (cm^3/g)
MCM41	728	32	0.61
MCM41-SO_3H-CG	706	27	0.47
MCM41-ETS-CG	620	16	0.26
MCM41-OTS-HG	635	17	0.30
MCM41-SO_3H -HG	394	20	0.20
SBA15-SO_3H -CC	447	72	0.88

B. Diffuse Reflectance Infrared Spectroscopy Fourier Transform (DRIFTS)

As widely documented in the literature, the bands observed in the 4000-3100 cm^{-1} range of the DRIFT spectrum can be assigned to the stretching vibration of surface –OH, while those in the 3100-2700 cm^{-1} range can be ascribed to CH_2/CH_3 groups [131, 199]. Upon functionalization, the disappearance of the free surface silanol band (**Figure 4.2**) is expected since the silylation consumes surface -OH groups to form Si*- O bonds and grafts the functional group (as in M-Si-O-Si*-R, where M-Si-O and –R correspond to the silica wall and functional groups, respectively). Therefore, the density of the remaining surface silanol groups after functionalization can be used as an indicator of the effectiveness of the functionalization procedure. Along with the disappearance of silanol, a rise in the C-H bond band intensity is expected in the 3100-2700 cm^{-1} range. However, examination of the spectra shows that all the samples functionalized with trialkoxy-organosilanes by the conventional grafting (CG) method exhibit a high content of residual free surface silanols and a low intensity of alkyl chain bands (**Figure 4.2a**). In fact, the differences with the un-functionalized MCM41 are minor. That is, the DRIFTS analysis

indicates a low extent of Si*-O bond formation. It is clear that when using trialkoxy-organosilanes as silylating agent, the temperature used (40^{o}C) was not high enough to activate the silylation reaction with the surface silanols. Moreover, increasing the synthesis temperature up to 110°C did not enhance the extent of sylilation (MCM41-SO_3H-CG (110C) sample much. By contrast, when the trialkoxy compound was replaced by a trichloro organosilane a clear disappearance of the free surface silanols was observed, along with a clear increase in the signal of the C-H vibration, even at the lower temperature treatment (see sample MCM41-ETS-CG (40C) in **Figure 4.2a**). Evidently, this difference is due to the higher reactivity of the trichloro-organosilanes compared to that of the trialkoxy-organosilanes. It is possible that even higher temperatures might be necessary to activate the trialkoxy compounds. However, the use of solvents in conventional synthesis procedures limits the temperature that can be used for grafting to the boiling point of the solvent. Therefore, it is desirable to eliminate the use of a solvent altogether. By doing so, one could operate at higher temperatures and minimize the presence of water during the synthesis procedure, which is the basis of the high-temperature grafting (HG) method proposed here.

In addition, since in the HG method the organosilane precursor is impregnated on the silica support until the point of incipient wetness, the $(CH_3O)_3Si$-R moieties completely fill the pores of the solid without any excess on the external surface of the solid. So, when the temperature is high enough they should react with the internal silanols in an effective way. Consequently, this solvent-free procedure allows for a high degree of

functionalization and a uniform distribution of active sites across the support surface, minimizing cross condensation of organosilanes or decomposition.

As demonstrated in the spectra of **Figure 4.2b**, all the samples synthesized by the HG method present a complete conversion of the free silanols along with a large increase in the band assigned to the alkyl groups. The band appearing in the region around 2550 cm^{-1} is ascribed to the vibration of –SH groups (see sample MCM41-SH-HG). This band disappears upon oxidation by H_2O_2 to form the acidic $–SO_3H$ group (see sample MCM41-SO_3H-HG). The absence of -SH vibration signal on all of the acid-functionalized catalysts indicates that the oxidation process is complete.

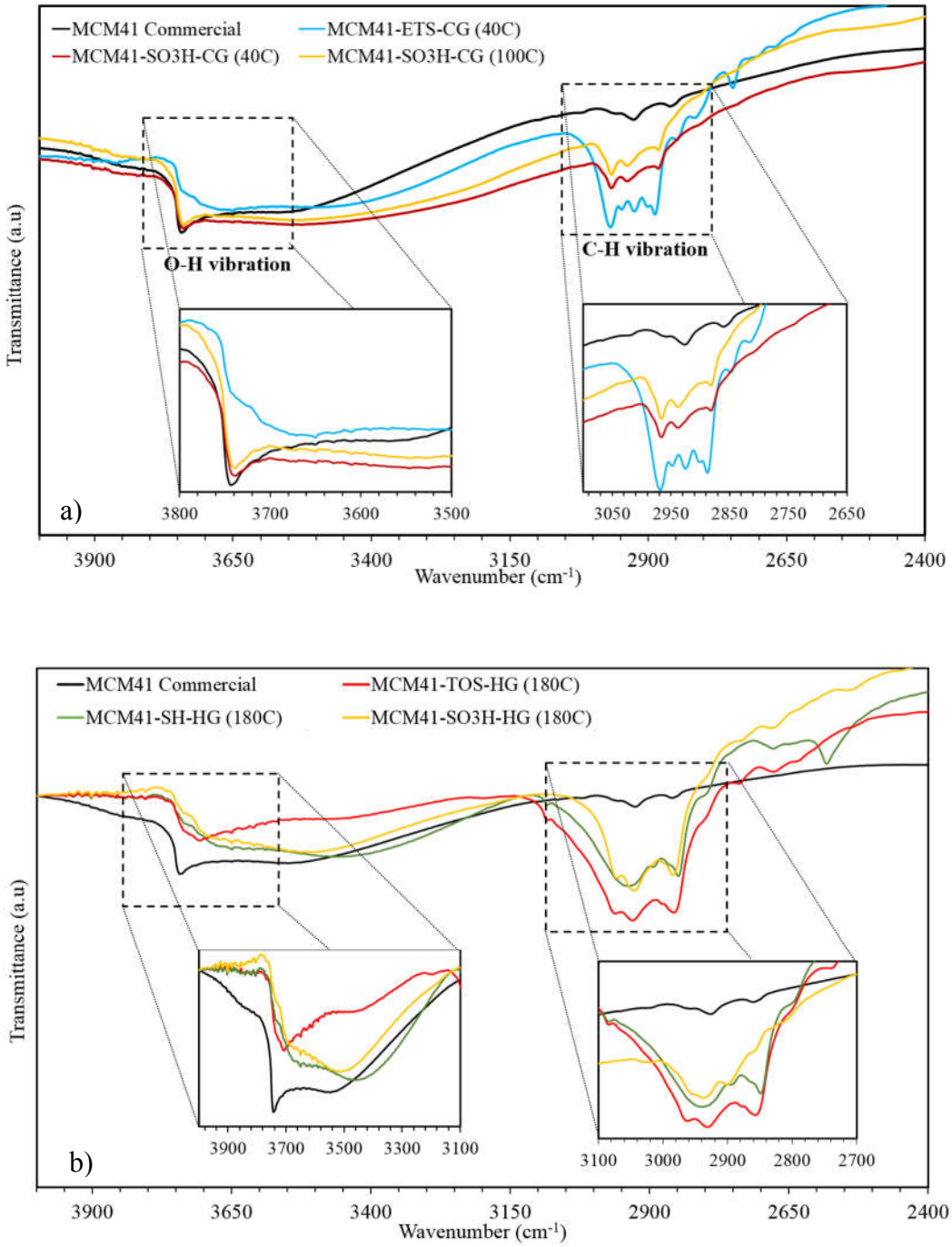

Figure 4.2 FTIR spectra at 50°C for the functionalized MCM41 synthesized by conventional grafting (CG) and high-temperature grafting (HG) with corresponding synthesis temperatures a) MCM41 functionalized by CG b) MCM41 functionalized by HG

C. Thermal Gravimetric Analysis (TGA)

We have used TGA to quantify the total load of organics in each sample. A typical TGA-TPO for a functionalized silica shows four characteristic regions (**Figure 4.3**). The first region (40-120°C) corresponds to elimination of adsorbed water. A second region (120-300°C) shows a mass plateau without any detectable MS peak. Moreover, the IR characterization (**S3-Supplementary Information**) demonstrates no decrease in the bands corresponding to the functional groups below 300°C. The 300-500°C region displays a significant mass loss attributed to the thermal degradation of functional groups. In this region, the Si-C, C-C and C-S bonds are thermally decomposed into CO_2, SO_2 and H_2O. The mass loss and corresponding MS signal of evolved gases were used to quantify the degree of functionalization on the mesostructured silica (see **Table 4.2**). The mass loss zone starting at 550°C can be ascribed to a small extent of thermal dehydroxylation of remaining single and germinal silanols [200].

As shown in **Table 4.2**, it can be obviously seen that the functionalization with trialkoxy organosilane (ex: MPTS) precursor when using the conventional CG method resulted in a low silylation yield (0.31 mmol/g). In contrast, the ETS precursor was much more effective when using the same method due to its higher reactivity. The resulting functionalization loading in this case was significantly higher (2.71 mmol/g). As mentioned above, 40°C is too low a temperature to activate the relatively unreactive trialkoxy organosilanes precursors. In fact, by increasing the functionalization temperature and conducting the silylation in a well-controlled environment (via the HG method), a substantial improvement in the level of the functionalization with trialkoxy

organosilanes was exhibited (2.1 mmol/g). Even though high degree of functionalization on MCM41-SO_3H-HG resulted in the decreased crystallinity, the catalyst could still maintain high fraction of ordered hexagonal arrangement (**Figure S4c-d. Supplementary Information**). No much difference in grafting efficiency can be noted between two synthesis methods when ETS (CG) and MPTS or OTS (HG) were used (~35-40%), demonstrating that at high temperature the reactivity of trialkoxy silane is as high as tricholo silane. The density of functional groups on MCM41-SO_3H-HG was calculated to be about 2.34 groups/nm^2, which is smaller than the density of available silanols of the parent MCM41. It indicates that all of functional groups are deposited inside the hexagonal pores rather than the external surface.

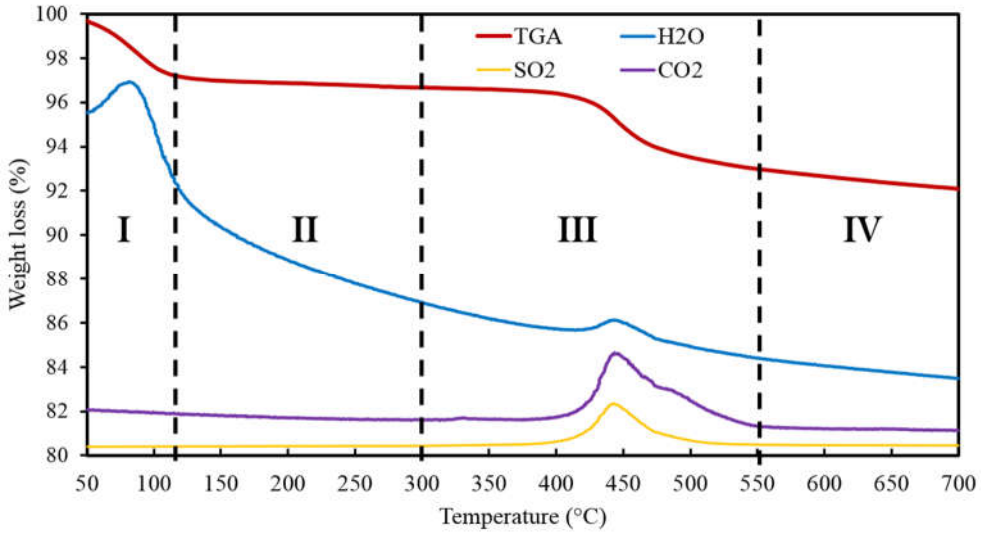

Figure 4. 3 Thermal Gravimetric Analysis (TGA) of MCM41-SO_3H-CG. The TGA results of the other samples investigated are shown in **Figure. S1-Supplementary Information**

Table 4. 2 Composition of the mesostructured silica after functionalizing by different methods

Materials	Synthesis methods	Precursor (mmol/g cat)[a]	Functionalization temperature, ^{o}C	Functionalization (mmol/g cat)[b]	Density, groups per nm^2
MCM41	Commercial	-	-	3.11-3.74 (Si-OH)[c]	3[c]-5.8[d]
MCM41-SO_3H	CG	MPTS (5.11)	40	0.31	0.26
MCM41-ETS	CG	ETS (7.11)	40	2.71	2.44
MCM41-OTS	HG	OTS (5.11)	180	1.8	1.87
MCM41-SO_3H	HG	MPTS (5.11)	180	2.1	2.34
SBA15-SO_3H	CC	MPTS (5.11)	100	0.97	0.91

CG: Conventional Grafting, CC: Co-condensation, HG: High-temperature grafting.
[a] Amounts of functional moieties used in the synthesis procedure
[b] Calculated from the TGA-TPO results (See **Figure S1- Supplementary Information**).
[c] Theoretical estimation of the -OH groups on the surface reported by Ref [196-198, 200]
[d] Based on our AIMD simulations

D. Solid State NMR Cross Polarization Magic-Angle Spinning (CPMAS)

NMR $^{1}H1$-^{29}Si CPMAS analysis can be used to determine the different structures of functionalized moieties on the silica surface [146, 162, 200]. As summarized in **Scheme 4. 1**, two families of signals are typically obtained on functionalized silicas. The first family of signals (Q_n) arises from Si species in the silica surface, giving different shifts depending on the coordination to bridging O or terminal silanols, that is Q_n=Si-$(OSi)_n$-$(OH)_{4-n}$, with n=2–4. The possible structures include siloxane tetra-coordinate Si-$(OSi)_4$ (Q_4 at -111 pm), single silanol Si-$(OSi)_3$-(OH) (Q_3 at -101 ppm), and geminal silanol Si-$(OSi)_2$-$(OH)_2$ (Q_2 at -92 ppm). The second family of signals (T_m) corresponds to Si species in the organosilane structures (T_m=RSi$(OSi)_m$-$(OH)_{3-m}$, m=1–3) with varying degrees of bonding to the surface. That is, triple bonded (T_3 at -65 ppm). double bonded (T_2 at -57 ppm), and single bonded (T_1 at -50 ppm).

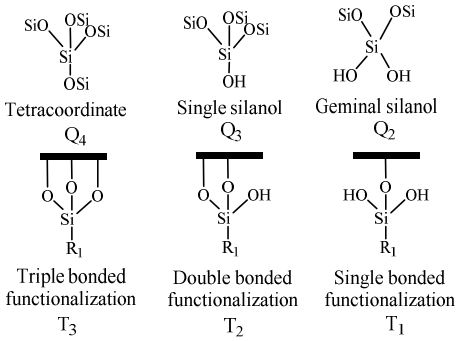

Scheme 4. 1 Different grafting modes on MCM41-MPTS/ETS/OTS [194, 200]

As shown in **Figure 4.4**, the two samples described above as those with the highest extent of functionalization (MCM41-ETS-CG and MCM41-SO_3H-HG) indeed display a high intensity for the bands representing multi-bonded functional moieties (T_2 and T_3). This increase goes in parallel with a decrease in the intensity of the Q_2 and Q_3 bands corresponding to species associated with geminal and single silanols, respectively. Clearly, the high-temperature grafting methods favor the generation of trialkoxide-bonded species while MCM41-ETS-CG shows higher density of bipodal T_2 species. It seems that a high grafting temperature facilitates the formation of tri-bonded functional sites on the surface, even for the less active trialkoxy precursor (MPTS). In contrast, weak T_n signals as well as a high density of unreacted silanols (Q_3) are observed in the case of MCM41-SO_3H-CG, in agreement with the above discussion relative to the XRD, IR and BET results.

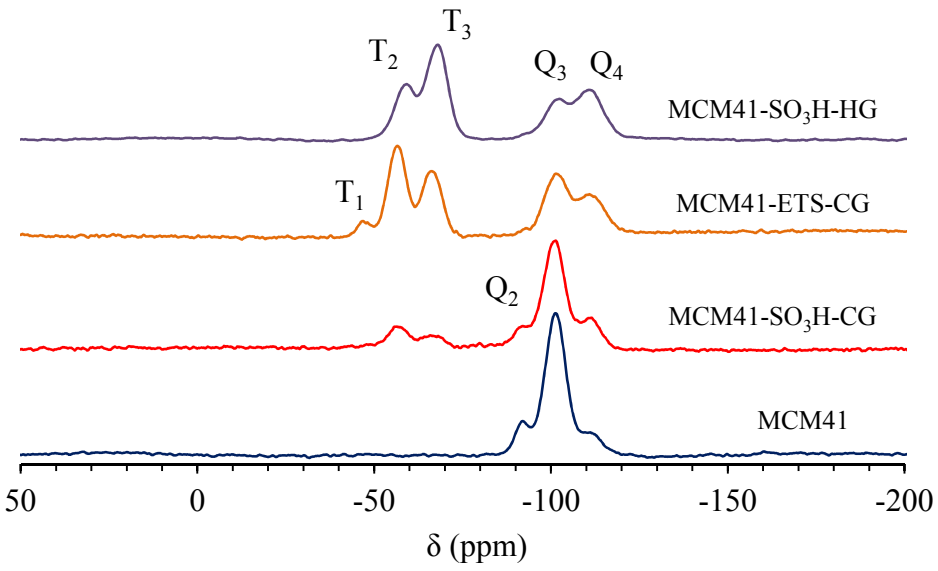

Figure 4. 4 NMR ^{1}H-^{29}Si CPMAS spectra of parent and functionalized MCM41

E. Hydrothermal stability of functionalized materials in the presence of water

The hydrothermal stability of functionalized MCM41 was evaluated as described in Ref [201]. In this test, 500 mg of catalysts was placed into a Teflon container inside a 50 mL autoclave. Water was added into the system at the bottom of the autoclave without direct contact with the catalysts. The system was heated to 200°C or 250°C to generate steam under autogenic pressure. The amount of water added was varied to control the state of water inside the system, which is determined by the n/n_o ratio, with n = amount of water in the system and n_o = amount of water needed to reach the saturation point. That is, n includes the amount of water added plus the amount of water already present in the catalyst (~0.015 g, as determined by TGA). In our conditions (T = 200°C, V = 50 ml, gas compressibility factor = 0.96, vapor pressure of water = 15.31 atm). The amount of water necessary to reach the saturation of the water vapor is n_o = 0.34 g. That is, when n/no < 1

water is only in the vapor phase; when n/no=1 water starts condensing; when n/no >1 the system contains both vapor and liquid water. After the hydrothermal treatment, the catalysts were dried at 100ºC and analyzed by several techniques to evaluate the impact of the water attack on the structure.

As shown in **Figure 4.5**, the XRD analysis indicates that the crystalline structure of the bare MCM41 completely collapsed when the mesoporous material was exposed to vapor water at 200ºC ($n/n_o = 0.2$). In parallel, as shown in **Table 4.3**, the surface area (S_{BET}) and pore volume (V_{pore}) were severely affected, dropping from 728 to 32 m^2/g and 0.61 to 0.15 cm^3/g, respectively. It is clear that the bare MCM41 was extremely susceptible to water attack (hydrolysis) at high temperature (200ºC). Moreover, even calcining the MCM41 at 600ºC for 6 h prior to water treatment did not increase the resistance to water, as demonstrated in **Figure 4.5** and **Table 4.3**. Similarly, the functionalized material prepared by conventional grafting MCM41-SO_3H -CG catalyst was susceptible to water vapor attack, but to a lesser degree than the bare material. That is, XRD indicates that the long-range crystallinity was maintained at low n/n_o values. However, in the presence of liquid water (i.e., $n/n_o \geq 1$), the structure was severely damaged. The specific surface area decreased moderately (from 706 to 609 m^2/g). The presence of the propyl-sulfonic groups in the functionalized material obviously enhanced the hydrothermal stability of the catalyst compared to the non-functionalized ones. However, the most remarkable enhancement in water tolerance was observed on the sample prepared by the high-temperature grafting method. As shown in **Figure 4.5** and **Table 4.3**, the MCM41-SO_3H-HG sample displayed excellent resistance to water attack

both in the vapor and liquid states. Additionally, it was observed that a highly-saturated-surface sample (MCM41-ETS-HG 6x) synthesized by the HG method with an excess amount of ETS (30.6 mmol of ETS precursor used per gram of MCM41) also exhibited similar high hydrothermal stability. Contrary to the large effect of the n/n_o ratio exhibited by the less functionalized samples, the ones prepared by high-temperature grafting kept the same crystallinity, surface area, and pore volume as well as exceptional stability against water attack from n/n_o= 0 to 4 (**Figure 4.5** and **Table 4.3**).

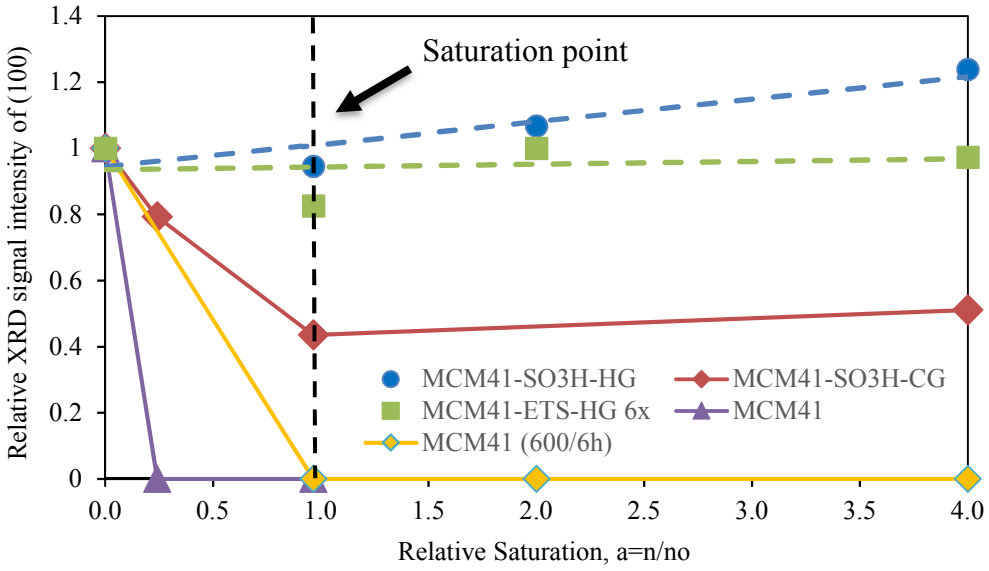

Figure 4. 5. Effect of the hydrothermal attack by vapor or liquid water on the structural stability of bare and functionalized MCM41. The corresponding XRD spectra are included in **Figure S5-Supplementary Information**

In agreement with the XRD analysis, the ^{1}H-^{29}Si CPMAS data (**Figure S6-Supplementary Information**) indicate that there are no substantial changes in the surface structure of the MCM41-SO_3H-HG sample after water attack with n/n_o ratios varying from 0.2 to 2. A minor modification of the organosilane structure can be inferred from a slight changeover in signal intensity from T_2 into T_3 as n/n_o increases. That is,

while the total functional group density (based on the total area of T_m signal) remained the same, the intensity ratio of T_3/T_2 increased. Then, this changeover might be a reflection of further reaction, at the increasingly severe hydrothermal conditions, between the di-bonded functional groups and the available surface silanols, becoming tri-bonded groups.

Table 4. 3 Porosity of MCM41 before and after hydrothermal treatment

Sample	n/n_o (at 200°C)	Surface Area (m^2/g)	Average Diameter (Å)	Pore Volume (cm^3/g)
MCM41	Before treatment	728	32	0.61
	0.2	32	185	0.15
MCM41 (600°C/6h)	Before treatment	780	28	0.54
	1	18	122	0.06
	2	12	110	0.03
MCM41-SO_3H-CG	Before treatment	706	27	0.47
	0.2	653	28	0.46
	1	609	27	0.41
	4	618	29	0.45
MCM41-SO_3H-HG	Before treatment	400	20	0.2
	0.2	432	20	0.21
	1	477	19	0.23
	4	495	19	0.24
MCM41-ETS-HG (6x)	Before treatment	185	19	0.1
	1	199	19	0.1
	4	190	20	0.1

F. AIMD simulations of functionalized materials

We performed ab initio molecular dynamics (AIMD) simulations to model MCM41 functionalized with hydrophobic groups. The MCM41 unit cell was taken from a previous report [193]; the wall thickness of this structure is about 1 nm and the pore diameter is about 3 nm. When running AIMD simulations at 320 K, we noticed that the hexagonal structure deformed slightly. We introduced 4 OTS molecules into the porous structure,

each connected with the MCM framework in the aforementioned T_1 configuration. We tested and compared the T_2 adsorption mode as well for a lower density (1 OTS per MCM unit cell) and didn't observe significant difference in terms of the dynamics and configuration of the OTS. When 4 OTS ligands are introduced, the OTS density is about 0.4 OTS/nm^2. The simulations run for more than 10 ps, and the snapshots are shown in **Figure 4.6**.

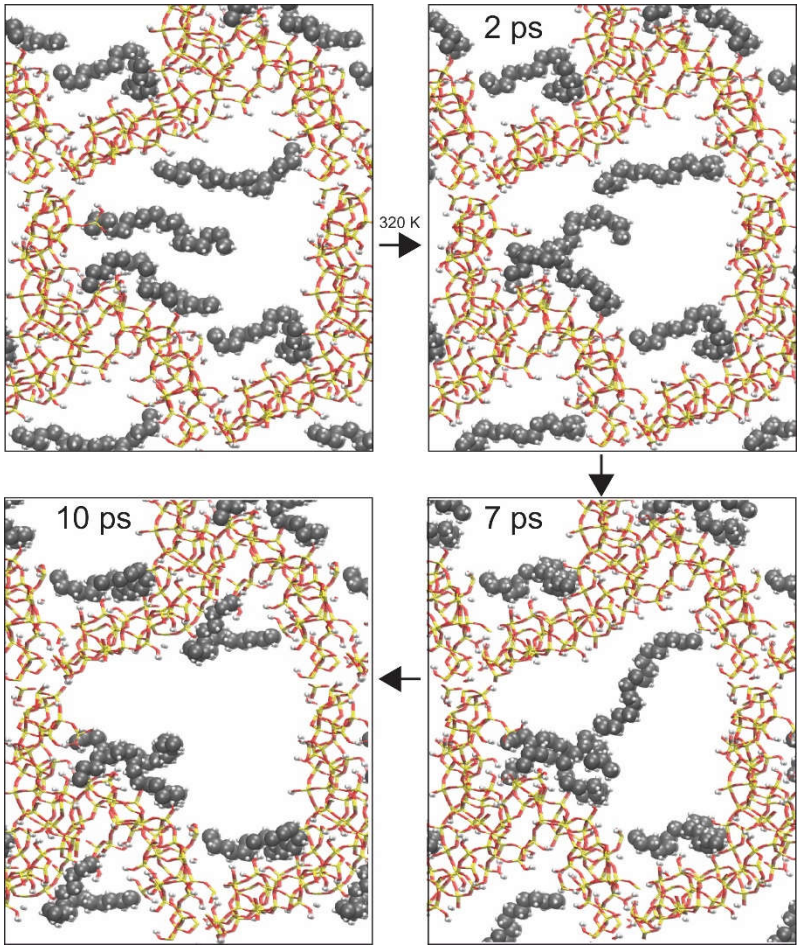

Figure 4. 6 Snapshots from AIMD simulations over 10 ps of OTS-functionalized MCM41. The Si, O, C and H atoms are colored yellow, red, grey, and white, respectively.

In the initial configuration, the OTS moieties protrude toward the center of the pore. During the simulation, OTS moieties may contact with each other temporarily driven by the intermolecular interaction (see at 2 ps and 7 ps simulation time), however, the interaction with the wall of the MCM41 tends to drive the OTS to be attached to the framework, at least at this OTS density; One would expect more inter-molecular contact at higher OTS densities. Note in this model of MCM41, the wall is rather hydrophilic [193]; The surface OH density is 5.8 per nm^2. The driving force for the OTS to lean toward the MCM41 framework seems to be the van der Waals interactions. The AIMD simulations thus indicate that, as a result of the OTS functionalization, the pore volume and diameter decrease quite significantly, in line with the experimental finding.

4.3.2 Catalytic activity of the acid-functionalized mesostructured silicas

The reaction of cyclopentanol (CPOL) with m-cresol was used as a probe to test the different catalytic materials. As illustrated in **Scheme 4.2**, a few reaction pathways can occur from these two reactants. First, CPOL can undergo self-etherification to produce dicyclopentyl ether (DPE) as well as cross-etherification with m-cresol (O-alkylation) to form cyclopentyloxy methylbenzene. However, we did not observe the latter in any of the runs. The main products were those from acid-catalyzed alkylation. It is well known that in the presence of an acid catalyst, CPOL can be readily dehydrated to generate cyclopentene (CPEN). Then, either CPOL or CPEN can attack the aromatic ring via alkylation, forming a C_{12} product dimer, which can subsequently react further to produce the trimer C_{17}. Both the alcohol (CPOL) and the olefin (CPEN) are alkylating agents, as

demonstrated in our previous work with the isopropanol/m-cresol system [9]. No trace of tri-alkylated product (tetramer) was detected, even at high overall conversions (~90%).

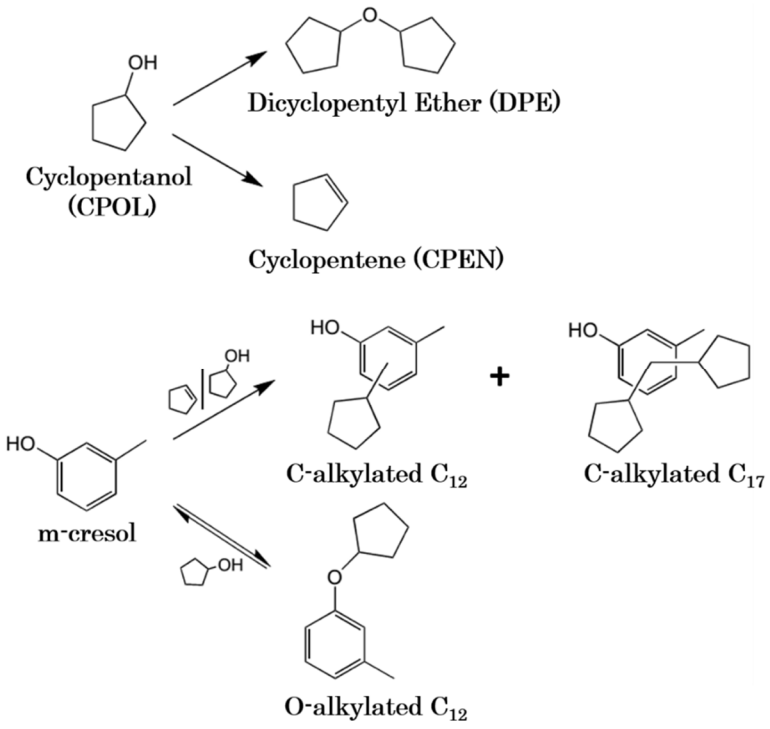

Scheme 4. 2 Reaction pathways from CPOL and m-cresol.

The product distributions from the several samples obtained with the different preparation methods, MCM41-SO_3H-CG, MCM41-SO_3H-HG, and SBA15-SO_3H-CC are compared in **Table 4. 4.** It can be seen that all samples exhibited high activity for the alkylation reaction with excellent carbon balance (>90%) in most cases. In decalin solvent, CPEN was the most abundant intermediate product due to a rapid dehydration of CPOL at the reaction temperature of 250^{o}C.

Table 4. 4 Activity of different functionalized catalysts for alkylation reaction between cyclopentanol and m-cresol. Reaction condition: Feed ratio: 1.0 M m-cresol - 0.5 M cyclopentanol (CPOL) in the case of decalin solvent and 6.6 M m-cresol – 3.3 M cyclopentanol (CPOL) in the case of using pure chemical (solvent free); Temperature: 250^{o}C; Pressure: 850 psi N_2; Reaction time: 2h

Catalysts	Solvent	Disappearance of CPOL, %	Yield, %				Carbon balance, %
			CPEN	C_{12}	C_{17}	DPE	
MCM41-SO_3H-CG	Decalin	80.6	43.2	18.1	3.5	1.8	86
SBA15-SO_3H-CC	Decalin	100	81.2	16.4	4.4	0.4	102.3
MCM41-SO_3H-CG	Pure CPOL/ m-cresol	44.4	24	15.3	1.6	3	99.5
SBA15-SO_3H-CC	Pure CPOL/ m-cresol	97.1	32	50.2	20.1	0.2	105.4
MCM41-SO_3H-HG	Pure CPOL/ m-cresol	96	40	39.9	9.6	0.6	94

Among the possible reaction paths from **Scheme 4.2**, the C-alkylation is shown to be more favorable compared to O-alkylation for most cases. It can be seen that at lower concentrations of CPEN (on MCM41-SO_3H-CG), more DPE was produced (1.8%) compared to only 0.4% yield of DPE in the case of higher concentration of CPEN (on SBA15-SO_3H-CC). This result indicates that CPEN only reacts via C-alkylation while CPOL promotes both C- and O-alkylation, as reported in our previous study with isopropanol/m-cresol [9].

In pure CPOL/m-cresol medium, MCM41-SO_3H-CG catalyst showed lower activity for CPOL dehydration. In this case, a lower concentration of CPEN led to higher yields of DPE, as expected. Very high conversion (>90%) and yield of C_{12}+C_{17} (~70%) were observed on SBA15-SO_3H-CC. The catalyst synthesized by high-temperature method (MCM41-SO_3H-HG) also demonstrated comparable activity toward C-alkylation, producing roughly 50% yield of C-C adducts. A general trend can be seen, that is, the

formation of bulky C_{17} adduct is promoted in pure medium with high concentrations of both CPOL, CPEN and m-cresol substrate. While in the first reaction cycles, all samples behaved rather similarly; significant differences were observed in subsequent cycles, as described below.

As mentioned in the Experimental section, a leaching test was implemented to quantify the possible leaching of the active species during reaction. That is, after the initial alkylation reaction, the catalyst was separated from the reaction mixture. After analysis, the liquid mixture was sent back to the clean reactor and re-run under the same conditions, but without the presence of a solid catalyst. Therefore, any conversion in this step must be ascribed to acid species leached from the catalyst. **Figure 4.7** compares the r_{homo}/r_{hetero} ratio, which demonstrates the relative rate of the homogeneous and heterogeneous activity on different catalysts. CPEN is an intermediate (alkylating agent) which reacts quickly with m-cresol to form C-C coupling products. Therefore, CPEN yield was not shown here to avoid confusion.

Under a polar medium (e.g. m-cresol/CPOL mixture), the samples MCM41-SO_3H-CG and SBA15-SO_3H-CC experienced severe leaching of functional moieties, as observed by the high r_{homo}/r_{hetero} value. That is, the observed activity during the second step must be ascribed to homogeneous reaction catalyzed by the solubilized sulfonic groups in the reaction mixture. It must be noted that no thermal reactions were detected under the evaluated conditions with any of the reactants, intermediates, and products in the absence of solid catalysts or leached moieties. The extent of leaching, as determined from this test seems to strongly depend on the sample and type of solvent used. For

instance, leaching of active moieties was clearly observed when the SBA15-SO_3H-CC sample was used, in both polar and non-polar solvents. However, it did not occur with the MCM41-SO_3H-CG sample when a non-polar solvent (decalin) was used, but it did leach under the polar solvent. Most interestingly, the catalysts synthesized by the high-temperature method did not show any leaching, even in the presence of a polar medium (**Figure 4.7**). In this case, the minor CPEN consumption (not shown in the graph) is attributed to physical loss (evaporation) during the leaching test procedure since CPEN is highly volatile.

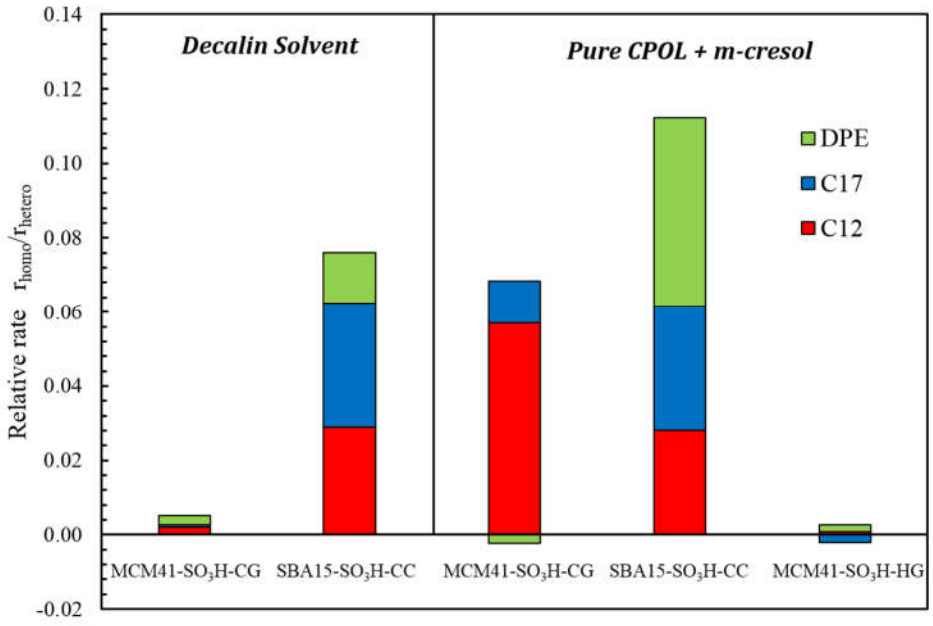

Figure 4. 7 The net change of product concentrations after leaching test. The reaction was first carried out at 250°C, 850 psi of N_2 for 2h. The obtained filtrate was then re-run at 250°C, 850 psi of N_2 for another 14 h without the addition of solid catalysts

4.3.3 Analysis of the leaching process

It is clear that the propensity for leaching of a given functionalized organosilane from a mesoporous silica is a strong function of the method used for grafting these functional groups. In this section, we analyze the possible causes of leaching and what precautions can be taken to minimize it.

A. Internal bond cleavage

Previous studies have proposed a leaching mechanism involving the cleavage of the Si-O [146, 165] or the Si-C bond [167, 168] via water-assisted hydrolysis (**Scheme 4.3a**). For instance, for the grafted SBA15 catalyst, it has been suggested that the losses of functional groups are mostly due to leaching of monopodal species (T_1) via Si-O bond cleavage. In this case, disappearance of the T_1 signal is observed after hydrothermal treatment (sample suspended in liquid water at 120°C for 7 days) while T_2 and T_3 species are less affected [146].

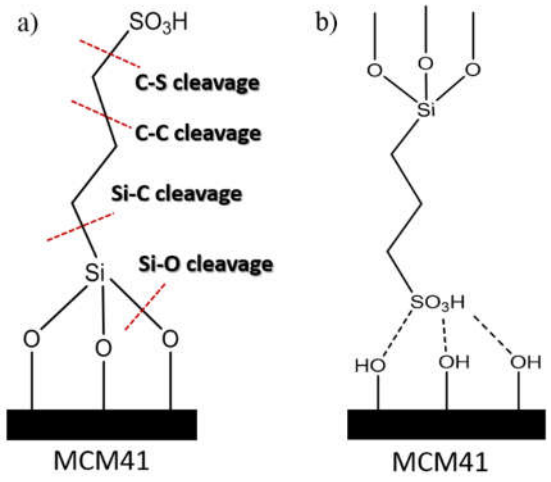

Scheme 4. 3 Possible causes of leaching a) Internal bond cleavage b) Weak interaction of functional groups

To clarify this mechanism in our system, we characterized the structure of the surface functional groups and carried out a quantitative analysis of the relative intensity of the ^{1}H-^{29}Si CPMAS bands (**Figure 4.8**). As discussed in the previous text, there are two types of bands in ^{1}H-^{29}Si CPMAS including the Si in the silica structure (Q_2, Q_3 and Q_4) and the Si in organosilane structures (T_1, T_2, T_3). Equations 1 and 2 can be used to calculate the fraction of each type of Si bonding mode, organosilane and silica, respectively. The values of T_m and Q_n signals were obtained from integrating the corresponding peaks in ^{1}H-^{29}Si CPMAS spectra, which were deconvoluted using Gaussians. The results are shown in **Figure 4.8**.

$$Composition\ of\ organosilane\ structure\ =\ \frac{T_m}{\sum_{m=1}^{3} T_m} \quad (1)$$

$$Composition\ of\ silica\ structure = \frac{Q_n}{\sum_{n=2}^{4} Q_n} \quad (2)$$

Our data demonstrates that the organosilane composition of the spent catalyst (MCM41-SO_3H-CG-S) displayed a decrease in T_2 (from 62% to 29%) and also the total organosilanes signal, indicating that T_2 species in MCM41-SO_3H-CG leached under our conditions (**Figure 4.8a**). However, even though high proportion of the T_2 bonded mode was observed in MCM41-SO_3H-HG catalyst (~37%), no leaching was detected in this case. In general, there is no clear relationship between extent of leaching and nature of bonding mode of the functional groups since the T_2 species leached in the case of MCM41-SO_3H-CG but did not in the case of MCM41-SO_3H-HG. Moreover, the fraction of surface silanols (Q_2 and Q_3) of spent catalysts did not change when the leaching

happened (**Figure 4.8b**). If the Si*-O bonds breaking is the cause of leaching, the regeneration of surface silanols would be expected. Therefore, the cleavage of the Si*-O bonds, in our system, may not be the original cause of leaching since it could not explain the observed significant differences of leaching behavior between the CG and HG samples under the same reaction conditions (i.e., CPOL/m-cresol at 250^{o}C). In a similar manner, it would be not reasonable to expect that Si-C, C-S, or C-C bond breaking is the main cause of leaching.

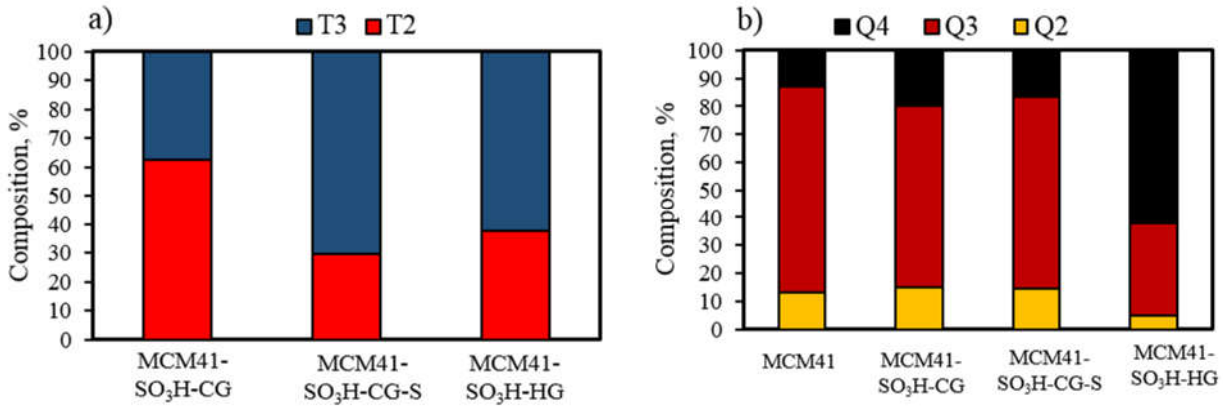

Figure 4. 8 Surface composition of the functionalized MCM41 a) T_m b) Q_n b) Weak interaction between functional groups and the surface silanols

B. Weak interaction between functional groups and the surface silanols

The second possible explanation for the observed leaching is that a diversity of strengths of interaction existed between the functional groups and the surface. For example, instead of a strong chemical Si*-O bond some functional groups could be grafted via a weaker interaction (H-bonding or Van de Walls forces) (**Scheme 4.3b**). As a consequence, a strong interaction between the polar solvent (CPOL + m-cresol) with

the sulfonic groups would be able to remove these physically adsorbed species off the surface at elevated temperatures. This option is plausible since the results from N_2 adsorption-desorption, FTIR, and ^{1}H-^{29}Si CP MAS NMR showed that the CG method did not result in the formation of strong chemical bonds, at least not to a great extent. However, as further discussed below, we believe that this is not the main path for leaching neither.

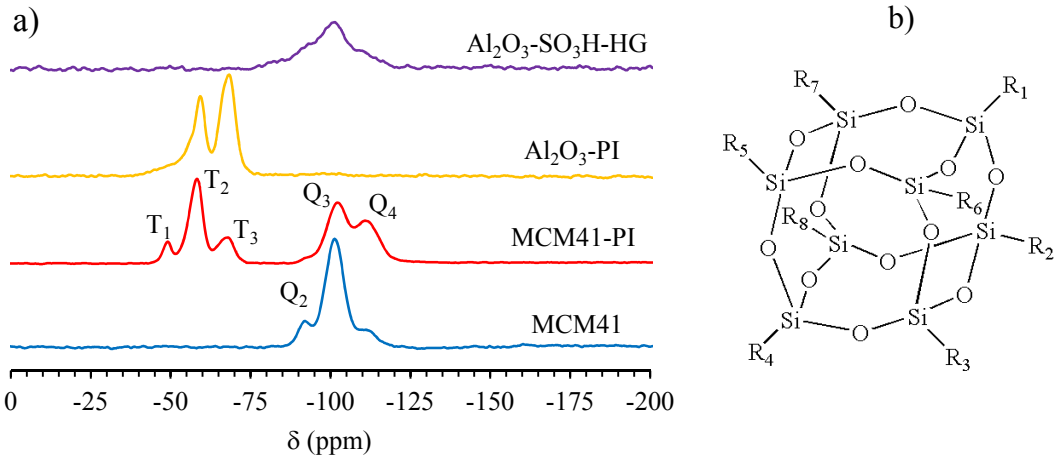

Figure 4. 9 a) NMR ^{1}H-^{29}Si CPMAS spectra of physically impregnated MCM41 and Al_2O_3 b) POSS (Polyhedral Oligomeric Silsesquioxane) structures

To further examine the nature of the physically adsorbed organosilanes on the catalyst surface we utilized the ^{1}H-^{29}Si CP MAS NMR data. A sample (MCM41-PI) was prepared by physical impregnation of MCM41 with MPTS at room temperature, without any further treatment. Surprisingly, the NMR data indicated the presence of T_1, T_2 and T_3 structures on the impregnated sample, which indicates that the appearance of T_m bands is not a strong indication of chemically bonded functional groups (**Figure 4.9a**). In fact, to rule out the possibility that the silylation could occur even at low temperatures, a similar procedure was conducted on Al_2O_3 which does not possess surface silanols. As shown in

Figure 4.9a, the Al_2O_3-PI sample also showed T_m bands. That is, without silanols, formation of Si*-O bonds could not occur on alumina. Therefore, we can conclude that the observed T_m bands in both samples should be due to the physically adsorbed species, reacting with themselves. These species could form mono- or poly- organosilanes, such as the well-known POSS structures (Polyhedral Oligomeric Silsesquioxane) [202-204] (**Figure 4.9b**). To further prove this concept, the Al_2O_3-PI sample was oxidized and washed with methanol to produce the Al_2O_3-SO_3H-HG sample. The disappearance of T_m signals from this sample (**Figure 4.9a**) indeed proves that all of the physical adsorption of organosilanes can be completely removed by a single step of methanol washing. Therefore, it should be concluded that observation of T_m signal in ^{1}H-^{29}Si CPMAS can be due to either chemically bonded functional groups or physically adsorbed species. The bands observed on the functionalized MCM41-SO_3H-CG and MCM41-SO_3H-HG samples are indeed due to actual chemical Si*-O bonds, in good agreement with other analysis techniques (FTIR, XRD, N_2 adsorption-desorption, TGA, etc). However, one must be careful assuming that T_m bands will always indicate formation of strong surface grafting via chemical bonds.

To gain a greater understanding on the leaching of MCM41-SO_3H samples synthesized by the CG method, the stability of the catalyst was further tested via multiple sequential washes with MeOH at 200°C (**Figure S7a-Supplementary Information**). After each wash, the solid was recovered and re-run for alkylation reaction at 250°C, 850 psi of N_2. It was observed that the activity of MCM41-SO_3H-CG gradually decreased after each methanol wash, which illustrates the severe leaching of functional moieties

when placed in contact with a strong polar medium, such as methanol. The extent of leaching for the MCM41-SO_3H-HG catalyst was less severe, with the activity dropping 27% initially, but stabilizing after the second wash (**Figure S7b-Supplementary Information**). This result suggests that the removal of physically adsorbed species during alkylation reaction does not cause the leaching. As discussed previously, a single methanol wash at high temperature is sufficient to clean the surface of loosely attached species. Therefore, if the activity keeps decreasing with subsequent washes, another more severely damaging effect should be occurring.

Moreover, the MS signal accompanying the TGA profiles (**Figure 4.3**) shows no evidence of organosilanes species desorbing (nor significant mass losses) in the second region (120-300^{o}C), which is at a temperature high enough to desorb physically adsorbed species from the surface. These results strongly suggest that most of the physically adsorbed or un-reacted organosilanes are completely removed after the ethanol wash during the catalyst preparation. In conclusion, physical adsorption or any other form of weakly interacting organic moieties with the surface cannot be the cause of the observed leaching.

As discussed previously, FTIR analysis (**Figure 4.2**) indicates that the MCM41-SO_3H-CG catalyst has a high density of free silanols. NMR analysis in **Figure 4.8b** also shows the similarity between the parent MCM41 and the functionalized MCM41-SO_3H-CG with high fraction of free silanols (Q_2 and Q_3) on the surface. Previous studies in our group have shown that silanol-terminated defects are responsible for the low tolerance of some zeolites in hot water [201]. In good agreement with the previous studies, the

hydrothermal stability experiments reported here (**Table 4.3** and **Figure 4.5**) reflect a high susceptibility of MCM41 and MCM41-SO_3H-CG to water. From these results, we can propose that the observed leaching in water or polar solvent media may be due to an attack on silanol-terminated sites on the silica surface, leading to partial dissolution of the solid surface structure, which results in massive leaching. In the next section, we will further elaborate this hypothesis.

C. The attack of water or polar species on silanol sites

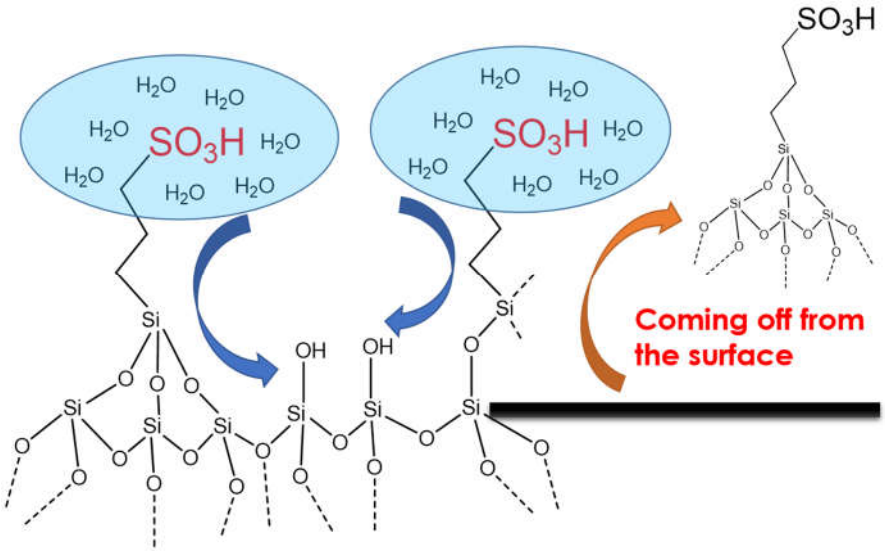

Figure 4. 10 Proposed leaching mechanism: Water attacks the silanol-terminated sites leading to structural damage

A possible mechanism of leaching is illustrated in **Figure 4.10**. First, a thin liquid layer could be formed around hydrophilic centers, such as the sulfonic group on which water or polar compounds can nucleate. The remaining silanol-terminated sites would facilitate the attack of liquid water (or methanol) via hydrolysis (or methanolysis). The process starts hydrolyzing the surface, gradually spreading into the bulk solid phase and

destroying the structure. The leached species are, in fact, the functional groups attached to a fraction of silica wall, as illustrated in **Figure 4.10**. This explains why the leaching is associated with structural damage, as observed in the methanol wash experiments. This idea is also consistent with the relationship observed between the hydrothermal stability and leaching of the silica-based catalysts, which essentially depends on the density of free silanols. The MCM41-SO_3H-HG catalysts are highly resistant to hydrolysis/leaching because they have a low density of silanol groups due to the more effective functionalization. As shown in **Figure S8-Supplementary Information**, this concept is also applicable to other silica-based catalysts, such as SBA15. As shown, the SBA15-SO_3H-CC sample synthesized by co-condensation experienced severe leaching in either polar and non-polar solvents. By contrast, when the fresh SBA15-SO_3H-CC was grafted with ETS in excess amounts via HG method (30.6 mmol ETS precursor per gram of the catalyst), a highly functionalized, hydrophobic surface was obtained. This heavily functionalized catalyst essentially showed no leaching at 250^oC in pure CPOL/m-cresol medium. It is obvious that by capturing the free silanols by functionalization, the leaching could be completely shut down on the SBA15-SO_3H-CC catalyst.

The proposed leaching mechanism is in line with similar effects of surface silanols reported about the stability of zeolites in hot liquid water [201]. In that case, it was proposed that water molecule clusters nucleated by free silanols, wetted the surface, and accelerated the hydrolysis of Si-O-Si sites, which led to the collapse and partial dissolution of the zeolite structure. It was found that hydrophobization of the zeolites by organosilanes was an effective method to enhance hydrothermal stability [201]. Previous

studies have also emphasized the important role of hydrophobicity of the surface in the resistance against hydrolysis and leaching [205-207]. For example, Fierro *et al.* have demonstrated that the leaching of functional group depends on the hydrophobicity of the surface. That is, the introduction of hydrophobic linkers provides a "protection" that enhances the stability of S-containing group [205]. Similarly, Yang *et al.* have shown that octyl linkers prevent the leaching of active species by tangling with the acid sites to increase its stability against leaching agent [206]. As proposed here, the "protection" should include two simultaneous effects: (i) expelling the liquid water from the catalyst surface and (ii) capping the free silanols, which are the potential nucleation sites for hydrolysis. Even though the leaching phenomenon has been observed in many studies, the connection between hydrothermal stability/leaching and silanol density has not been fully described before mostly due to the complexity of the functionalized surface.

4.4 Conclusion

As a conclusion, we postulate that the origin of leaching of functional groups from mesoporous silicas can be attributed to the high susceptibility of silicas to water/polar species when the surface is terminated with silanol groups. That is, a high concentration of silanol groups on the surface favors the solvent attack and greatly diminishes the hydrothermal stability of the silica, speeding up the leaching process. Therefore, the three essential factors that regulate the resistance to leaching of functionalized mesoporous silica are (a) the degree of functionalization, (b) the density of free silanol groups and (c) the surface hydrophobicity. In fact, theses parameters are not independent parameters but strongly dependent. That is, increasing the degree of functionalization reduces the silanol

density and slows down the hydrolysis process. The surface hydrophobicity also plays an important role in keeping the liquid water away from the surface and preventing the dissolution of the outer layers of the solid. Accordingly, we have proposed a novel method to address these factors and obtain a non-leaching functionalized mesoporous silica. This method could open up promising opportunities for applying this type of catalyst to reactions that require to be operated under severe conditions (e.g., polar solvents and high temperatures), such as those found in biomass conversion in the condensed phase.

Chapter 5 - Self and Cross Aldol Condensation of Cyclopentanone and Acetone over ZSM-5.

The Factors Determining Cross- and Self- Selectivity

5.1 Introduction and Literature Review

5.1.1 Introduction

An excellent selectivity of cyclopentanone (CPO) obtained from furfural hydrogenation/ring rearrangement (**Chapter 2**) has encouraged us to design different chemistries to incorporate this molecule into gasoline/diesel fraction. Besides hydroxyalkylation, the self-aldol condensation of CPO and the cross-aldol condensation of CPO with another ketone are other potential pathways to produce long-chain hydrocarbons. Since acetone could be selectively produced from the ketonization of acetic acid, one of the most abundant species in the first stage of torrefraction, the utilization of this small ketone has an intriguingly practical advantage as a means to vary molecular weights of the hydrocarbon products, depending on a specific demand or requirement. For example, aldol condensation of the cyclopentanone/acetone mixture could produce four different dimers and a few trimers with the chain length ranging from C_8 to C_{15}. The potential to obtain high yields of those condensated products is high since scientific community has extensively demonstrated the similar concept for several ketone mixtures on heterogeneous catalysts [208-213]. The mechanism of the reaction on basic catalysts has been extensively investigated in the literature while that on acid catalysts such as zeolites is less well-understood [214]. Furthermore, the factors that control the product selectivity to narrow down the diversity of the product chain length are not amply addressed. Therefore, the main purpose of this chapter is to give some fundamental insights into the matter.

5.1.2 Literature Review

a/Mechanism of acid-catalyzed aldol condensation

The acid-catalyzed aldol condensation of a wide range of ketones and aldehydes have been reported on zeolites [209, 215-218], Amberlyst [91, 168], acid-functionalized mesoporous materials [219, 220], $CoAlPO_4$-5 [221], and MOF [222]. The mechanism for the acid-catalyzed aldol condensation is initiated by the simultaneous tautomerization and protonation. The former step can be activated by both Lewis and Brønsted acid sites. Herrmann *et al.* [223] have proposed that the Brønsted acid sites on large pore zeolites (BEA, FAU, MCM41) are responsible for the tautomerization of an adsorbed acetone. The acetone is first adsorbed on the surface via the interaction between the O atom of the carbonyl group with the surface proton (**Scheme 5.1**). The adsorbed species then undergoes the tautomerization with a concerted configuration on the Brønsted acid site. The concerted mechanism is in agreement with several previous studies [224, 225]. DFT calculations show that the proton does not completely transfer to the adsorbed acetone but instead stabilizes the molecule via H-bonding, which agrees with a ^{13}C NMR study for the adsorption of acetaldehyde on HZSM-5 [226, 227]. The former enol undergoes an electrophilic attack on the C atom of the gas phase acetone (Eley-Rideal mechanism) to produce an aldol adduct [223]. In the second step, the C-C bond is formed simultaneously with a proton transfer in which the enol donates an α-proton to the O atom of the zeolite surface while accepting a proton from the Brønsted acid site to the O atom of the carbonyl group, as also suggested by Solans-Monfort *et al*. [225]. The diacetone alcohol is quickly dehydrated to produce mesityl oxide, which can be further isomerized to isometyl oxide

(**Scheme 5.1**). In contrast, other authors [224, 228-230] have reported that the most stable surface-species is a silyl-ether complex, which is the protonated adsorbed acetone at the transition state. The formed enol is bound to the Brønsted site via a weak π interaction [224]. The questions as to whether a Brønsted or a Lewis acid site is essential for the reaction and which step is kinetically relevant (tautomerization or C-C coupling) have been addressed repeatedly in the literature.

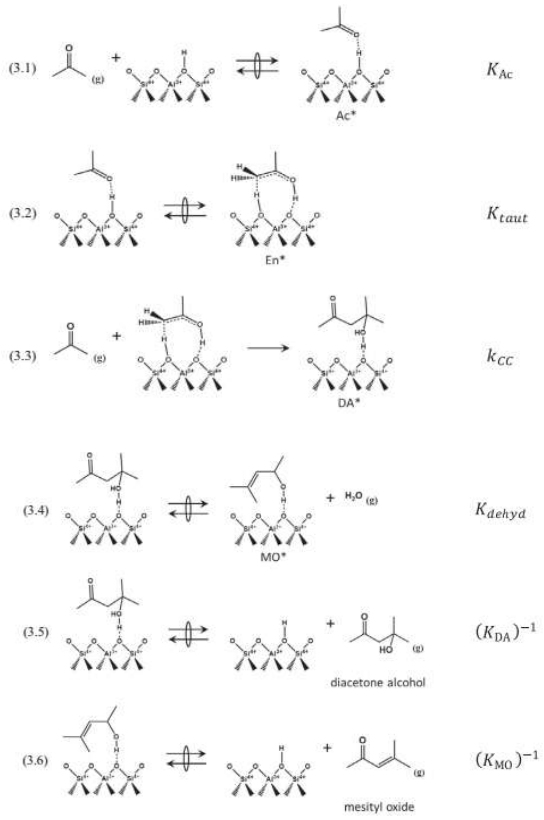

Scheme 5. 1 Proposed mechanism of acid-catalyzed aldol condensation of acetone on a zeolite surface. Reproduced with permission from Ref. [223]

b/ Site requirements

Activation (enolization) by Brønsted sites:

Kikhtyanin *et al.* [208, 231] have suggested that the Brønsted acid sites on zeolites (HZSM-5, HBEA, HMOR and HSDUSY) play a crucial role in the aldol condensation of furfural/acetone. It was shown that regardless of the zeolite crystal framework structures, all the catalysts in H-form were all active for the reaction [208] whereas the NH_4-form was nearly inactive. Moreover, two H-BEA catalysts with similar Brønsted acidity but different Lewis acidity exhibited similar activity, suggesting that the Brønsted acid sites are more important.

Herrmann *et al.* [223] have reported a similar value of rate constants calculated from the first order rate expression for several MFI and BEA zeolites with different Si/Al ratios (MFI: 17-168, BEA: 12-43) and H^+/Al ratios (MFI: 0.65-1.03, BEA: 0.22-1.04). There are three main points that back up their conclusion of an Eley-Rideal mechanism with C-C coupling as the kinetically relevant step: (i) the surface was nearly saturated with H-bonded acetone as confirmed by FTIR and DFT calculations under the reaction conditions; (ii) the acetone condensation rate was first order in the partial pressure of acetone in the gas phase; and (iii) no isotope effect was observed when acetone-d_0/H_2 vs. acetone-d_6/D_2 were used, indicating that the kinetically relevant step does not involve a proton-transfer process (i.e., formation/breaking of C-H/O-H bonds).

On the other hand, some DFT studies on the acetone/formaldehyde system using cluster models have revealed that the tautomerization of acetone is the rate-limiting step on different zeolites: HZSM-5 [224, 225, 232], HY [232], H-FER [224], and HMCM-22 [224], which is in agreement with an experimental gas phase study [233].

Activation (enolization) by Lewis sites: Dumitriu *et al.* [209] have found out that silicalite-1 is also active for the aldol condensation of a mixture of acetaldehyde and formaldehyde. This material does not have any strong Brønsted acid sites, except for some weak acidity from terminal Si-OH groups. The authors have attributed the catalytic activity to the catalytic action of Lewis acid sites in combination with silanol groups, acting as the Brønsted acid sites (**Scheme 5.2**). The role of the Brønsted acid sites is to protonate the acetone to render the C of the carbonyl group electrophilic while that of the Lewis acid is to facilitate the tautomerization of the adsorbed ketone. However, the nature of the Lewis sites on this material was not mentioned. Biaglow *et al*. [234] have stated that acetone condensation could be catalyzed by non-framework Al species. The cooperation effect of both types of acid sites has also been invoked to explain the high activity observed in heteroatom modified-MFI zeolites (Fe, Al, Ge, B), which have both Brønsted and Lewis sites. The Lewis acid site can bind to acetone, enhancing the electrophilicity of the carbonyl group's C atom, which is very similar to the protonation effect caused by Brønsted acid sites [234]. However, this hypothesis has not been tested experimentally.

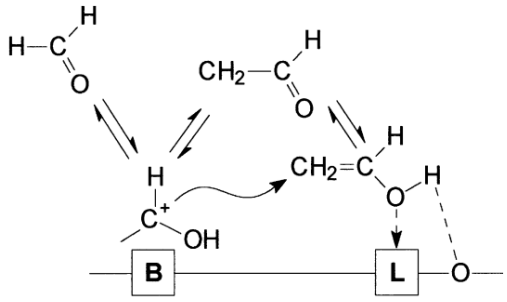

Scheme 5. 2. Proposed mechanism of cooperative catalysis of Brønsted and Lewis acid sites. Reproduced with permission from Ref. [209]

Panov *et al.* [235] have utilized FTIR to investigate the adsorption/condensation of acetone on alumina and USY, HY, HZSM-5 zeolites at 105 °C. They observed that on alumina, which possesses only Lewis acid sites, the reaction occurred at a much faster rate than on zeolites (containing both Brønsted and Lewis acid sites). In contrast, an HZSM-5 zeolite sample without non-framework aluminum exhibited zero activity. A linear relationship between the initial rate and density of Lewis acid sites. In contrast, no clear trend was observed with respect to Brønsted site density, suggesting that the Lewis acid sites are kinetically relevant. From FTIR spectra, it was shown that acetone could adsorb on both Lewis and Brønsted sites characterized by different stretching vibration frequencies of the carbonyl group (1650-1690 cm^{-1} for Brønsted sites and 1690-1705 cm^{-1} for Lewis sites). This observation suggests a combined role for both types of active sites. In this manner, the Lewis sites would tautomerize the acetone while the Brønsted sites would adsorb the co-reactant for the C-C coupling step. If this is the case, close proximity between Brønsted and Lewis sites would be a crucial requirement for the cooperative effect. The lack of adjacent sites could lead to a low condensation rate, even when there is a high density of Brønsted sites available. On alumina, the absence of Brønsted sites leads to an Eley-Rideal mechanism, in which the tautomerized acetone picks up the co-reactant from the gas phase. The C-C coupling might be proposed as the rate-limiting step without further explanation. However, this assumption cannot explain the faster reaction rate observed in the case of alumina.

The activation of aldehydes by Lewis acid sites has also been reported in other catalysts such as $CoAlPO_4$-5 [221] and MOF [222]. Kikhtyanin *et al.* [222] have studied

the role of Lewis acid sites in MOF materials for the aldol condensation of furfural and acetone. MOF catalysts investigated included Cu-BTC (Basikite C300) and Fe-BTC (Basolite F300). They showed an opposite catalytic behavior even though both materials have a similar density of Lewis acid sites (~2.3-2.5mmol/g). While Cu-BTC showed poor activity for aldol condensation, Fe-BTS exhibited 10-fold higher activity. The authors proposed that the Fe-BTS catalyst possessed weak Brønsted acidity originating from the promoting effect of water. However, the nature of the active sites was not reported. Hypothetically, they suggested that Fe^{3+} could hydrolyze the water molecules in their first coordination sphere to generate a metal aqua complex which could donate a proton to activate the ketone. The poor activity of Cu-BTC indicates that Lewis acid sites alone are were not sufficient to initiate the aldol condensation reaction, which probably suggests that the rate-limiting step, in this system, is C-C coupling.

There are two issues that have been widely discussed in the literature, but without a clear conclusion. In fact, conflicting proposals have often been reported.

- The Brønsted acid site could participate in either tautomerization or protonation. The former renders the activated species nucleophilic (enol formation) while the latter makes the carbonyl carbon more electrophilic towards the attack by the enol [226, 236]. The question is which pathway would be more favorable than the other if a carbonyl compound is introduced to a surface that has mostly Brønsted acid sites. In fact, the difference in the activation energy between these steps has never been compared in the literature. This is important, especially for the systems having more than two carbonyl groups, since the reaction pathway and product

selectivity could be different. An extensive investigation of this matter is necessary.

- Similarly, the roles of Lewis acid sites are still unclear. Compared to Brønsted acid-catalyzed aldol condensation, the Lewis acid-catalyzed case is less well-understood. Some questions to be addressed include whether Lewis sites alone can catalyze aldol condensation, whether the Lewis site requires the assistance or cooperative catalysis of an adjacent Lewis or Brønsted site, and what is the essential requirement for an active Lewis acid catalyst.

Selectivity of self- and cross- aldol condensation

Several studies have been conducted on the aldol condensation of the mix ketone/aldehyde systems including: furfural/acetone, hydromethylfurfural/acetone, formaldehyde/ acetaldehyde, citral/acetone, acetone/formaldehyde, benzaldehyde/n-heptaldehyde, aromatic aldehydes/acetone over basic catalysts: MgO and alkali promoted MgO [237], hydrotalcites [212, 213], Mg,Al-mixed oxides [238], MgO–ZrO_2 [140], amine-functionalized MCM41 [239], Al-MCM41 supported MgO [240] and acidic catalysts: HZSM-5, HBEA, HMOR and HSDUSY zeolites [208-211], Lewis acidic zeolites (Hf-, Sn-, Zr- beta) [241], MWW family of different structure types (MCM-22, MCM-49, MCM-56 and MCM-36) [231], etc.

In general, the aldol condensation of a ketone mixture could produce a complex mixture of aldol adducts including the self-aldol condensation of ketones that bear α-H and the cross-aldol condensation of those ketones with the second carbonyl compound. The factors that govern the selectivity toward the self- or cross- aldol condensation vary, depending on the ketone mixtures, catalysts as well as reaction conditions (feed ratio,

temperatures, etc). For example, in the furfural (or HMF)/acetone or aromatic aldehydes/acetone systems over zeolites [208, 222, 241], it has been reported that the cross-aldol condensation dominated with over 90% selectivity. In the other mixtures such as citral/acetone, a high selectivity toward the cross- aldol condensation of citral and acetone (pseudoionone) was also observed while the self- aldol condensation of acetone or citral was found with a trace amount over basic hydrotacites and Mg,Al-mixed oxides at 333K even though a high acetone/citral ratio of 3-17 was employed. Acidic zeolites (HY and HBEA) exhibited negligible activity in this case [211]. It is interesting to note that the self- aldol condensation of acetone has been obtained with a moderate yield over basic catalysts such as hydrotalcites [212], MgO and alkali-treated MgO [237, 242] and zeolites [217]. This indicates that the negligible rate of the acetone self- aldol condensation observed in the mixture with other carbonyl compounds could be due to the competitive adsorption or relatively higher activation barriers of the enolization or C-C bond formation steps compared to that of the other ketones. In fact, when a high acetone/citral ratio was used, a higher yield of acetone self- aldol adduct was observed, which illustrates the inhibition effect of citral to the reactivity of acetone [212].

Ungureanu *et al.* have examined the gas-phase aldol condensation of the mixture of formaldehyde/acetaldehyde over ZSM-5 and semicrystalline zeolitic-mesoporous UL-ZSM-5 [243]. The authors have reported that the ratio of acrolein (cross-aldol adduct) over crotonaldehyde (self-aldol adduct) increased from 3 to 10 when temperatures were varied from 250 to 350^{o}C. In another study, Dumitriu *et al.* have also stated that high temperature favored the formation of acrolein on silicalite-1 and HZMS-5 (in the range of 275-375^{o}C) [209]. However, in this case the maximum cross-/self- ratio was only 1.5,

which was much smaller than the value reported by Ungureanu *et al.* [243]. The lower selectivity of crotonaldehyde at a high temperature was attributed to the coke formation caused by the polymerization of the product itself [210]. A change in the product distribution was also seen on HZSM-5 with different Si/Al ratios, in which the acrolein selectivity increased with increasing Al contents [210]. In this case, the nature of acid sites as well as their distribution on the surface obviously plays a crucial role.

As previously discussed, Dumitriu *et al.* have proposed the cooperative effect between Brønsted and Lewis acid site, in which the Lewis site activates a ketone via enolization and the Brønsted site protonates another ketone to enhance the electrophilicity of its C-carbonyl. Then, the enol picks up the adjacent polarized ketone for the aldol addition step. As a result, the selectivity toward the cross- or self- products for a given enol might depend on the availability of the adsorbed or polarized carbonyl molecules. For example, it has been shown that the O-atom of acetadehyde has a higher electronic density than that of formaldehyde, which could facilitate the polarization of the acetaldehyde on a Brønsted acid site [209]. In contrast, another study has proposed that the Brønsted site is responsible for the enolization while the Lewis site is involved in the polarization. High density of Lewis acid sites facilitated the cross-aldol condensation selectivity [243].

Another factor that could play a role is the relative activation barrier (free energy) of the C-C coupling step between a given enol with other carbonyl compounds. Recently, Iglesia *et al.* have shown that the rate of the cross- aldol condensation for the formaldehyde/acetone mixture over TiO_2 was a 1000 -fold higher than that of the acetone self- aldol condensation [244]. The value varied between different mixtures of

formaldehyde and other carbonyl compounds with an increasing chain length. According to the authors's analysis, the cross-/self- selectivity is determined by the $\Delta G^{TS}_{i,j-i,i} = \Delta G^{TS}_{i,j} - \Delta G^{TS}_{i,i}$ factor, which is the difference in the free activation energy of the C-C coupling step between cross- and self- aldol condensation. The crucial parameter that controls the variation in product distribution is the chain-length or size of the alkyl substituents of the carbonyl compounds. This factor greatly affects the entropy component ($\Delta S^{TS}_{i,j}$). DFT calculations have shown that the entropy loss increased for larger electrophiles (C_2-C_4 carbonyls), resulting in a greater difference in the activation entropy between cross- and self- coupling ($\Delta S^{TS}_{i,j-i,i}$). Difference in the activation enthalpy, $\Delta H^{TS}_{i,j-i,i}$, on the other hand, was not influenced much by the ketone sizes. Overal, the difference in activation free energy was greater for the coupling of HCHO with larger enols, resulting in a more significantly higher cross-aldol selectivity with the increasing ketone chain length.

5.2 Experimental Methods

5.2.1 Chemical and materials:

Zeolite NH_4ZSM-5 CBV 3024E (Si/Al=15) and CBV 8014 (Si/Al=40) were obtained from Zeolyst International. Before being used, the zeolites were calcined at 600^{o}C for 5 h in 150ml/min air flow to produce H^+ form. Na-ZSM-5 (Si/Al=40) was synthesized via ion-exchange method. First, zeolite NH_4ZSM-5 CBV 8014 (Si/Al=40) was stirred with 2M NaCl solution at 80^{o}C for 12 h. The ion exchange was conducted three times. The obtained solid was dried at 110^{o}C overnight, followed by calcination at 600^{o}C for 5 h in 150ml/min air. Cyclopentanone (>99%), acetone (HPLC grade, >99%) and cyclohexane (HPLC grade, >99.9%) were purchased from Sigma Aldrich. Cyclopentanone was

distilled to remove impurities before use while acetone and cyclohexane were employed as provided.

5.2.2 Catalytic reaction measurements:

The aldol condensation of cyclopentanone and acetone was carried out in a Parr reactor at 250°C, V_{total}=120ml, 500psi N_2 pressure in cyclohexane solvent over 0.5 g HZSM-5 (Si/Al=15 and 40), at an initial concentration of cyclopentanone and acetone of 900 mM. At first, 90ml of cyclohexane and the catalysts were placed in a stainless steal vessel. A 30ml mixture including cyclopentanone and acetone in cyclohexane was placed inside a feeding cylinder. After the reactor temperature reached 247°C, the feed was injected into the reaction mixture. The temperature was stabilized at 250°C after 5 minutes and the reaction time began to be counted.

The product mixture was analyzed by Shimadzu QP2010S gas chromatograph/mass spectrometer (GC-MS) and quantified by GC-FID Agilent 6890 equipped with a flame ionization detector for quantification. Both GC's were equipped with a Zebron ZB-1701 column with the dimensions of 60m x 0.25 mm x 0.25 μm.

The conversion of cyclopentanone (X_C), conversion of acetone (X_A), yield of a product based on cyclopentanone or acetone initial concentration were calculated as:

$$X_C = \frac{C_{C-in} - C_{C-out}}{C_{C-in}}; X_A = \frac{C_{A-in} - C_{A-out}}{C_{A-in}}$$

$$Y_i = \frac{C_i}{C_{C-in}} \text{ or } \frac{C_i}{C_{A-in}};$$

The formation rate r_i (mmol.g^{-1}.s^{-1}) and turnover frequency TOF_i (s^{-1}) of a product were calculated as

$$r_i = \frac{n_i}{m_{cat} \times t}; TOF_i = \frac{n_i}{n_{H^+} \times t}$$

n_i: Number of Mol of a product (mmol)

m_{cat}: mass of catalysts (g)

n_{H+}: Number of protons or active sites (mmol)

t: Reaction time, (s)

The carbon balance for the cyclopentanone ($C_{C\text{-}bl}$) and acetone ($C_{A\text{-}bl}$) were calculated as:

$$C_{C-bl} = \frac{C_{C-out} + C_{C\to P}}{C_{C-in}}; C_{A-bl} = \frac{C_{A-out} + C_{A\to P}}{C_{A-in}}$$

where $C_{C(in,\ out)}$, $C_{A(in,\ out)}$: Concentration of cyclopentanone and acetone before and after reaction (mM);

$C_{C\to P}$ and $C_{A\to P}$: Concentration of cyclopentanone and acetone convered to detectable products and the concentration of a product (mM);

5.3 Results and Discussions

5.3.1 The reaction mechanism and rate limiting step on ZSM-5 zeolites

According to the literature, the acid-catalyzed aldol condensation of a ketone undergoes 3 main steps: tautomerization (enolization), C-C coupling and de-protonation. Over acid zeolites, it has been reported that the rate limiting step could be either the activation of the ketone (tautomerization) or the C-C coupling step of the enol with

another ketone, which corresponds to the 1st and 2nd reaction order, respectively. Experimental data [233] as well as DFT calculations on the acetone/formaldehyde system over different zeolites: HZSM-5 [224, 225, 232], HY[232], H-FER[224], HMCM-22 [224] have revealed that the tautomerization of acetone is the rate limiting step, which corresponds to the 1st order reaction. Herrmann *et al.* have also observed the 1st order rate expression for the gas phase self-aldol condensation of acetone over MFI and BEA zeolites with different Si/Al ratios. However, in this case the C-C coupling is the slow step and the surface is nearly saturated with the adsorbed acetone, resulting in the 1st order dependence of the measured rate on the acetone partial pressure in the gas phase [223]. To investigate this matter in the liquid phase aldol condensation of cyclopentanone (C) and acetone (A), a Langmuir Hinshelwood model was established with an assumption that the rate determining step is the tautomerization of the ketones

1/The tautomerization of C and A

$$C + * \underset{}{\overset{K_C}{\rightleftharpoons}} C*$$
$$C* \xrightarrow{k_{C-tau}} [C]*_{enol}$$

$$A + * \underset{}{\overset{K_A}{\rightleftharpoons}} A*$$
$$A* \xrightarrow{k_{A-tau}} [A]*_{enol}$$

With C, C*, [C]*enol are cyclopentanone, adsorbed cyclopentanone and activated cyclopentanone (the enol), respectively; A, A* and [A]* are acetone, adsorbed acetone and activated acetone (the enol), respectively; K_C, K_A, $k_{C\text{-}tau}$, $k_{A\text{-}tau}$ are the adsorption

constant of cyclopentanone, adsorption constant of acetone, rate constant of cyclopentanone tautomerization and rate constant of acetone tautomerization, respectively.

2/The C-C coupling

For the cross- aldol condensation of C and A, the activated ketones ([C]*enol or [A]*enol) can couple with either adsorbed cyclopentanone or acetone (C* or A*) to produce four different dimer products ([C]A, [C]C, [A]A and [A]C). The dimers could also react with another activated ketone to generate longer chain hydrocarbons (trimers). However, for simplification, the formation of those trimers is not included in this model. In fact, experimental results show that the formation of those trimers are negligible compared to that of the dimers.

$$[C]^*_{enol} + A^* \xrightleftharpoons{K_{[C]A-coupling}} {}^*[C]A^+ + *$$
$$^*[C]A^+ \xrightleftharpoons{K_{[C]A-deprot}} {}^*[C]A$$
$$^*[C]A \xrightleftharpoons{K_{-[C]A}} [C]A + *$$

$$[C]^*_{enol} + C^* \xrightleftharpoons{K_{[C]C-coupling}} {}^*[C]C^+ + *$$
$$^*[C]C^+ \xrightleftharpoons{K_{[C]C-deprot}} {}^*[C]C$$
$$^*[C]C \xrightleftharpoons{K_{-[C]C}} [C]C + *$$

$$[A]^*_{enol} + A^* \xrightleftharpoons{K_{[A]A-coupling}} {}^*[A]A^+ + *$$
$$^*[A]A^+ \xrightleftharpoons{K_{[A]A-deprot}} {}^*[A]A$$
$$^*[A]A \xrightleftharpoons{K_{-[A]A}} [A]A + *$$

$$[A]^*_{enol} + C^* \xrightleftharpoons{K_{[A]C-coupling}} *[A]C^+ + *$$

$$*[A]C^+ \xrightleftharpoons{K_{[A]C-deprot}} *[A]C$$

$$*[A]C \xrightleftharpoons{K_{-[A]C}} [A]C + *$$

With [C]C, [C]A, [A]A and [A]C are the dimer products of C-C coupling, *[C]C, *[C]A, *[A]A and *[A]C are the adsorbed dimers; *[C]C$^+$, *[C]A$^+$, *[A]A$^+$ and *[A]C$^+$ are the protonated form of the adsorbed dimers; $K_{C\text{-}C\ coupling}$, $K_{C\text{-}A\ coupling}$, $K_{A\text{-}A\ coupling}$ $K_{A\text{-}C\ coupling}$ are the equilibrium constants of the C-C coupling steps; $K_{C\text{-}C\ deprot}$, $K_{C\text{-}A\ deprot}$, $K_{A\text{-}A\ deprot}$ $K_{A\text{-}C\ deprot}$ are the equilibrium constants of the deprotonation of the dimers; $K_{[C]C}$, $K_{[C]A}$, $K_{[A]A}$, $K_{[A]C}$ are the adsorption constants of the dimers

The total formation rate of the products originated from [C] and [A] enols could be written as:

$$r_{[C]} = \mathrm{r}_{[C]C} + \mathrm{r}_{[C]A} = k_{C-tau} K_C (C)(*)_v \qquad (5.1)$$

$$r_{[A]} = \mathrm{r}_{[A]A} + \mathrm{r}_{[A]C} = k_{A-tau} K_A (A)(*)_v \qquad (5.2)$$

$$\frac{r_{[A]}}{r_{[C]}} = \frac{k_{A-tau} K_A (A)}{k_{C-tau} K_C (C)} \qquad (5.3)$$

With (C), (A) and $(*)_v$ are the concentration of cyclopentanone or acetone in the bulk phase and the concentration of vacant sites, respectively.

The selectivity of [C]C and [C]A; [A]A and [A]C could be derived as

$$\frac{r_{[C]A}}{r_{[C]C}} = \frac{[C]A}{[C]C} = \frac{\dfrac{K_{[C]A-cpl}K_{[C]A-deprot}K_A K_C k_{C-tau}(C)(A)}{K_{[C]A}}}{\dfrac{K_{[C]C-cpl}K_{[C]C-deprot}K_C{}^2 k_{C-tau}(C)^2}{K_{[C]C}}}$$

$$= \frac{\dfrac{K_{[C]A-cpl}K_{[C]A-deprot}K_A(A)}{K_{[C]A}}}{\dfrac{K_{[C]C-cpl}K_{[C]C-deprot}K_C(C)}{K_{[C]C}}} = \frac{K_{[C]A-tot}K_A(A)}{K_{[C]C-tot}K_C(C)} \qquad (5.4)$$

$$\frac{r_{[A]A}}{r_{[A]C}} = \frac{[A]A}{[A]C} = \frac{\dfrac{K_{[A]A-cpl}K_{[A]A-deprot}K_A(A)}{K_{[C]A}}}{\dfrac{K_{[A]C-cpl}K_{[A]C-deprot}K_C(C)}{K_{[C]C}}} = \frac{K_{[A]A-tot}K_A(A)}{K_{[A]C-tot}K_C(C)} \qquad (5.5)$$

With $K_{[i]\text{-}j\text{-}tot}$ is the product of $K_{[i]\text{-}j\text{-}deprot}$, $K_{[i]\text{-}j\text{-}cpl}$, K_j and $K_{[i]\text{-}j}^{-1}$

From equation (5.1), (5.2) and (5.3), it can be seen that if the measured rate is limited by the activation of the ketones, the total formation rate of [A] products, the total formation rate of [C] products and the ratio of those two rates would be linearly proportional to the acetone bulk concentration, the cyclopentanone bulk concentration and the ratio of the two concentrations, respectively. Equation (5.4) and (5.5) also indicate that the ratio of [C]A/[C]C and [A]A/[A]C are also in proportion to the ratio of acetone and cyclopentanone bulk concentration.

When the feed ratio A/C increased (increasing concentration of A while maintaining concentration of C), the formation rate of [A] products ([A]A+[A]C) increased proportionally while the formation rate of [C] products remained at the same value

(**Figure 5.1)**. The formation rates of [C] products were comparable when the single feed of C (0.9M) or the mixture of A/C (0.9M of C + 0.9M of A) was used. The formation rate of [A] products in the single feed of A (0.9M of A) was also equal to that in the mixture of A/C (0.9M of C + 0.9M of A). Different initial concentrations of C in the single feed experiments (0.45M, 0.9M and 1.8M of C) yielded a proportional formation rate of [C] products, indicating 1st reaction order. Additionally, experimental data from **Figure 5.1** show that the ratio of total [A] over total [C] products, [C]A/[C]C and [A]A/[A]C proportionally depend on A/C feed ratio as clearly described in equations (5.3), (5.4) and (5.5). It strongly indicates that the activation of the C and A (tautomerization or enolization) is the kinetically relevant step. The finding also holds true for HZSM-5 with higher Si/Al ratio (40) as presented in **Figure 5.2**.

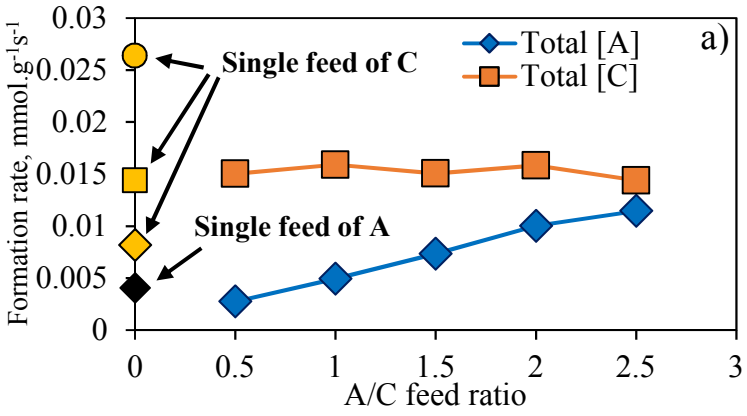

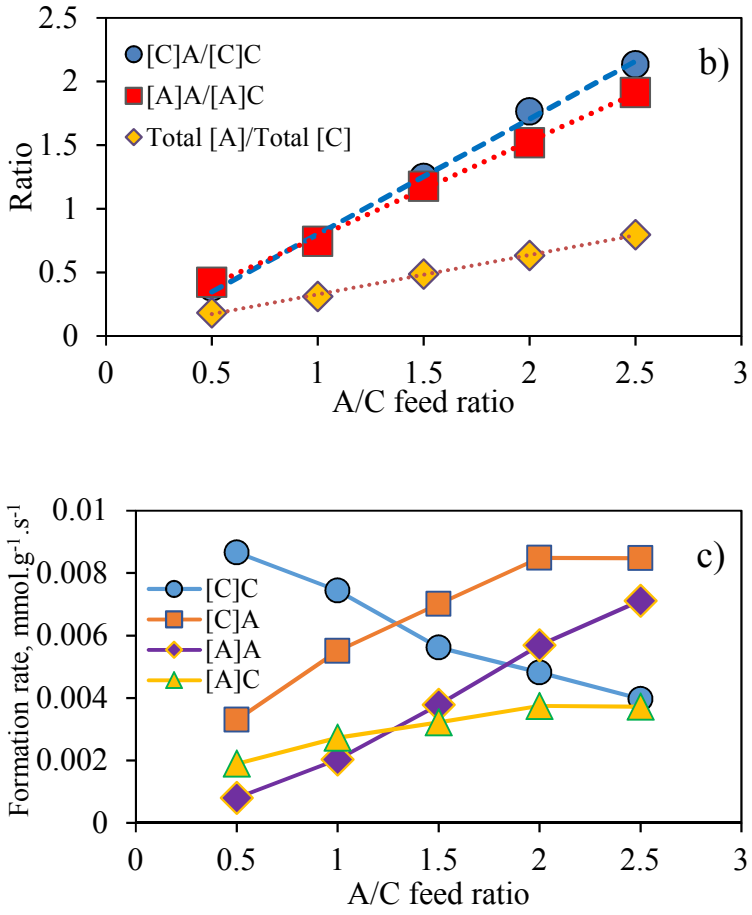

Figure 5. 1 The effect of acetone/cyclopentanone feed ratio (A/C) on a) The total formation rate of [A] and [C] products. The yellow circle, square and diamond correspond to a single feed experiments with 0.45, 0.9 and 1.8M of C; The black diamond correlates to a single feed experiment with 0.9M of A; and to b) Cross- and self- selectivity and c) Product distribution over ZSM-5 (Si/Al=15)

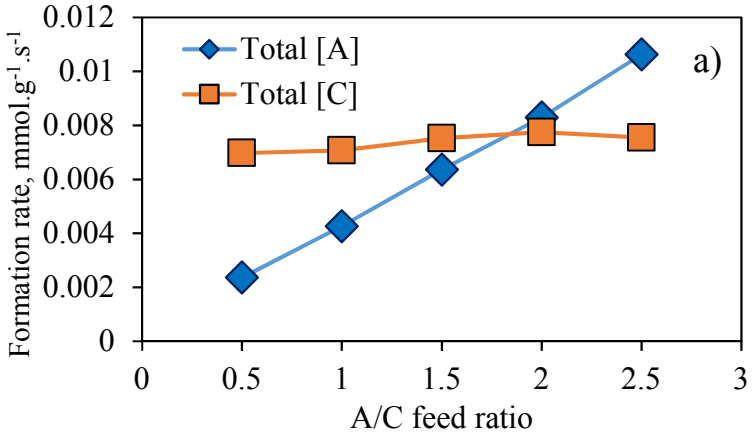

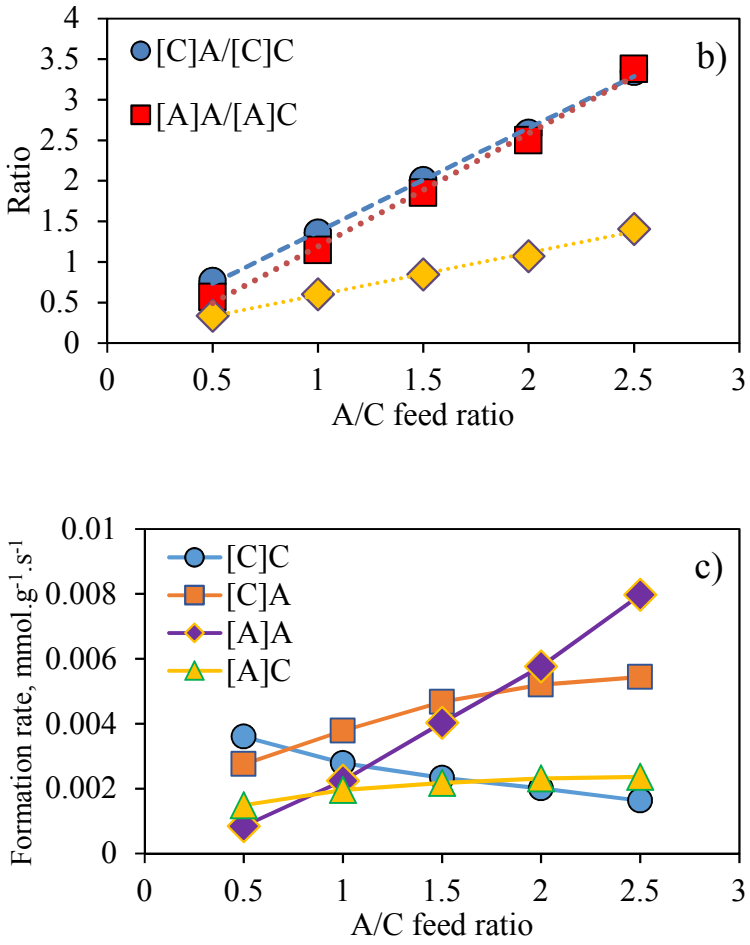

Figure 5. 2 The effect of acetone/cyclopentanone feed ratio (A/C) to a) The total formation rate of [A] and [C] products and b) Cross- and self- selectivity and c) Product distribution over ZSM-5 (Si/Al=40)

Consequently, the formation rate of [C] and [A] products is controlled by the formation rate of the enols. Therefore, a higher formation rate of total [C] products than that of total [A] at an equal A/C feed molar ratio observed from **Figure 5.1** and **5.2** would be due to the difference in the enolization reactivity of the ketones. Swain *et al.* have reported that the enolization of a ketone undergoes a step-wise mechanism in which the O-atom of the ketone is protonated first, followed by the abstraction of an α-H by the conjugate base of the Brønsted acid site. The C-H bond cleavage or the H-abstraction is

the rate limiting step [245-247]. By conducting a substitution of tritium (T) and deuterium (D) at the α-C of the ketones, the authors observed a dramatic decrease in the rate of acid-catalyzed enolization. The isotopic effects were reported to be $k_{C-H}/k_{C-T} = 10$ and $k_{C-H}/k_{C-D} = 5$ [245]. The conclusion was later agreed by Ref [248]. The enolization reactivity of a ketone, therefore, would depend on the acidity of an α-H of the ketone. From DFT calculations, Gómez-Bombarelli *et al.* have reported the value of pKa for acetone and cyclopentanone which are 19.6 and 16.5 in the gas phase, 20.9 and 19.7 in the aqueous phase, respectively [249]. Computational calculations from our group have also calculated that the deprotonation energies of the α-Hs of cyclopentanone and acetone are 1453 $kJ.mol^{-1}$ and 1461 $kJ.mol^{-1}$ respectively. Moreover, a lower barrier for the H-abstraction of cyclopentanone compared to that of acetone on MgO (100) was also observed (51 kJ/mol compared to 60 kJ/mol). These evidences firmly indicate a stronger acidity of the α-Hs of C compared to A, resulting in the higher formation rate of [C] enols as well as the total [C] coupling products.

At an equal initial feed molar ratio of A/C, the selectivity to [C]A and [C]C (or ([A]A and [A]C) would depend on the relative equilibrium constants of the coupling step, the deprotonation step, the adsorption constants of A and C and the adsorption constants of [C]A and [C]C products, as demonstrated by Eqn. (5.6) - (5.7).

$$\frac{[C]A}{[C]C} = \frac{\dfrac{K_{[C]A-cpl}K_{[C]A-deprot}K_A}{K_{[C]A}}}{\dfrac{K_{[C]C-cpl}K_{[C]C-deprot}K_C}{K_{[C]C}}} = \frac{K_{[C]A-tot}K_A}{K_{[C]C-tot}K_C} \quad (5.6)$$

$$\frac{[A]A}{[A]C} = \frac{\dfrac{K_{[A]A-cpl}K_{[A]A-deprot}K_A}{K_{[C]A}}}{\dfrac{K_{[A]C-cpl}K_{[A]C-deprot}K_C}{K_{[C]C}}} = \frac{K_{[A]A-tot}K_A}{K_{[A]C-tot}K_C} \quad (5.7)$$

with $K_{i\text{-}tot}$ is the product of $K_{i\text{-}cpl}$, $K_{i\text{-}deprot}$ and K_i^{-1}

Experimental data in **Figure 5.3** show that at A/C molar ratio =1, over HZSM-5 (Si/Al=15), the coupling of the enols with C is more favorable, resulting in the higher yields to [C]C and [A]C compared to [C]A and [A]A, respectively. Interestingly, the opposite trend was observed on HZSM-5 with a higher Si/Al ratio (40), in which the coupling of the enols with A has a higher rate than that with C, resulting in the higher selectivity of [C]A than [C]C and that of [A]A than [A]C. The switch of the product distribution with the Si/Al ratios is caused by mass transfer limitation which is prevalent on this catalyst for the aldol condensation reaction. Consequently, the order observed here is apparent and would not reflect the true order of the reaction. Further investigation is needed. One of the most important objective of the future work is to address this matter.

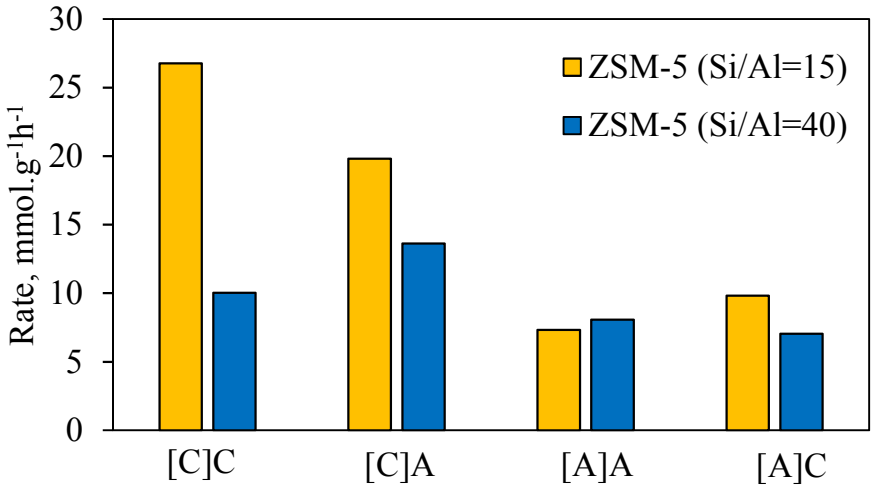

Figure 5. 3 Product distribution of the aldol condensation of C and A on HZSM-5 zeolites

5.3.2 The nature of the active sites

As previously demonstrated by Iglesia *et al.*, the titration technique for the gas phase aldol condensation of acetone could be applied to measure the most relevant active sites for the reaction by co-feeding a deactivation agent into the reaction mixture. On acid zeolites, a base (such as pyridine or dimethyl pyridine) has been used. In this work, a similar concept has been applied for the liquid phase aldol condensation of cyclopentanone and acetone in cyclohexane solvent, which allows us to determine the true kinetically relevant sites for the reaction as well as quantify the density of the active sites at the same time. It can be seen from **Figure 5.4a** that the formation rates of the aldol-adducts over HZSM-5, HBEA and HY did not change with an increasing amount of pyridine, indicating that the system is in the internal mass transfer limitation regime. This could be owning to the small pore size entrance of those microporous zeolites, which might inhibit the diffusion of the reactants and release of the coupling adducts. For example, HZSM-5 zeolite has the pore size of 0.55-0.56nm, which is close to the kinetic

diameter of acetone (~ 5nm) [250] (**Table 5.1**). Catalytic activity did not change with different stirring speeds, ruling out the effect of the external mass transfer limitation (**Figure 5.4b**).

Interestingly, a linearly decaying formation rate of the aldol adducts with an increasing amount of pyridine added was observed over MCM41-SO_3H-HG. It is obvious that over the mesoporous silicas with a large pore and a well-order hexagonal structure, the diffusion of the aldol adducts could be significantly facilitated. As a result, the condensation rate over MCM41 was controlled by the surface reaction, manifested by an instant drop of the measured rate with the pyridine addition.

Table 5. 1 Pore size, surface area and Brønsted acid density of some zeolites

Zeolite	Pore Size (nm)	Surface area[a] (m^2/g)	Brønsted acid sites density (mmol/g)			Lewis acid sites density (mmol/g)
H-ZSM5 (Si/Al=15)	0.55-0.56	405	-	0.61 [c]	0.56 [d]	0.56 [d]
H-ZSM5 (Si/Al=40)	0.55-0.56	425	0.39 [b]	0.38 [c]	0.33 [d]	0.29 [d]
HY (Si/Al=30)	0.66-0.67	720	0.29 [b]	-	-	-
H-Beta (Si/Al=19)	0.74	710	0.54 [b]	-	-	-
MCM41-SO_3H-HG	3	549	0.353 [b]	-	-	-

[a] of ammonium form, according to manufacturers; [b] IPA-TPD (isopropyl amine)[c] Obtained from Ref [223] [d] Calculated from pyridine titration and B/L ratio reported by Ref [251]

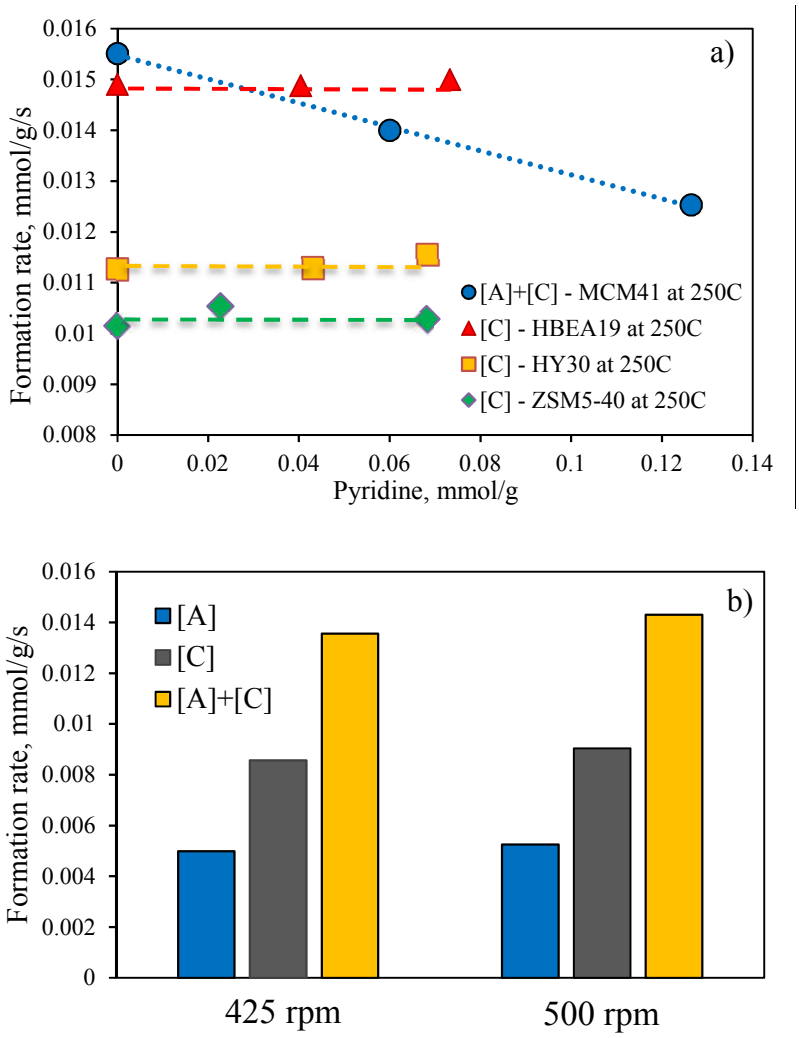

Figure 5. 4 a) The total formation rate of the aldol-adducts with different amounts of pyridine co-fed into the reaction. A mixture of A+C with C_C=C_A=0.9M was used in the case of functionalized MCM41 while a single feed CC=0.9M was used for the other catalysts. Reaction condition: 250°C, 0.5h, cyclohexane solvent **b)** The effect of stirring speeds to the catalytic activity of HZSM-5 (Si/Al=40)

When a small amount of pyridine was added into the cross-aldol condensation of C and A reaction mixture over HZSM-5 zeolites, initially the formation rate of [A], [C] and [A]+[C] did not change due to the excess active sites. However, with more pyridine added, the rates started linearly dropping, indicating that the all of the excess active sites have been deactivated from pyridine titration. Up to this point, the system was controlled

by the surface reaction regime. The extrapolation of [A]+[C] curve in **Figure 5.5a)** and **b)** allows the quantification of acid density on HZSM-5 zeolites, which are 1.12 and 0.63 mmol/g for Si/Al ratios of =15 and 40, respectively. It should be noted that both Brønsted and Lewis acid sites can be titrated by pyridine. The value obtained here might be the total number of Brønsted and Lewis sites. The Brønsted/Lewis ratios for HZSM-5 (Zeolyst) with Si/Al=15 and 40 have been reported to be 0.99 and 1.11, respectively [251]. The calculated Brønsted acid density of HZSM-5 zeolites shown in **Table 5.1** strongly agrees with the value obtained from IPA-TPD and from Ref [223]. An equivalent density of Lewis acid sites was obtained. However, the Lewis acid sites alone are much less active than when both Brønsted and Lewis ones are present as shown in **Figure 5.6a**. The low activity of Na-ZSM-5 zeolite contradicts with some studies in the literature, stating that the Lewis acid site of zeolites by itself could catalyze the aldol condensation [234, 235]. The obtained result indicates that the Brønsted acid is the most kinetically relevant site for the aldol condensation reaction, in agreement with Refs [208, 223, 231]. Iglesia *et al.* have shown similar values of rate constant (normalized by the number of H^+) on MFI and BEA zeolites for the aldol condensation of acetone [223] as also observed in our data (**Figure 5.6b**). By normalizing the total formation rate of aldol adducts ([C]+[A]) with the number of H^+ (from **Table 5.1**) on the two zeolites, a comparable TOF value was obtained (**Figure 5.6b**), indicating that the Brønsted sites are more kinetically relevant for the reaction. It should be noted that the Lewis acid density of HZSM-5 (Si/Al=40) and Na-ZSM-5 should not be much different. Therefore, the tremendous difference in the activity between those catalysts is a strong evidence against the involvement of the Lewis sites in the enolization step. However, it could not be ruled out

that the elimination of the Brønsted acid sites on Na-ZSM-5 could induce the change of the rate limiting step from the enolization to the C-C coupling, leading to the lower activity on Na-ZSM-5. Further investigation into this problem is needed.

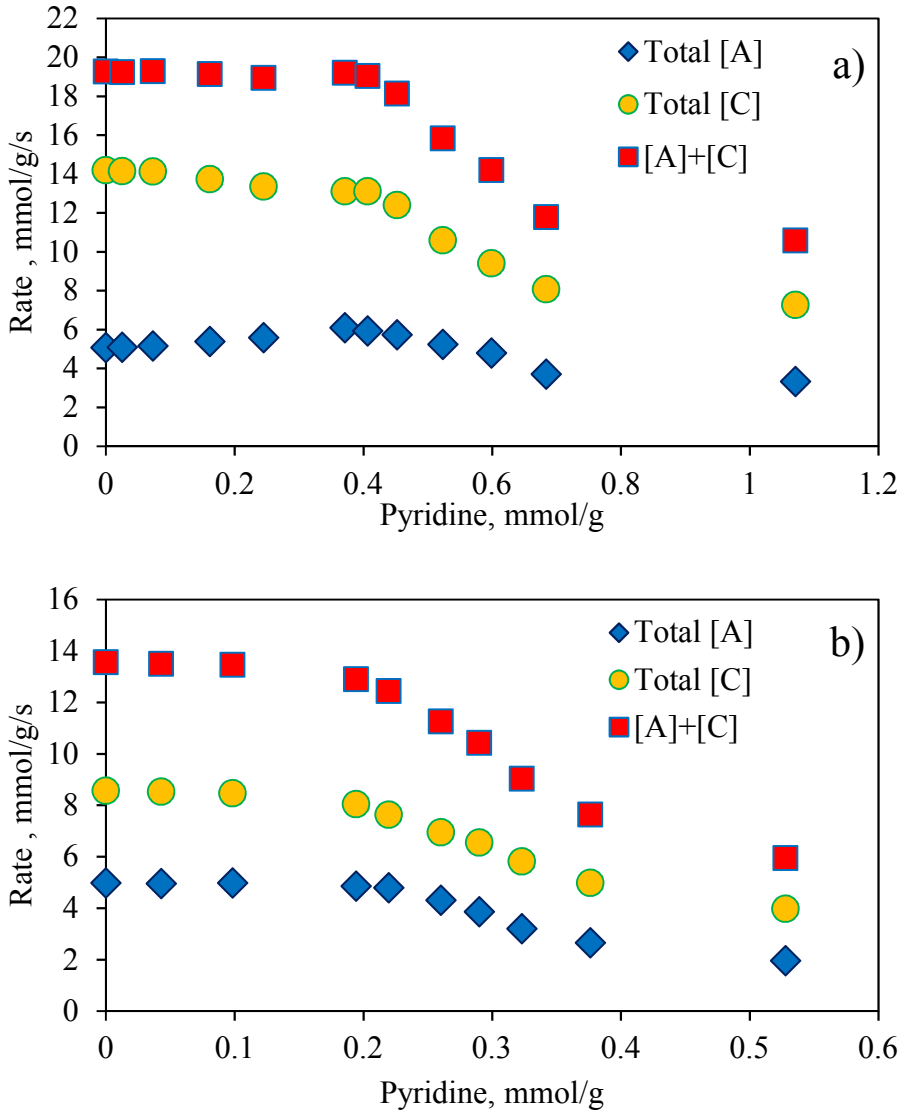

Figure 5. 5 The formation rate of aldol adducts with increasing amounts of pyridine added over HZSM-5 zeolite a) Si/Al=15 and b) Si/Al=40

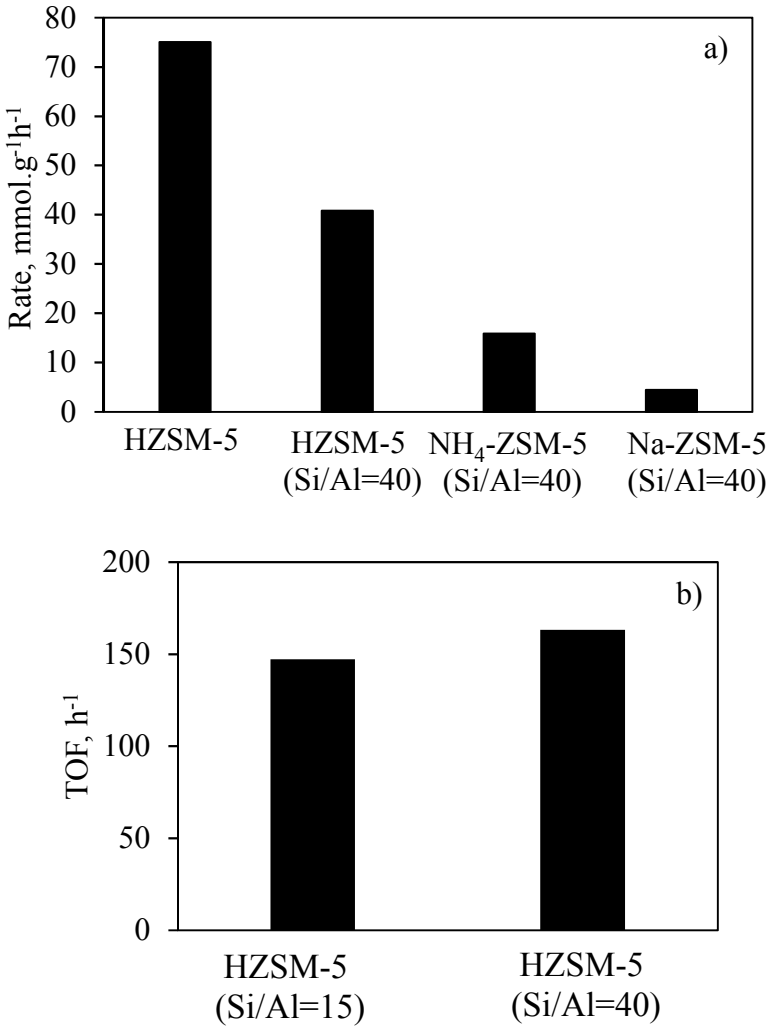

Figure 5. 6 a) Catalytic activity comparison of different zeolites (NH_4-ZSM-5 catalyst was used as provided from Zeolyst) **b)** TOF for aldol adduct formation on HZSM-5 zeolites (per H^+)

5.3.3 The role of mass transfer limitation and acid density of HZSM-5 zeolites on the cross- and self- selectivity

The product distribution of the aldol adducts on HZSM-5 (Si/Al=40) dramatically changed as the system transitioned from the mass transfer to the surface reaction regime. Specifically, the reaction favors the formation of [C]A and [A]A in the mass transfer limitation region then switches to [C]C and [A]C in the surface-reaction controlled

regime (**Figure 5.7**). On the other hand, HZSM-5 (Si/Al =15) initially yielded higher [C]C and [A]C and the selectivity of those dimers kept increasing until the system reached the regime transition point. Above this point, both [C]A and [A]C decreased due to the reduced number of the kinetically relevant sites (**Figure 5.8**).

The mass transfer limitation could tailor the product selectivity by controlling the availability of each reactant surrounding the activated enols, based on their different diffusivities in the pore. In fact, a smaller molecule such as acetone would have higher diffusivity than cyclopentanone. For the lower acid density HZSM-5 (Si/Al=40) with fewer numbers of active sites located on the exterior area, both A and C have to diffuse deep into the inner pore. Due to the higher diffusivity of A, the local concentration of A in the inner pore should be higher than C, resulting in [C]A>[C]C and [A]A>A[C]. However, when the system is controlled by the surface reaction regime, [C]C and A[C] are more favorable thanks to an equivalent local concentration of acetone and CPO.

For a higher acid density HZSM-5 (Si/Al=15), because of a higher amount of the exterior active sites, the local concentration of A and C around the activated enols is comparable, leading to [C]C > [C]A and [A]C > [A]A. The product distribution does not considerably change in the surface reaction regime. The coupling of the enols with C at the equivalent A and C local concentration is easier, which might be caused by the charge stabilization effects of the ring and/or the enhanced Van der Waals interaction of the ring with the surface. DFT calculations are being processed to give some fundamental insights into the results. Favorable enol-CPO coupling has also been observed in other catalyst systems such as MgO.

It is important to address why the product distribution changed with an increasing amount of pyridine on HZSM-5 (Si/Al=15) in the mass transfer limitation regime, but such behavior was not observed on the lower acid density zeolite. It is hypothesized that:

- The acetone is more favorably adsorbed on the surface, leading to favor Langmuir-Hinshelwood mechanism for the enol-acetone coupling
- Even though the surface is dominantly occupied by the adsorbed acetone, the capture of CPO in the bulk phase (Eley-Rideal mechanism) by the enols is still easier due to the more energetically favorable enols-cyclopentanone coupling step

In the light of those assumptions, on HZSM-5 (Si/Al=15), the reduced amount of the acid sites (Brønsted or/and Lewis), especially the ones on the exterior area, caused by the pyridine titration could decrease the concentration of the adsorbed acetone, leading to the more favorable [C]C and [A]C formation. In fact, our adsorption experiments have demonstrated that the acetone uptake is 2 times higher than that of cyclopentanone on both zeolites at room temperature (**Figure 5.9**). Even though the uptake value should be different at the reaction temperature (250^{o}C), it is expected that the more favorable adsorption of acetone on the catalyst surface is still valid. On HZSM-5 (Si/Al=40), due to the lower active sites on the exterior area, the rate of pyridine deactivation might be slower as pyridine has to diffuse into the inner pores. The lower diffusivity of pyridine compared to A and C might cause such delay in the change of product selectivity observed in the mass transfer limitation regime. Moreover, the higher local concentration of acetone in the inner pore could facilitate the enols-acetone coupling.

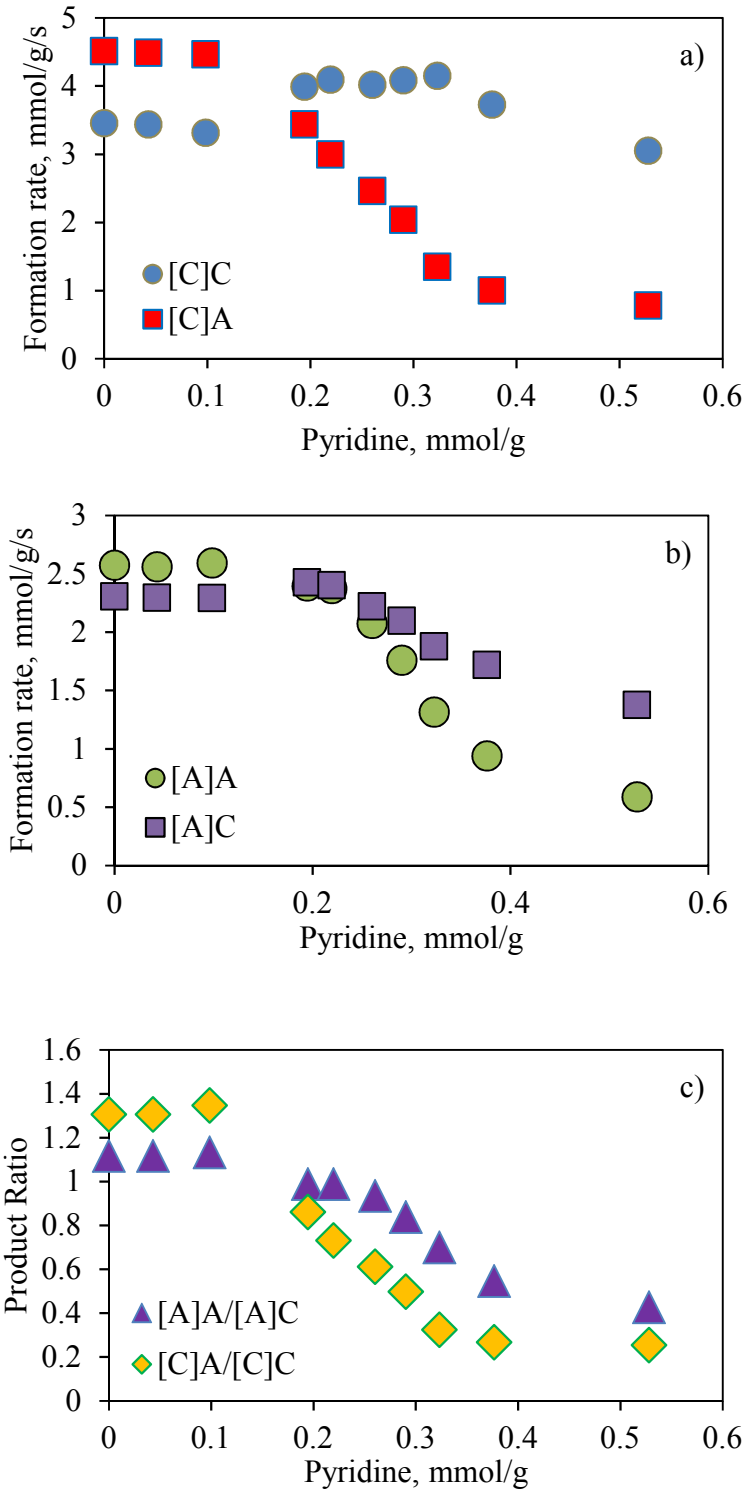

Figure 5. 7 The formation rate of a) [C]C and [C]A products and b) [A]A and [A]C products and c) Product selectivity between the coupling of the enolates ([A] and [C]) with A or C at different amounts of pyridine over HZSM-5 40

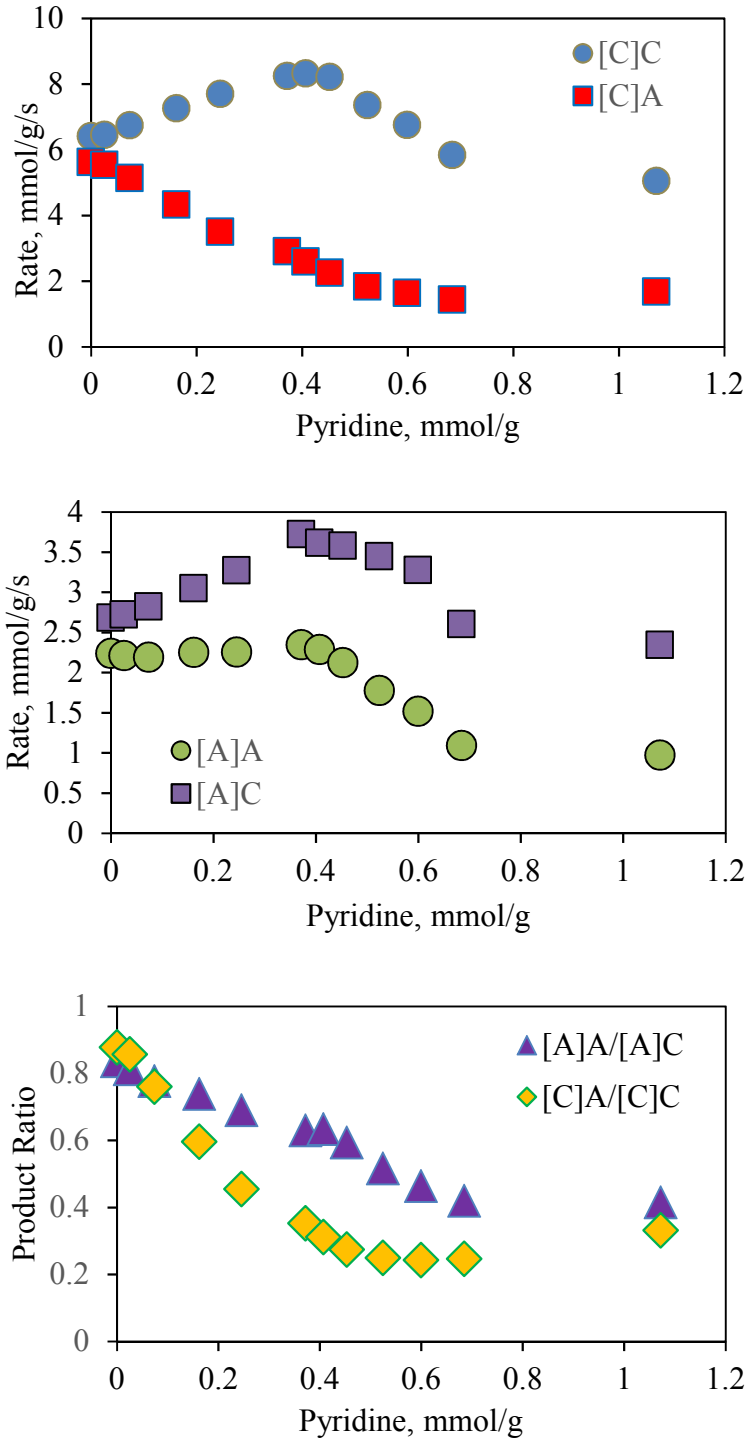

Figure 5. 8 The formation rate of a) [C]C and [C]A products and b) [A]A and [A]C products and c) Product selectivity between the coupling of the enolates ([A] and [C]) with A or C at different amounts of pyridine over HZSM-5 15

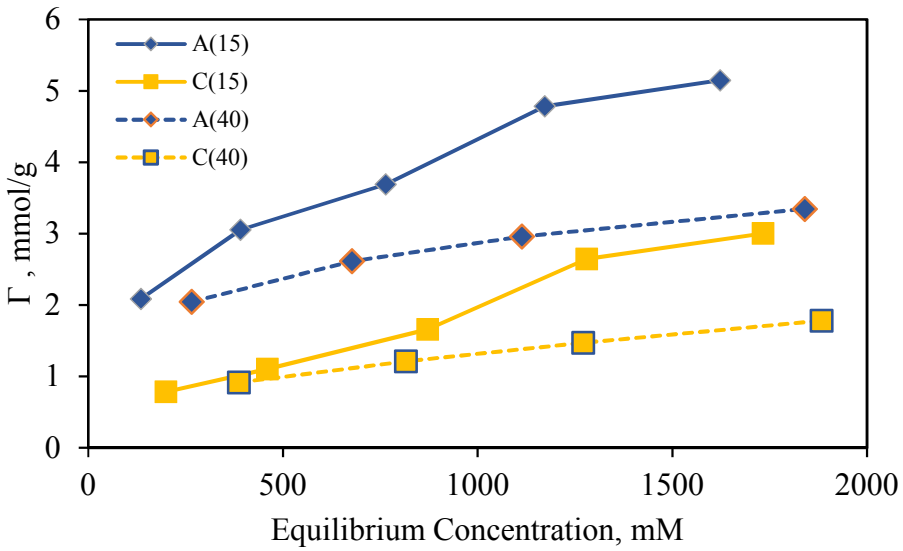

Figure 5. 9 Acetone and Cyclopentanone uptake on HZSM-5 (Si/Al=15 and 40). A(15) and A(40) stand for the adsorption of acetone on HZSM-5 with Si/Al=15 and 40, respectively. C(15) and C(40) stand for the adsorption of cyclopentanone on HZSM-5 with Si/Al=15 and 40, respectively

5.4 Conclusion

The enol formation has shown to be the rate limiting step for the aldol condensation of cyclopentanone and acetone on HZSM-5 zeolites, manifested by the 1st order dependence of the condensation rates on the ketone concentrations. Since both Brønsted and Lewis acid sites coexist on the zeolites, the Brønsted ones are more likely to be the most kinetically relevant, which directly tautomerizes the ketones to form the enols. However, the involvement of the Lewis sites cannot be completely ruled out, which requires further investigation.

The selectivity toward cross- or self- aldol condensation could be manipulated by tailoring the local concentration of the reactants in the inner pore via controlling reaction regimes (mass transfer limitation or surface reaction). Acid density and the adsorption of

the reactants on those sites have shown to be the crucial factors that govern the selectivity. Even though the pyridine titration provides a useful tool to examine the mass transfer/surface reaction regimes, the method still has some weaknesses. A few of those are the non-selective titration on both Brønsted and Lewis acid sites; and the competitive diffusivity of pyridine with other reactants that could greatly affect the catalytic performance.

Chapter 6 - The Effects of Water on the Rate of C-C Coupling and Dehydration Reactions

6.1 Introduction and Literature Review

Water has been one of the most abundant components in biomass conversion [130, 252-254]. However, the use of water as a solvent for subsequent bio-oil upgrading is not practically feasible due to the low solubility of oxygenates generated from the biomass thermal treatment in an aqueous phase. An organic solvent, on the other hand, has been shown to be beneficial for lignocellulosic biomass conversion [255-257]. Depending on the amount of an aqueous phase existing in an organic phase, water can be considered as a co-solvent as in the biphasic system [132, 258, 259] or an impurity that could potentially yield different effects on the catalytic performance as well as product selectivity as widely reported on many catalyst systems including oxides [260, 261], zeolites [262, 263] and metals [264-268].

The rate enhancement effect of water has been previously reported by Breslow *et. al* back in 1983 for the Diels-Alders reaction in the absence of catalysts. The authors observed that when water was used as a solvent, the coupling rate was dramatically enhanced compared to when other organic solvents were employed [269-272] (**Table 6.1**). For example, the measured rate constant of cycloaddition of N-ethylmaleimide and hydroxymethylanthracene at 45^{o}C in water was 200 times higher than that in acetonitrile [269]. The phenomenon has been explained in terms of "enforced hydrophobic interactions" which occurs when non-polar species favor to associate with each other at

the transition state to minimize the interfacial hydrocarbon-water surface with the surrounding aqueous phase [269]. Engberts *et al.* have later shown that the free energy of activation (at 25°C) for the Diels-Alder reaction of cyclopentadiene with different dienophiles decreased with an increasing molar fraction of water in C_1-C_4 alcohol solvents (**Figure 6.1a**), divided into three different regions: alcohol-rich solutions, non-ideal alcohol-water mixture and highly aqueous solutions [273].

Table 6.1 Second-order rate Constants for the Diels-Alder Reaction of 1,3-Cyclopentadiene with Methyl Vinyl Ketone in Various Solvents. Reproduced with permission from Ref[272]

Solvent	Rate constant; k x 10^5 M^{-1} s^{-1} (20°C)	Ref
Iso-octane	5.94 ±0.3	[269]
Methanol	75.5	
Water	4400±70	
Formamide	318±4	[272]
Ethylene glycol	480	

In the highly aqueous solution region (water molar fraction ~1) (**Figure 6.1b**), upon the addition of a small amount of apolar solvent (the alcohols), water became more organized due to the formation of hydration shells surrounding the apolar molecules. This is associated with a higher entropy loss ($-\Delta S^{TS}$) compensated by a decrease in the activation enthalpy (ΔH^{TS}). With more apolar species added to the solution (non-ideal alcohol-water mixture), highly dynamic clusters of apolar molecules was formed and consequently, the cycloaddition TS was more likely to be solvated by the apolar cosolvent. Up to this point, water started losing its aqueous character as well as the enforced hydrophobic effect, manifested by a dramatic increase of the activation free energy (ΔG^{TS}). At high alcohol content (alcohol-rich solutions), the rate gradually

decreased as the mixture approached the apolar solvent [273]. The proposed enforced hydrophobic effect was further solidified by observed chaotropic/antichaotropic effects (or salting-in/salting-out effects). A substance is chaotropic when upon addition, it increases the solubility of hydrocarbons in water by reducing the hydrophobic effect of water. In contrast, a substance that decreases the water solubility of hydrocarbons is called an antichaotropic agent. It has been reported that the addition of a chaotropic salt such as guanidinium chloride to water decreased the rate of the addition of N-ethylmaleimide to anthracene-9-carbinol by 3 times whereas a 2.5 -folds rate increase was observed with an antichaotropic salt such as lithium chloride [272]. Besides, the rate enhancement effect by water could be explained in term of the aggregation processes [274] and the high internal pressure of water [275, 276].

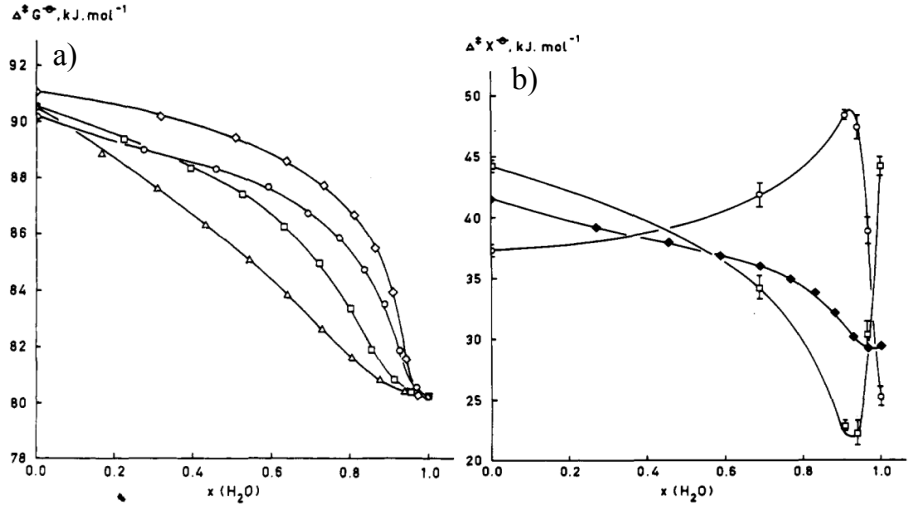

Figure 6. 1 a) Free energy of activation (25°C) for the Diels-Alder reaction of cyclopentadiene with alkyl vinyl ketones in the mixtures of water and methanol, ethanol and 1-propanol and 2-methyl-2-propanol as a function of the mole fraction of water b)Activation parameters (25°C) for the Diels-Alder reaction of cyclopentadiene with 5-hydroxy-1,4-naphthoquinones as a function of the mole fraction of water in the mixture

of water with 1-propanol: ΔG^{TS}, ΔH^{TS} and ΔS^{TS}. The values of ΔG^{TS} have been displaced downward by 40 $kJ.mol^{-1}$. Reproduced with permission from Ref [273]

The positive effects of water have been observed in several metallic catalyst systems [260, 268, 277-280] . For instance, Wang *et al.* have proposed that an appropriate amount of water could effectively enhance the hydrogenation activity of metallic sites Rh as well as the acidity of HY zeolites for the ring opening of naphthalene over Rh_2O_3/HY. Too much water, in contrast, decreases the catalytic activities due to the competitive adsorption of water on the catalyst surface [260]. In another study, water in a condensed phase has proved to be beneficial for Fischer-Tropsch reaction over Ru/carbon nanotube nanohydrid catalysts (**Figure 6.2**) [268]. In this case, liquid water might act as a more effective H-shuttle promoter than the adsorbed one on the surface, leading to a higher measured rate. Liquid water with higher degrees of freedom might easily accommodate the H atom at the most energetically favorable configurations. Moreover, the higher residence time of liquid water with adsorbate (*H) on the surface can also assist the H-transfer process [268]. The enhanced activity of FTS in the presence of water has also been ascribed to a reduced energy barrier of the CO dissociation step due to the water-CO interaction [277-279] or the oxidation of low coordination sites or surface reconstruction [280].

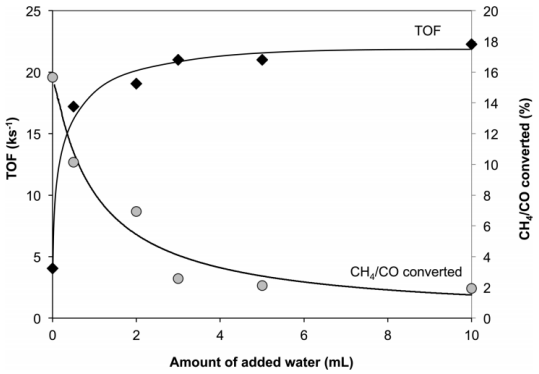

Figure 6. 2 Evolution of TOF and methanation as a function of initial amounts of liquid water added into decalin, keeping a total of 30ml of solvents. Reaction condition: T=473.15K, t=2h, syngas ratio $H_2/CO=2$. Reproduced with permission from Ref [268]

On zeolites, the exposure of the catalysts to vapor water can lead to a rate enhancement as observed in the alkylation of toluene with iso-butylene [263]. Water has been reported to be able to dissociatively adsorb on strong Lewis sites to produce new Brønsted acid sites, resulting in a higher catalytic activity [260, 281-285]. Moreover, water could retard deactivation by preventing coke formation. However, exceeding water contents lead to the passivation of Brønsted acid sites or capillary condensation [281]. Other studies have also stated that a minor amount of water promotes the catalyst activity while excess water reduces it [261, 263, 286, 287].

Several extensive studies have demonstrated that the interaction of water molecules with Brønsted acid sites of zeolites could generate different species on the surface such as hydronium ion H_3O^+ [288, 289], hydrogen-bonded form [290, 291], partially protonated form [292] or both hydronium ion form and hydrogen-bonded form coexisting on zeolite surfaces [293-295]. ^1H solid-state NMR study on HZSM-5 with different water contents have shown that water molecules can rapidly diffuse and hope between acid sites, thus easily participate in the proton exchange process with the Brønsted acid sites

[262]. The role of water is to accelerate the proton transfer by simultaneously interacting with the reactants and the acid sites via H-bonding to form a bimolecular-transition state with a lower energy barrier, ending up an increase in the C-H activation rate by a factor of 10 at the value of 1 water molecule per proton. Higher water loadings (2-3 water molecules per active site) promote the formation of thermodynamically favorable water clusters on the acid sites. According to the authors, the active role of water is to stabilize the transition state for those reactions that involve the participation of hydrophobic reactants [262].

Recently, DFT calculations on MFI-5 have demonstrated that two Brønsted acid sites in close proximity could substantially enhance the adsorption energy of a water molecule via a stronger H-bonding between water and the acid sites [296]. The increased interaction of water may result in the thermodynamically favorable delocalization of a proton of the acid pair (**Figure 6.3**). This results in a formation of a hydronium ion H_3O^+ which acts as a new acid site. The authors have suggested that the delocalization/deprotonation effect could be further enhanced with a larger water cluster, leading to a generation of a mobile proton network inside zeolite pores [296]. In fact, several previous studies on the adsorption of water on zeolites have observed such formation of protonated water clusters constituting of 4-5 water molecules [297-299].

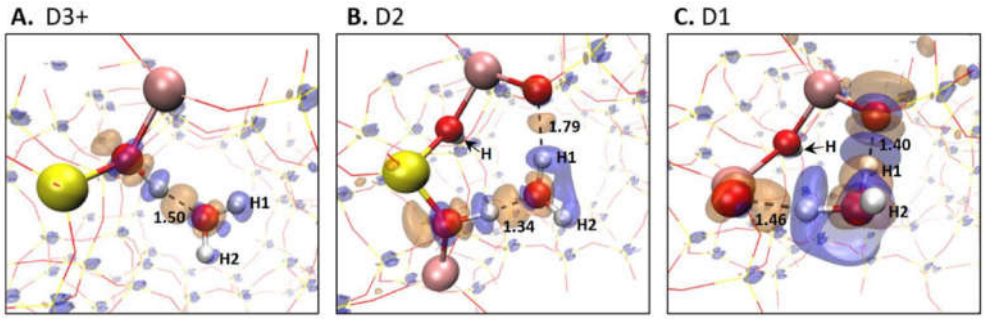

Figure 6. 3 Adsorption-induced changes in electron densities are shown with the orange portions being areas of electron density accumulation and blue areas of electron density depletion. The isosurface used to plot the charge density difference is ±0.03e A^{-3}. D3+, D2 and D1 are different distances between two adjacent Brønsted acid sites with the following order: D3+ > D2 > D1. Reproduced with permission from Ref [296]

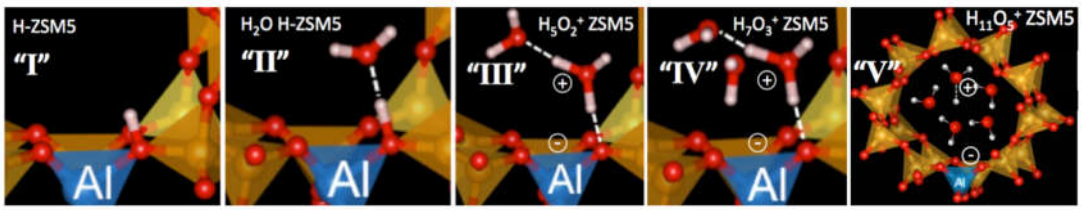

Figure 6. 4 DFT-optimized structures illustrating the process of hydrating the zeolite with increasing numbers of water molecules. For two or more water molecules, the proton dissociates from the T-site forming a hydronium ion with increasing degrees of hydration. The structure assignments of I, II, III, IV, and V are the species discussed in the interpretation of the XANES and IR spectra. The $H_9O_4^+$ species (not shown) is structurally similar to V. Reproduced with permission from Ref [300]

DFT calculations from Lercher's group have stated that a water cluster of at least 3 molecules can deprotonate a proton on tetrahedral Al group to form a network of hydronium cation (H_3O^+) with the properties close to a homogeneous H^+ [300] (**Figure 6.4**). Interestingly, it has been reported that in a confined environment such as in zeolite pores, where pronated water clusters are formed, a complete association of the hydronium ions with cyclohexanol is established. That is, all of the hydronium ion is associated with cyclohexanol inside the confined pores, manifested by the observed zero-order

dependence of the dehydration rate on the cyclohexanol concentration. In a homogeneous acidic solution, the first-order dependence of the dehydration rate on cyclohexanol concentration was observed. Experimental data indicated a much higher dehydration rate of cyclohexanol in the zeolite pores compared to that in the bulk H^+ solution (**Figure 6.5**). Furthermore, activation enthalpies, entropies and free energies at 443K calculated from the kinetic analysis and the transition state theory have shown that a lower activation free energy in the case of MFI and BEA compared to that in soluble acids is due to either lower activation enthalpy (MFI) or higher activation entropy (BEA) (**Table 6.2**). This is a typical compensation effect where the smaller pore zeolite (MFI) could further stabilize the TS, reducing the activation enthalpy but at the same time, increasing entropy loss due to a tighter TS. The opposite situation is expected in the larger pore zeolite (BEA) where a looser TS is formed. The combination of lower activation free energy and high coverage in MFI and BEA yields a substantially higher TOF compared to the homogeneous acids. The higher TOF in the case of FAU is only due to the better association of the hydronium ion with the alcohols [301, 302].

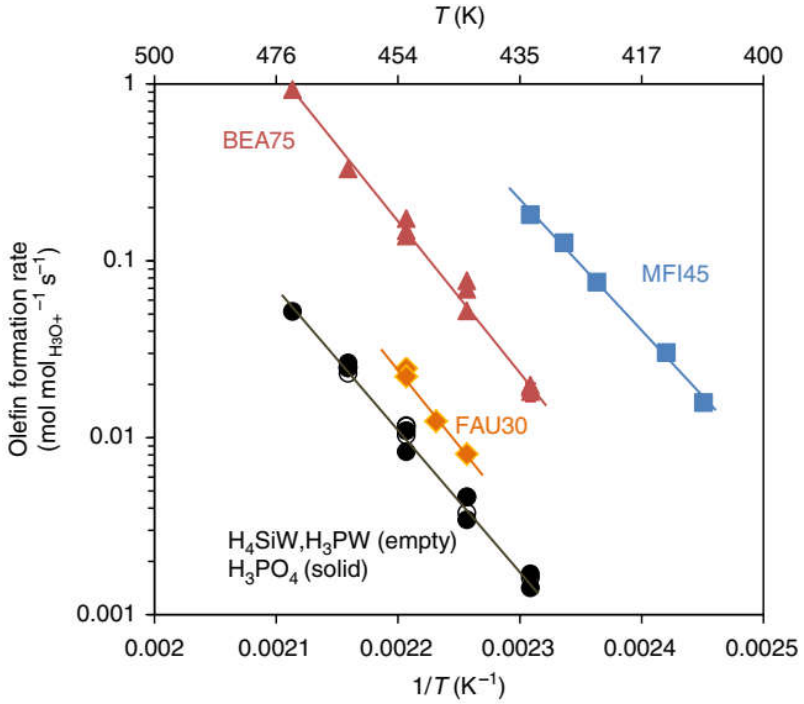

Figure 6.5. Measured turnover frequencies of cyclohexene formation in the aqueous-phase dehydration of cyclohexanol on different acid catalysts. For zeolites, the Si/Al ratio is denoted as the number following the framework-type code. H_4SiW and H_3PW stand for tungstosilicic and phosphotungstic acids. Rates were determined at conversion <10%. Solid lines are fits to the Arrhenius equation (note that the slopes are not identical). Reproduced with permission from Ref [301]

Table 6.2 Intrinsic activation parameters for the aqueous-phase dehydration of cyclohexanol.*Reproduced with permission from Ref [301]

Catalyst	$\Delta H^{o\ddagger}$ (kJ mol^{-1})	$\Delta S^{o\ddagger}$ (J mol^{-1} K^{-})	$\Delta G^{o\ddagger}_{443K}$ (kJ mol^{-1})
MFI	140 ± 5	62 ± 10	112 ± 1
BEA	159 ± 4	87 ± 9	120 ± 1
FAU	166 ± 4	88 ± 10	127 ± 1
Soluble acids	154 ± 4	68 ± 8	124 ± 1

*Standard enthalpies, entropies and free energies of activation (at 443 K) on zeolites and homogeneous acids, derived from kinetic measurements and the transition state theory formalism. The error bars for $\Delta H^{o\ddagger}$ and $\Delta S^{o\ddagger}$ represent the 1-σ s.d.'s, while the error bar for $\Delta G^{o\ddagger}$ represents the maximum error rounded up to the nearest integer (error analysis protocol detailed in Supplementary Methods).

Based on the information collected from the literature, we investigate, in this study, the effects of water on the catalytic performance of HY zeolite and functionalized

MCM41 for C-C coupling reactions. We have found that water has both negative and positive effects on the catalytic performance. As discussed previously in **Chapter 4** that liquid water can accelerate the leaching process on the functionalized MCM-41 catalysts. We have also found out that HY zeolite, upon being exposed to vapor water, also quickly deactivates without showing any enhancement effect. On the other hand, functionalized MCM-41 synthesized by the high grafting temperature method has displayed an enhanced activity for the alkylation reaction upon water addition. Later on, to fundamentally examine the water effects on acid catalysts, a simpler reaction such as dehydration of cyclohexanol in different solvents over HZSM-5 zeolites was chosen as a probe reaction.

6.2 Experimental Methods

6.2.1 Chemical and materials:

Zeolite NH_4ZSM-5 CBV 2314 (Si/Al=11.5) and CBV 8014 (Si/Al=40) were obtained from Zeolyst. Before used, the zeolites were calcined at 600^{o}C for 5 h in 150ml/min air flow to produce H^+ form. As-received mesoporous MCM41-Type A was dried at 120°C for 12 h under N_2 flow (99.999%, Airgas) prior to further treatment or use. MCM41 functionalized with sulfonic acid groups (MPTS) was synthesized via the high-temperature grafting method as described previously in Chapter 4 (denoted as MCM41-SO_3H-HG).

Cyclopentanone (>99%), cyclopentanol (99%), m-cresol (99%), decahydronaphthalene, mixture cis + trans (99%) (Sigma-Aldrich) and cyclohexane (HPLC grade, >99.9%) were obtained from Sigma Aldrich. Cyclopentanone was distilled

to remove impurities before used while other chemicals were employed as provided. Water (HPLC grade) was obtained from Fisher Chemical and used as provided.

6.2.2 Catalytic reaction measurements:

The self-aldol condensation of cyclopentanone over MCM41-SO_3-HG was carried out in a Parr reactor at 250^{o}C, V_{total}=120ml, 500psi N_2 pressure in cyclohexane solvent over 0.15 g MCM41-SO_3H-HG (0.353 mmol H^+/g), at an initial concentration of cyclopentanone of 900 mM. At first, 90ml of cyclohexane and the catalysts were placed in a stainless steal vessel. A 30ml mixture of cyclopentanone and cyclohexane was placed inside a feeding cylinder. After the reactor temperature reached 247^{o}C, the feed was injected into the reaction mixture. The temperature was stabilized at 250^{o}C after 5 minutes and the reaction time started to be counted.

The alkylation of cyclopentanol (CPOL) and m-cresol was conducted in a Mini Bench Top Parr high-pressure reactor (Model Parr 4564) equipped with a Parr 4848 Reactor Controller. Reactant concentrations of 1.0 M m-cresol and 0.5 M cyclopentanol (CPOL) were used in decalin solvent or as a pure m-cresol/CPOL mixture of 2:1 molar ratio. The reaction set up was conducted similarly to the aldol condensation as described above.

The product mixtures were analyzed by Shimadzu QP2010S gas chromatograph/mass spectrometer (GC-MS) and quantified by GC-FID Agilent 6890 equipped with a flame ionization detector for quantification. Both GC's were equipped with a Zebron ZB-1701 column with dimensions of 60m x 0.25 mm x 0.25 μm.

For the alkylation reaction, the conversion of CPOL (X), yield of a product (Y_i), and carbon balance ($C_{balance}$) were calculated as follows:

$$X = \frac{C_{CPOL-in} - C_{CPOL-out}}{C_{CPOL-in}} \quad Y_{CPOL \rightarrow Pi} = \frac{C_i \times n}{C_{CPOL-in}} \quad C_{balance} = \frac{C_{CPOL-out} + C_{CPOL \rightarrow P}}{C_{CPOL-in}}$$

$C_{CPOL\text{-}in}$ and $C_{CPOL\text{-}out}$: Initial and remaining concentration of CPOL (mM)

C_i and n_i : Concentration of the product i (mM) and the corresponding stoichiometric number

C_{in} and C_{out}: Initial and remaining amount of carbon existing in the system (mM)

For the aldol condensation reaction, the conversion of cyclopentanone (X_{CPO}), yield of a product were calculated as:

$$X_{CPO} = \frac{C_{CPO-in} - C_{CPO-out}}{C_{CPO-in}}; \; Y_i = \frac{C_i}{C_{CPO-in}}$$

The formation rate of a product r_i (mmol.g^{-1}.s^{-1}) and turnover frequency TOF (s^{-1}) were calculated as

$$r_i = \frac{n_i}{m_{cat} \times t}; TON = \frac{n_i}{m_{cat} \times d_{H^+} \times t}$$

The carbon balance for the aldol condensation reaction was calculated as:

$$C_{CPO-bl} = \frac{C_{CPO-out} + C_{CPO \rightarrow P}}{C_{CPO-in}}$$

where $C_{CPO(in,\ out)}$: Concentration of cyclopentanone before and after reaction (mM);

$C_{CPO \rightarrow P}$ and C_i: Concentration of CPO convered to detectable products and the concentraiton of a product (mM);

n_i: Number of Mol of a product (mmol)

m_{cat}: mass of a catalysts (g)

d_{H+}: acid density measured from TGA (mmol/g)

t: Reaction time, (s)

6.3 Results and Discussions

6.3.1 The rate enhancement effects of water on alkylation and aldol condensation reactions

Figure 6.6 presents the rate enhancement effects of water observed on zeolites and MCM41 for the alkylation reactions of cyclopentane and m-cresol. The presence of vapor water increased the formation rate of coupling products up to 2 folds. As the liquid water started to form, the catalytic activity substantially dropped due to the rapid deactivation (structure damage/collapse) or mass transfer limitation caused by a thin liquid film of water on the surface. The results are in agreement with the literature [260, 261, 263, 286, 287].

From Arrhenius plot, the apparent activation enthalpy and entropy of the alkylation reaction in the presence water vapor could be estimated (**Figure 6.7a** and **Table 6.3**). The result shows that as the amount of water increases, both the apparent activation enthalpy (ΔH_{app}) and the apparent activation entropy (ΔS_{app}) increase. The observed behavior suggests the typical compensation effect between an enthalpy gain and an entropy loss of a transition state (TS). Water reduces the entropy loss of the transition state by rendering it more mobile but consequently increases the activation barrier of the rate limiting step due to a looser-interaction of the TS with the active site. As the result, a lower apparent activation free energy (ΔG_{app}) leads to a higher alkylation rate in the presence of vapor water.

Table 6. 3 Apparent activation enthalpy and entropy of the alkylation reaction under the presence of water (calculated from Arrhenius plot in **Figure 6.7a**)

n/n_0	ΔH_{app}, kJ/mol	ΔS_{app}, kJ/mol
0	20.7	-178.5
0.45	26.9	-163.1
0.66	32.4	-150.5

Higher mobility of the activated complex suggests a hypothesis that water might form a bridge between an acid site and the TS via participating in the cyclopentene activation process or m-cresol adsorption, which could facilitate the proton transfer between the acid sites and the reactants. This water-assisted proton transfer process would give more freedom (configurations) to the transition state, leading to the lower entropy loss. Breslow *et al.* have reported similar activation enthalpy and entropy changes when a small amount of water was added into alcohol solvents for Diels-Alder reactions [273].

Similar behavior was observed for the self-aldol condensation of cyclopentanone on MCM41-SO_3-HG in decalin solvent (**Figure 6.7b**), in which the measured condensation rate was initially enhanced in the vapor region. However, once the liquid water started to form, the condensation rate decreased due to the deactivation/leaching or mass transfer limitation caused by the liquid films on the surface. On the other hand, HY zeolite suffered an instant deactivation even when exposed to vapor water. In this case, the hydrophobization is crucial to improve the catalyst resistance against water.

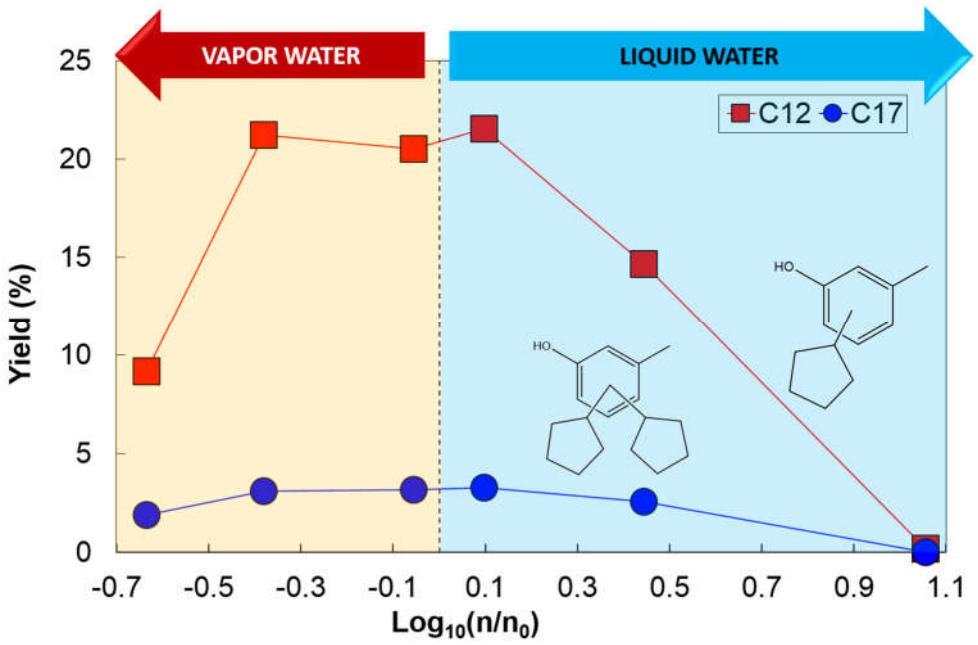

Figure 6. 6 The rate enhancement effect of water on the alkylation of cyclopentene and m-cresol. Reaction condition: m-cresol/CPEN=2:1, C_{CPEN}=0.5M, solvent: decalin, temperature: 200°C, pressure: 800 psia N_2, reaction time: 2h, mass of MCM41-SO_3H-DG catalyst: 150mg; (n_0: the amount of water needed to reach the saturation point where water starts to form liquid phase; n: the amount of water added to the system. At the value of n/n_0=1, the system reaches the saturation point).

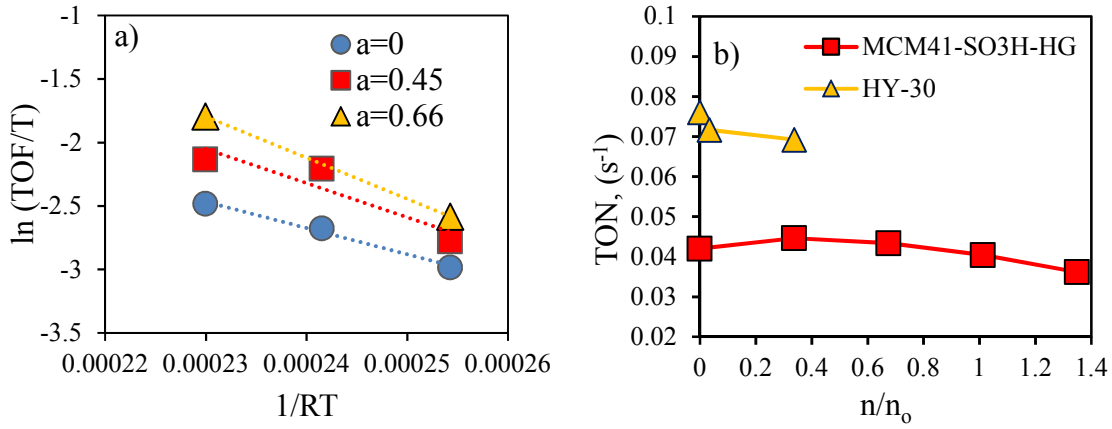

Figure 6. 7 a) The Arrhenius plot for the alkylation reaction with different amounts of vapor water b)The effect of water on the measured rate of the aldol condensation of CPO on different catalysts

6.3.2 The effects of water and solvents on the dehydration of cyclohexanol

C-C coupling reactions could generate a wide range of condensated products, possibly causing catalyst deactivation, especially in the presence of water. In that way, a fundamental investigation on the nature of water enhancement effect could be problematic. Therefore, a simpler and more robust reaction that only involves a single reactant and a corresponding product is desirable. In this study, the dehydration of cyclohexanol over HZSM-5 zeolites with different Si/Al ratios (40 and 11.5) in water and decalin solvents was chosen.

Acid density quantification on zeolites by pyridine titration

First, the acid density of HZSM-5 was determined by the pyridine titration in water solvent. A linearly decaying rate with an increasing amount of pyridine added indicates that the reaction is in a kinetically controlled regime (**Figure 6.8**). The extrapolation of the fitting line allows the acid density quantification of HZSM-5 zeolites, which is shown in **Table 6.4**. Even though the values determined from pyridine titration are deviated from the one obtained from IPA-TPD, a strong agreement could be seen on the effect of Si/Al ratio on the acid density of the zeolites. The value from the pyridine titration will be used for further analysis.

Table 6. 4 Acid density of HZSM-5 quantification by IPA-TPD and Pyridine titration

Cat	Density (Titration), mmol/g	Density (TPD), mmol/g
HZSM-5 11.5	0.645	1.01
HZSM-5 40	0.249	0.4

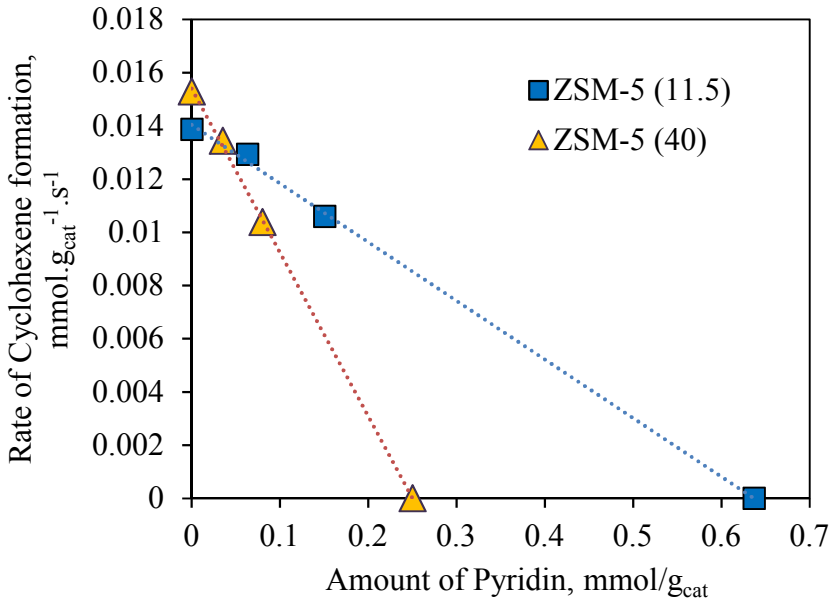

Figure 6. 8 Pyridine titration on the HZSM-5 zeolites for cyclohexanol dehydration in water solvent. Reaction condition: 0.32M cyclohexanol, 150°C, 730psi H_2, water solvent

Dehydration activity of HZSM-5 zeolites and homogeneous H_3PO_4 acid

Catalytic activities of HZSM-5 zeolites (Si/Al=11.5 and 40), homogeneous H_3PO_4 catalyst and a physical mixture of H_3PO_4 and silicalite-1 (MFI) are compared in **Table 6.5 and Figure 6.9.** The intrinsic activities per proton (TOF, s^{-1}) of HZSM-5 with Si/Al ratios of 40 and 11.5 are 150 and 50 folds higher than that of the homogeneous catalyst (H_3PO_4). A physical mixture of silicalite-1 and H_3PO_4 exhibited a comparable rate and TOF values with the homogeneous H_3PO_4 solution. Lercher *et al.* have proposed that the confinement in the zeolite pores could significantly enhance the association of the hydronium ions with cyclohexanol, leading to a higher activity of zeolites than homogeneous H_3PO_4 [301, 302]. The addition of silicalite-1 into bulk H^+ solution (H_3PO_4+silicaite-1) was expected to provide such a confinement environment for the protons. However, no detectable effect was observed upon this addition. That means the

incorporation of the homogenous protons into the confined zeolite pores is not sufficient to yield the higher rate as observed in the zeolites. Moreover, it should be noted that the intrinsic activity of the heterogeneous site is two orders of magnitude more active than the homogeneous one, indicating that the intrinsic strength of the proton originated from the zeolite framework is significantly higher than the bulk H^+.

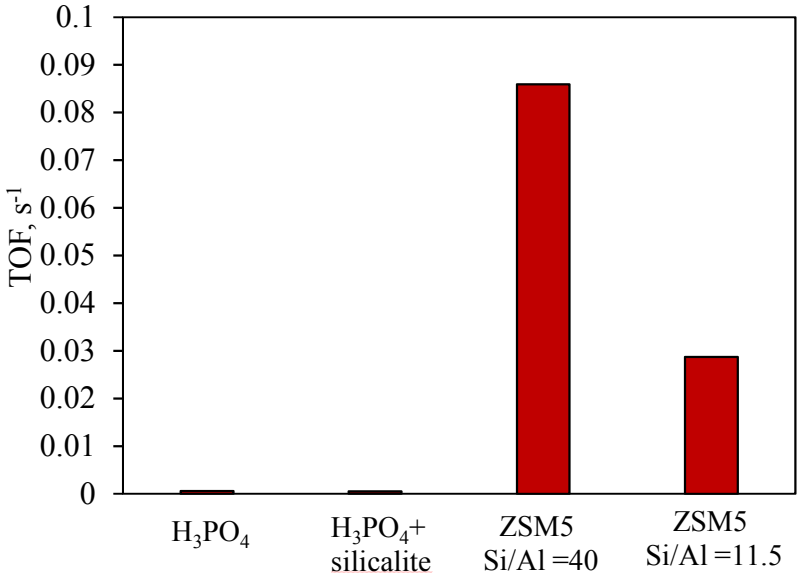

Figure 6. 9 Turnover frequencies of the solid acids and homogeneous acidic solution for the cyclohexanol dehydration in water solvent. Reaction condition: 0.32M cyclohexanol, 150°C, 730psi H_2, water solvent

Table 6. 5 Catalytic activity of HZSM-5 zeolites and homogeneous H_3PO_4 solution in water. Reaction condition: 0.32M cyclohexanol, 150°C, 730psi H_2, water solvent

Cat	**Mass,** mg	$\mathbf{n_{H+}}$, mmol	Conversion, %	Rate, mmol/g/s (x 10^3)	TOF, s^{-1} (x 10^4)
H_3PO_4	29.6	0.257	3.5%	5.05	5.82
H_3PO_4 + silicalite	29.7	0.258	3.13%	4.72	5.44
HZSM-5 Si/Al=40	30	0.0075	7.57%	21.4	859
HZSM-5 Si/Al=11.5	12.3	0.0079	5.05%	18.5	287

Co-feeding sodium chloride into the reaction over HZSM-5 (Si/Al=11.5) also leads to an activity degradation due to the ion exchange of the framework hydroxyl groups (H^+) with Na^+ cations (**Scheme 6.1 and Figure 6.10**). A linear decay of the dehydration rate was observed, confirming that the framework proton is a kinetically relevant site. The acid density of the zeolite extrapolated to the zero-rate point of cyclohexene formation would give an unrealistic huge value. In contrast to the irreversible poisoning of pyridine on Brønsted acid sites, the ion exchange with NaCl is a reversible process, which is much slower. Therefore, a substantially larger amount of NaCl is needed to yield observable effects on the measured dehydration rate.

It is important to point out that the ion exchange process replaces the framework hydroxyl groups with Na^+ cations bound to the framework Al and replenishes the surrounding solution with homogenous protons. That means, the total number of protons in a particular cage is nearly unchanged. The decaying rate observed during the ion exchange process indicates that the intrinsic activity of the homogeneous proton and the hydronium ion originated from the framework hydroxyl group is considerably different, which agrees with the results in **Figure 6.9.**

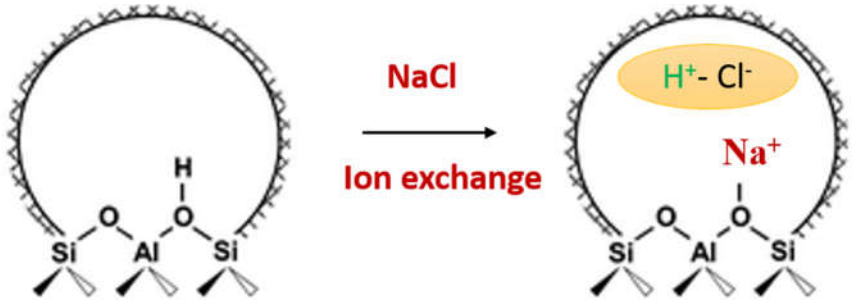

Scheme 6. 1 Illustration of the ion exchange of Na^+ with the framework hydroxyl groups within the zeolite pore

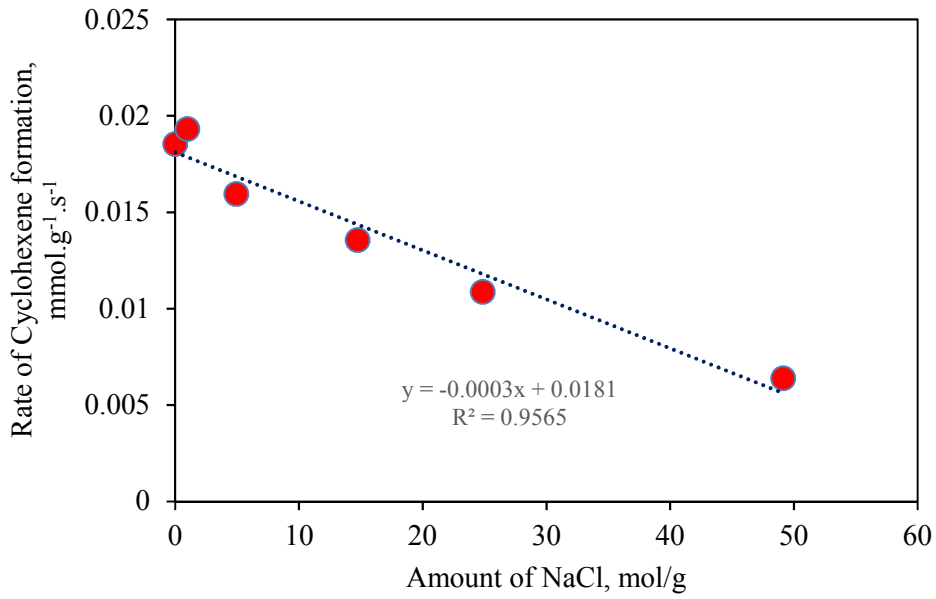

Figure 6. 10 Effects of the ion exchange with NaCl on the rate of cyclohexene formation over HZSM-5 Si/Al=11.5. Reaction condition: 0.32M cyclohexanol, 150°C, 730psi H_2, water solvent

Kinetic and activation parameter analysis for cyclohexanol dehydration

According to the transition state theory assuming that a quasi-equilibrium is established between a reactant and a TS, the rate constant of cyclohexanol dehydration could be written as:

$$k = \frac{k_B T}{h} \times e^{\Delta S^{\ddagger}/R} \times e^{-\Delta H^{\ddagger}/RT} = \frac{k_B T}{h} \times e^{-\Delta G^{\ddagger}/RT} \qquad (6.1)$$

k: rate constant of cyclohexanol dehydration (s^{-1}),

k_B: Boltzmann constant, 1.380648 x 10^{-23} (m^2. Kg. s^{-2}. K^{-1})

h: Planck constant, 6.62607 10-34 (m^2.Kg.s^{-1})

T: Temperature, K

$\Delta H^{\ddagger}$, $\Delta S^{\ddagger}$ and $\Delta G^{\ddagger}$ are the true activation enthalpy, entropy and free energy of the transition state (of the rate limiting step) with respect to the adsorbed cyclohexanol.

The turnover frequency of cyclohexene formation or cyclohexanol dehydration is identified as:

$$TOF = k \times \theta_A \qquad (6.2)$$

θ_A: coverage of cyclohexanol on the catalyst surface or degree of hydronium ion associated with cyclohexanol

From Eqn. (6.1) and (6.2):

$$TOF = \frac{k_B T}{h} \times e^{\Delta S^{\ddagger}/R} \times e^{-\Delta H^{\ddagger}/RT} \times \theta_A \qquad (6.3)$$

$$\ln \frac{TOF}{\theta_A \times T} = \frac{-(\Delta H^{\ddagger})}{R} \frac{1}{T} + \frac{\Delta S^{\ddagger}}{R} + \ln \frac{k_B}{h} \qquad (6.4)$$

A linear relationship of cyclohexene formation rate and initial concentration of cyclohexanol (<300nM) in H_3PO_4 solution indicates 1st order kinetic regime (**Figure 6.11)**. At the higher initial concentration of cyclohexanol, the curve reached a plateau corresponding to the 0th order regime. First-order dependence of the cyclohexene formation rate on cyclohexanol concentration was also observed in the case of the physical mixture of H_3PO_4 and silicalite-1. Lercher *et al.* have reported that the association of hydronium ion with cyclohexanol in H_3PO_4 solution is ~0.16 (in similar studied conditions) [302].

The association enhancement effect caused by the confinement has been proposed to be originated from the significantly higher water-uptake compared to cyclohexanol-

uptake of the zeolite pores. For instance, for 0.32M cyclohexanol solution in water, HBEA zeolite pore contains 1 cyclohexanol molecule together with 180 water molecules, resulting in a unity value of the coverage in this case [302]. Our experimental data shows that in an 0^{th} reaction order was also obtained on HZSM-5 (Si/Al=40) in non-polar solvent (decalin) (**Figure 6.12**). That means, the surface was also saturated even without the presence of water or the formation of hydronium ions. Interestingly, the order of the reaction decreased with an increasing amount of water added into the reaction (**Figure 6.12**). In pure water solvent, the reaction order estimated from the fitting was -0.5. Negative order is normally obtained for a reaction that requires two adjacent active sites which is not likely to be the case for a dehydration reaction. A possible explanation for this behavior is the deactivation which could be accelerated in water solvent. Another possibility is that the non-polar cyclohexene product, once produced, cannot detach from the hydronium ion due to the suppression of the surrounding water solvent. The competitive adsorption of the product could lead to a lower coverage/association of hydronium ion with cyclohexanol and consequently a lower rate at high initial concentration of cyclohexanol. It should be noted that a significant higher TOF was obtained in water compared to that in decalin. Higher concentration of cyclohexene would acceleration the deactivation/inhibition. Further investigation into this matter is needed.

However, up to this point, it is obvious that on HZSM-5, all of the proton either on the surface or in the form of hydronium ion is totally associated with the reactant, manifested by the 0^{th} order regime in decalin solvent. The coverage is, therefore, equal to 1, in agreement with the literature [301, 302]. In water solvent, even the

deactivation/competitive adsorption might occur, the coverage should not deviate much from the unity value. For simplification purpose, the coverage in water solvent is assumed to be 1.

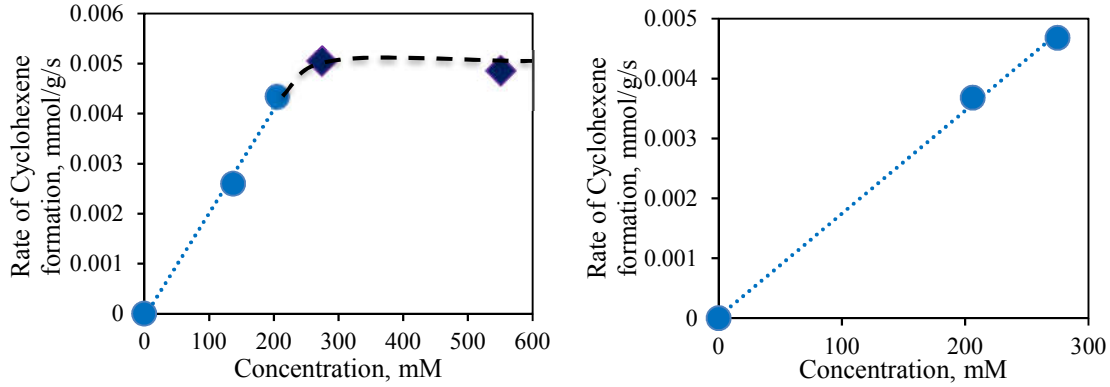

Figure 6. 11 Rate of Cyclohexene formation as a function of cyclohexanol concentration on a) H_3PO_4 and b) physical mixture of H_3PO_4 and silicalite-1. Reaction condition: 0.32M cyclohexanol, 150°C, 730psi H_2, water solvent

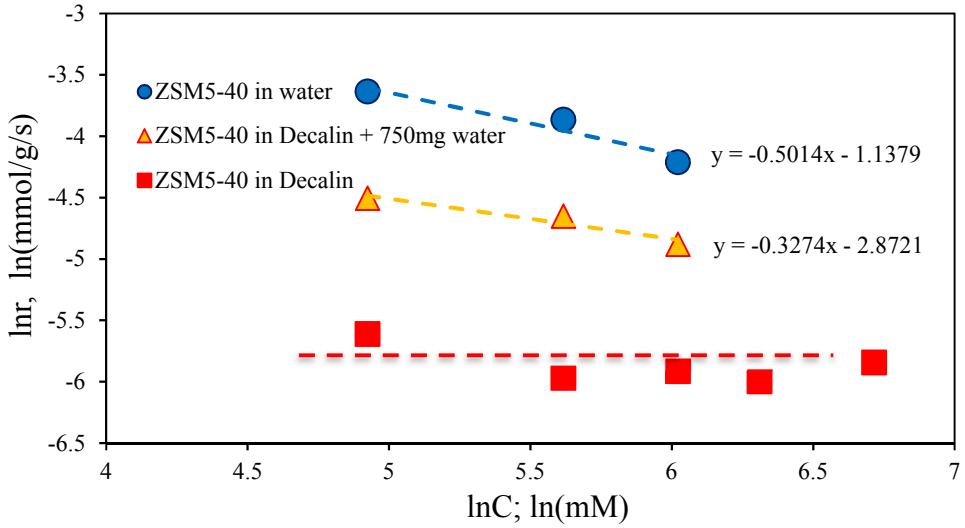

Figure 6. 12. Reaction order of cyclohexanol dehydration over HZSM-5 (Si/Al=40) in different solvents. Reaction condition: 0.32M cyclohexanol, 150°C, 730psi H_2

The true activation enthalpy, entropy and free energy estimated from fitting equation (6.4) with the experimental data are shown in **Table 6.6**. The $\Delta H^{\ddagger}$ and $\Delta S^{\ddagger}$ of the homogeneous H_3PO_4 are 149kJ/mol and 58 J/mol/K, which are close to the value reported by Lercher *et al.* [302]. The addition of silicalite-1 into the acidic solution results in a much lower activation enthalpy and a huge loss of activation entropy. Consequently, both catalyst systems ended up with a very close TOF value. The stabilization of the confinement obviously plays a crucial role in reducing the activation energy as also observed in the solid acid catalysts. Lower activation enthalpies are obtained on HZSM-5 with Si/Al=11.5 and 40, which are 83 and 93 kJ/mol, respectively. A much lower entropy loss in the case of the lower Si/Al zeolite (40) leads to the lower activation free energy and the higher intrinsic rate constant. Up to this point, three important conclusions need to be addressed:

- The addition of silicalite-1 into H_3PO_4 did not yield any detectable effect, indicating that (homogeneous protons + confinement) might be not sufficient to gain the higher dehydration rate as observed in the zeolites;
- The observed unity coverage in zeolites might not be caused by the confinement and higher water-uptake since the 0^{th} reaction order can also be achieved in decalin solvent. The strong adsorption of cyclohexanol on the acid sites is more likely to be the case;
- The confinement effect induced by the zeolite pores greatly reduced the intrinsic activation free energy, resulting in a higher TOF. The hydronium ion originated from the surface is more consequential than the homogeneous one.

That means the confinement effect is only active for the hydronium ion bound to the framework.

Table 6. 6 Intrinsic activation parameters for the cyclohexanol dehydration on different catalysts Reaction condition: 0.32M cyclohexanol, 120-180°C, 730psi H_2, water solvent

Catalysts	H_3PO_4	H_3PO_4 + silicalite-1	HZSM-5 Si/Al=11.5	HZSM-5 Si/Al=40
$\Delta H^{\ddagger}$; kJ/mol [a]	149	57	83	90
$\Delta S^{\ddagger}$; J/mol/K [a]	58	-173	-81	-56
$\Delta G^{\ddagger}$; kJ/mol [a]	124.5	130.1	117.3	113.7
k x 10^4 (150°C), s^{-1}	36.1	5.4	287	860
θ [b]	0.16	1	1	1
TOF x 10^4 (150°C), s^{-1} [c]	5.8	5.4	287	860

[a] Obtained from fitting experimental data with Eyring equation (3). [b] Adopted from Ref [302] [c] Experimental data

Effects of solvent to the catalytic activity of HZSM-5 zeolites with different Si/Al ratios

The change of solvents greatly influenced the rate of cyclohexanol dehydration on HZSM-5 zeolites (**Table 6.7**). In decalin solvent, considerably higher entropy losses were obtained on both zeolites, resulting in a much higher activation free energy. The water obviously rendered the TS more freedoms compared to the non-polar solvent, suggesting the formation of the water bridge between the framework-bound proton and the TS. Interestingly, in decalin solvent, the TOF for the olefin formation on HZSM-5 increased with an increasing amount of water added (**Figure 6.13**). The effect was dramatic in a small range of 0-0.05 water volume fraction (wvf.%). At a higher water content (from 0.05 to 0.25 wvf.%), the rate enhancement was slower, reaching a plateau. Above 0.5 wvf.%, the dehydration rate in the biphasic decalin/water is as high as that in pure water solvent (**Figure 6.13**)

Table 6. 7 Intrinsic parameters and turnover frequencies for the cyclohexanol dehydration on HZSM-5 in different solvents. Reaction condition: 0.32M cyclohexanol, 120-150°C, 730psi H_2, water solvent

Catalysts	HZSM-5 Si/Al=11.5		HZSM-5 Si/Al=40	
	Water	Decalin	Water	Decalin
$\Delta H^{\ddagger}$; kJ/mol	83	55	90	59
$\Delta S^{\ddagger}$; J/mol/K	-81	-166	-56	-144
$\Delta G^{\ddagger}$; kJ/mol	118	124.8	114	120.4
k x 10^4 (150°C), s^{-1}	287	36	860	102
Θ	1	1	1	1
TOF x 10^4 (150°C), s^{-1}	287	36	860	102

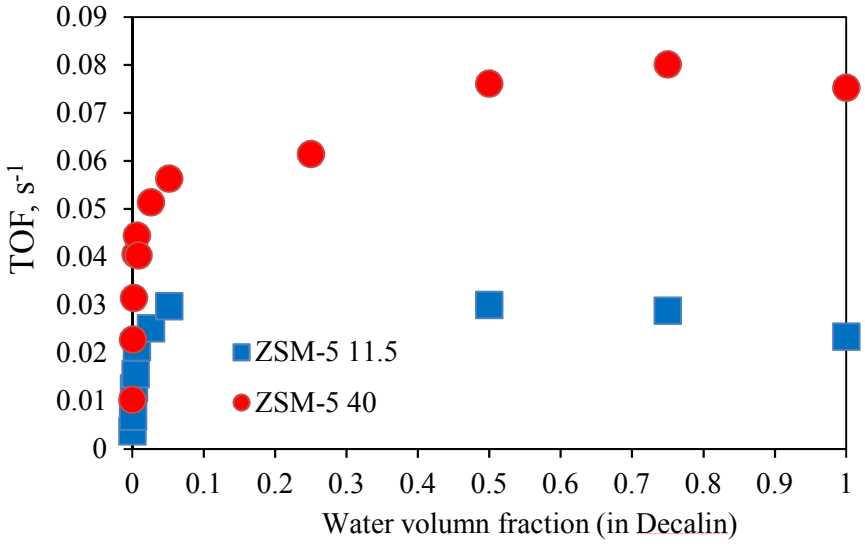

Figure 6. 13 The effect of water addition to the turnover frequencies of cyclohexanol dehydration on HZSM-5 zeolites. Reaction condition: 0.32M cyclohexanol, 120-150°C, 730psi H_2, water volume fraction is identified as the ratio of water volume over decalin volume

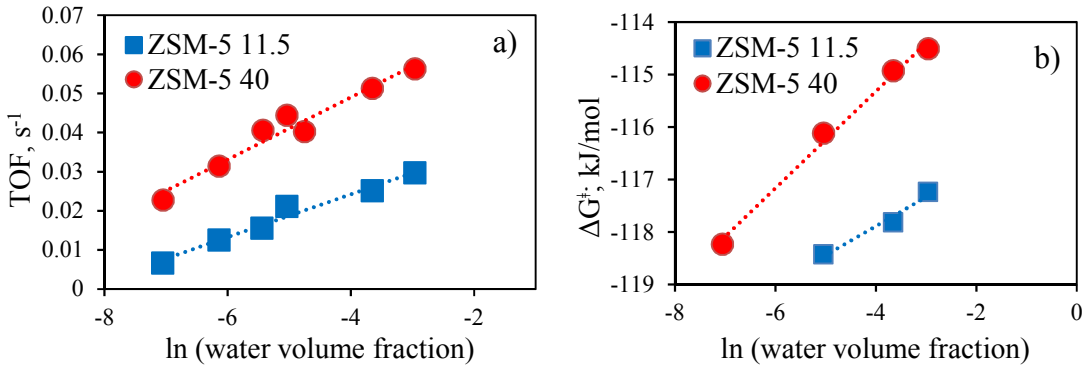

Figure 6. 14 Linear relationship of TOF and $\Delta G^{\ddagger}$ versus water contents

Interestingly, when the TOF of cyclohexene formation was plotted versus the natural logarithm of water volume fraction in the range of 0-0.05, a linear trend was observed (**Figure 6.14a**). Calculated intrinsic activation free energy also exhibited a linear relationship with ln(water volume fraction) parameter (**Figure 6.14b**). Furthermore, it can be seen from **Table 6.8** that the increasing amount of water enhances the activation barrier while reduces the entropy loss of the TS. At the point of 0.025 wvf.% corresponding to 3g of water added, the maximum TOF was reached and the TS actually gained some small entropy compared to the adsorbed state. Above this value, the lower $\Delta H^{\ddagger}$ is completely compensated by an increase in entropy loss, leading to an almost constant value of $\Delta G^{\ddagger}$. The biphasic system of decalin/water started to behave similarly to the pure water solvent.

Table 6. 8. The effect of water to the activation enthalpy, entropy and free energy on HZSM-5 zeolites. Reaction condition: 0.32M cyclohexanol, 120-150°C, 730psi H_2, decalin solvent

Amount of water, g	Water fraction	HZSM-5 Si/Al=11.5			HZSM-5 Si/Al=40		
		$\Delta H^{\ddagger}$	$\Delta S^{\ddagger}$	$\Delta G^{\ddagger}$	$\Delta H^{\ddagger}$	$\Delta S^{\ddagger}$	$\Delta G^{\ddagger}$
Decalin solvent	0	54.7	-166.8	125.3	59.2	-144.5	120.4
0.10	0.00086	-	-	-	78.6	-93.6	118.2
0.75	0.0065	116.2	-5.2	117.6	93.5	-53.3	116.1
3.00	0.025	119.8	4.75	118.5	120.8	13.8	114.9
6.00	0.051	115	-5.1	116.4	109.1	-12.7	114.5
Water solvent	1	83	-81	105.1	90	-56	113.5

The intriguing result of $\Delta G^{\ddagger}$ dependence on water contents indicates the direct involvement of water in the TS complex structure that leads to the observed rate enhancement. Since the 0^{th} reaction order is established in decalin solvent over HZSM-5 zeolites, the role of water is not likely to assist the adsorption or association of cyclohexanol with the active sites. In fact, Lercher *et al.* have proposed such water-associated TS complex for the cyclohexanol dehydration on HBEA zeolite in water solvent [302]. The cyclohexanol dehydration is proposed to undergo three elementary steps (E1 mechanism) including: protonation of cyclohexanol from the solvated cyclohexanol-hydronium complex, C-O and C-H bond cleavages, corresponding to three different TS complexes: $[C_6H_{11}^{+}\ldots H_2O + (H_2O)_{n+1}]$; $[C_6H_{11}^{+} + (H_2O)_{n+2}]$ and $[C_6H_{10}\ldots H_3O^{+} + (H_2O)_{n+1}]$, respectively. The decrease in $\Delta G^{\ddagger}$ with increasing water contents (in the range of 0-0.05 volume fraction) could be due to the increase in size of the water cluster that facilitates the deprotonation of the framework proton. Several groups from literatures have stated that the nucleation and deprotonation/delocalization effect of large water clusters (constituting of at least 3 molecules) on Brønsted acid sites

are more thermodynamically favorable than a single water molecule [262, 296, 300]. The more favorable delocalization effect induced by a larger water cluster makes the proton more detached from the surface, as the results, resulting in gaining more entropy for the water-associated TS complex as shown in **Table 6.8**. As indicated by Lercher *et al.*, for a water cluster with size larger than 4 molecules (such as $H_9O_4^+$, and $H_{11}O_5^+$), the positive charge of the hydronium ion does not change with the addition of more water molecules [300]. This could explain the plateau at higher water content as seen in **Figure 6.13**

6.4 Conclusion

Zeolites with confined pores has shown a tremendous effect on the rate of cyclohexanol dehydration in water solvent compared to a plain acidic solution via the stabilization of the TS complex rather than the enhancement cyclohexanol-hydronium ion association. This is in line with considerably lower $\Delta H^{\ddagger}$ and $\Delta S^{\ddagger}$ obtained on HZSM-5 zeolites and a 0^{th} to negative reaction orders obtained on HZSM-5 in decalin and water solvent, respectively. Furthermore, the addition of silicalite-1, a non-acidic silica-based material with a similar porous structure as HZSM-5, into H_3PO_4 solution did not yield any positive effect on cyclohexene formation rate compared to the plain H_3PO_4 solution, indicating that a physical combination of hydronium ions and confined pores might be not sufficient to enhance the dehydration rate. The hydronium ion originated from the framework hydroxyl group is essential for the high TOF value observed in the zeolites.

Compared to water solvent, the cyclohexene formation is slower in decalin solvent. The addition of a small of amount water is beneficial for the reaction as a much faster rate is observed. This process associates with a gradual increase in the intrinsic activation

enthalpy which is compensated by a fast decrease in the entropy loss, resulting in the lower activation free energy. This intriguing catalytic behavior could be caused by the increase in size of the water clusters that might thermodynamically mediate the deprotonation/delocalization of the framework proton as well as the H-transfer process in the kinetically relevant C-H bond cleavage step. This effect is cancelled out as the water cluster grows bigger, corresponding to the unchanged rate at the point above 0.25 water volume fraction.

Appendix A: Supplementary Information for Chapter 4

High-Temperature Silylation for Minimizing Leaching of Acid Functionality from Hydrophobic Mesoporous Silicas

Tuong V. Bui‡, Santiago J. Umbarila‡, Bin Wang, Tawan Sooknoi, Daniel E. Resasco*

‡Both authors contributed equally to this work

*Corresponding Author: resasco@ou.edu

School of Chemical, Biological and Materials Engineering, The University of Oklahoma, Norman, OK 73019, USA

A. THERMO GRAVIMETICAL ANALYSIS

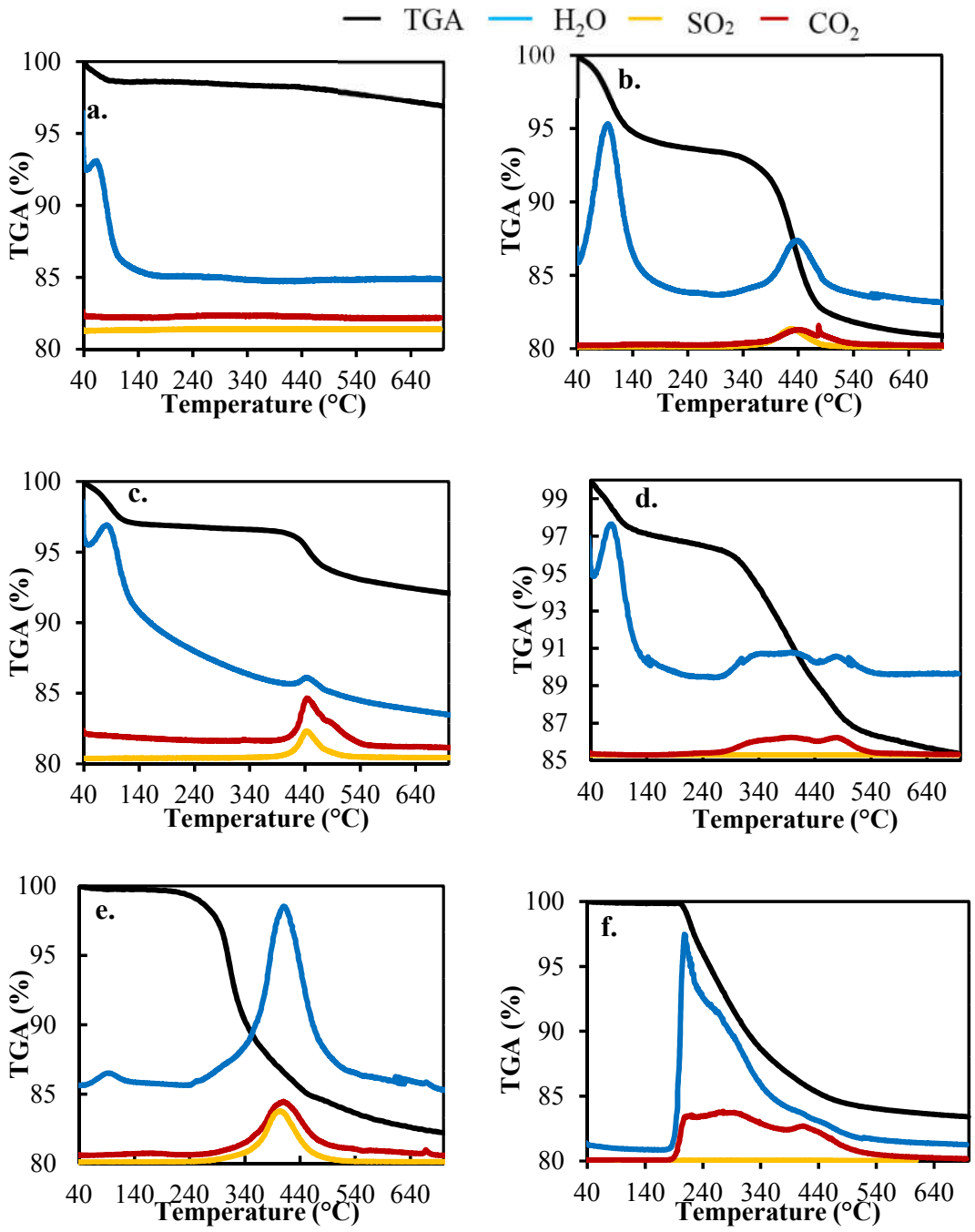

Figure S1. TGA-TPO decomposition analysis for the functionalized silica: a) MCM41, b) SBA15-SO_3H-CC, c) MCM41-SO_3H-CG, d) MCM41-ETS-CG, e) MCM41-SO_3H-HG, f) MCM41-OTS-HG.

B. N_2 ADSORPTION-DESORPTION ISOTHERMS

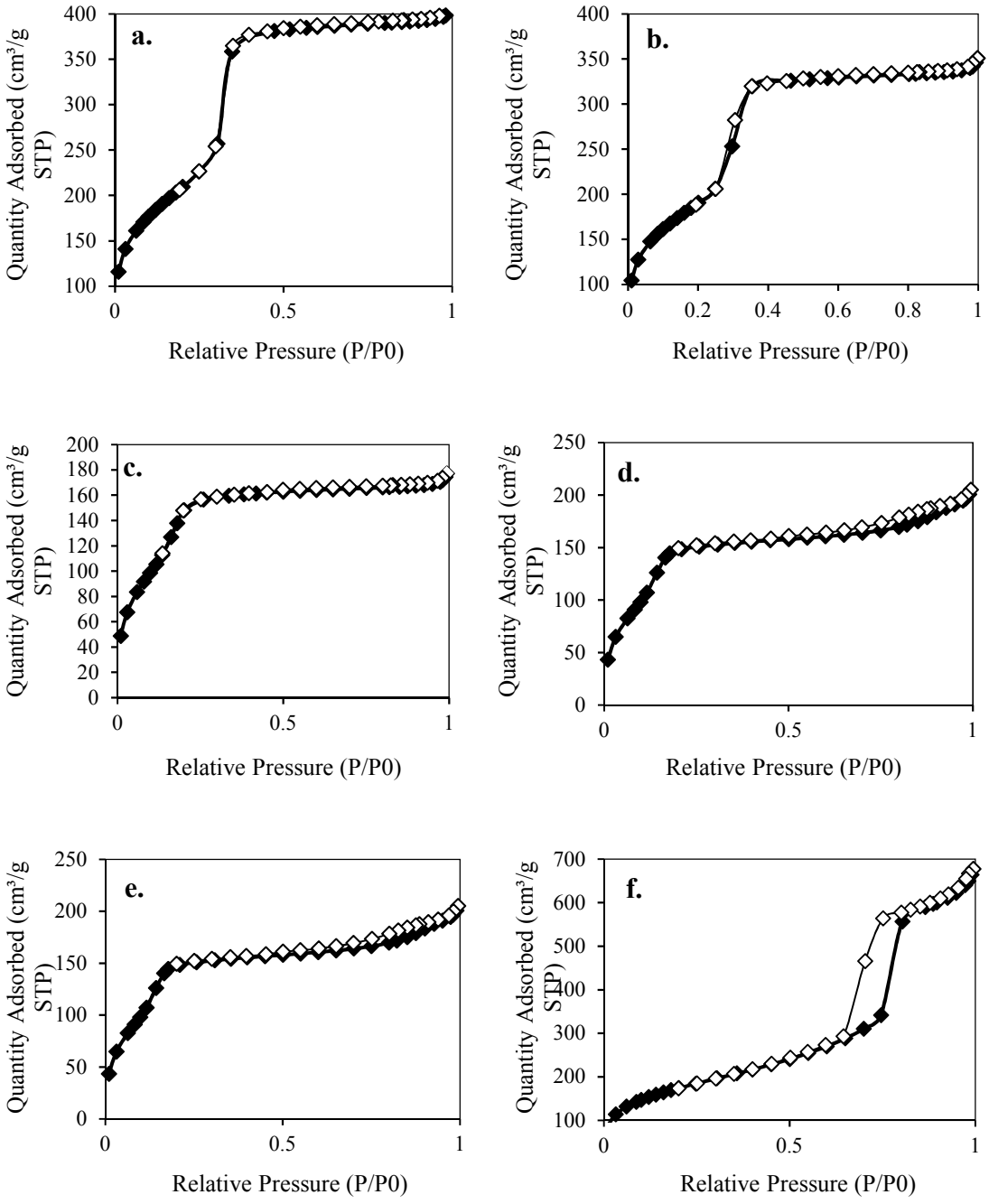

Figure S2. Isotherms of adsorption and desorption for: a) MCM41, b) MCM41-SO_3H-CG, c) MCM41-ETS-CG, d) MCM41-SO_3H-HG, e) MCM41-OTS-HG f) SBA15-SO_3H-CC. (♦) Adsorption isotherms, (◊) Desorption isotherms.

C. THERMO STABILITY OF MCM41-SO_3H-HG

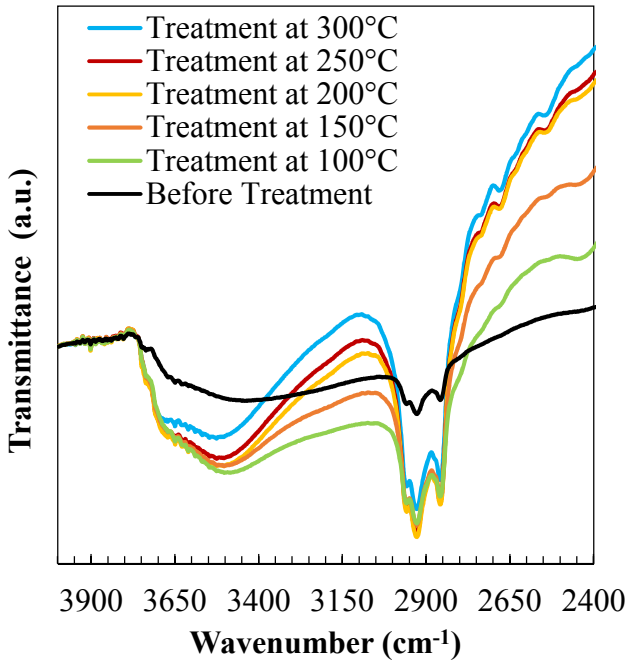

Figure S3. DRIFT spectra at 50ºC of MCM41-SO_3H-HG. The samples were pretreated at different temperatures in constant flow of He

The thermal stability of MCM41-SO_3H-HG was evaluated by using FTIR cell (High temperature DRIFT HVC cell). The sample was heated up in-situ under He flow with ramping rate of 10°C/ min until reaching the desired temperature which is kept constant for 1 h during experiment. The cell was cold down to 50°C and the DRIFT spectra was collected. The results are presented in the **Figure S3**. The increases of the signal in the region of 3700 to 3100 cm^{-1} (corresponded to the O-H stretching vibration) along with the increasing temperature is due to the desorption of physisorbed water on the surface, leading to the reduction of interference on the IR signal. The pretreatment of samples helps to produce clear and stable signals in the C-H vibration region (2800-2600 cm^{-1}). No loss of functionalization was detected up to 300ºC.

D. TRANSMISSION ELECTRON MICROSCOPY IMAGES OF THE FUNCTIONALIZED SILICA

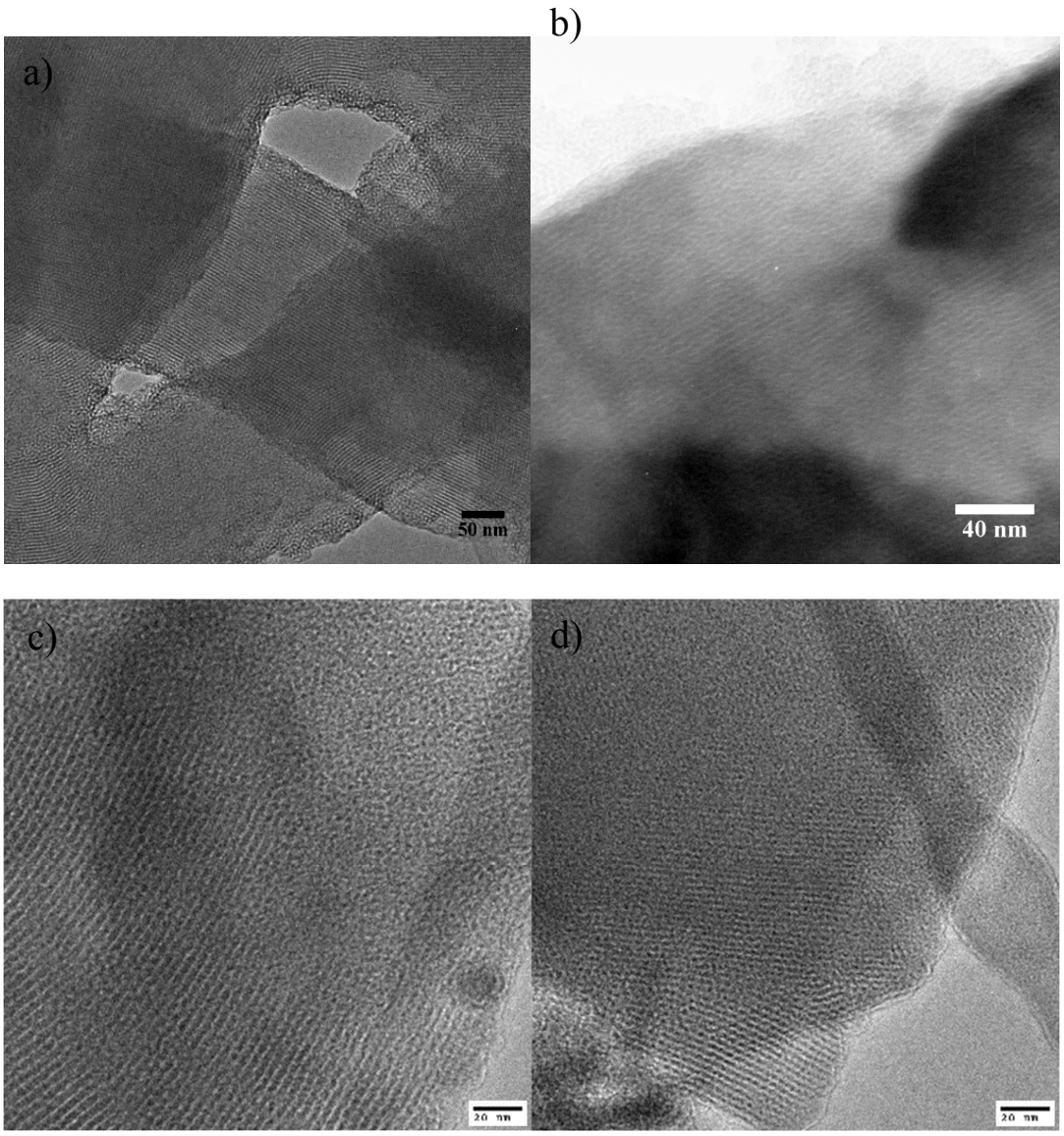

Figure S4. HRTEM for the parent and functionalized MCM41: a) parent MCM41, b) MCM41-SO_3H-CG c-d) MCM41-SO_3H-HG

E. XRD OF HYDROTHERMAL TREATED CATALYSTS

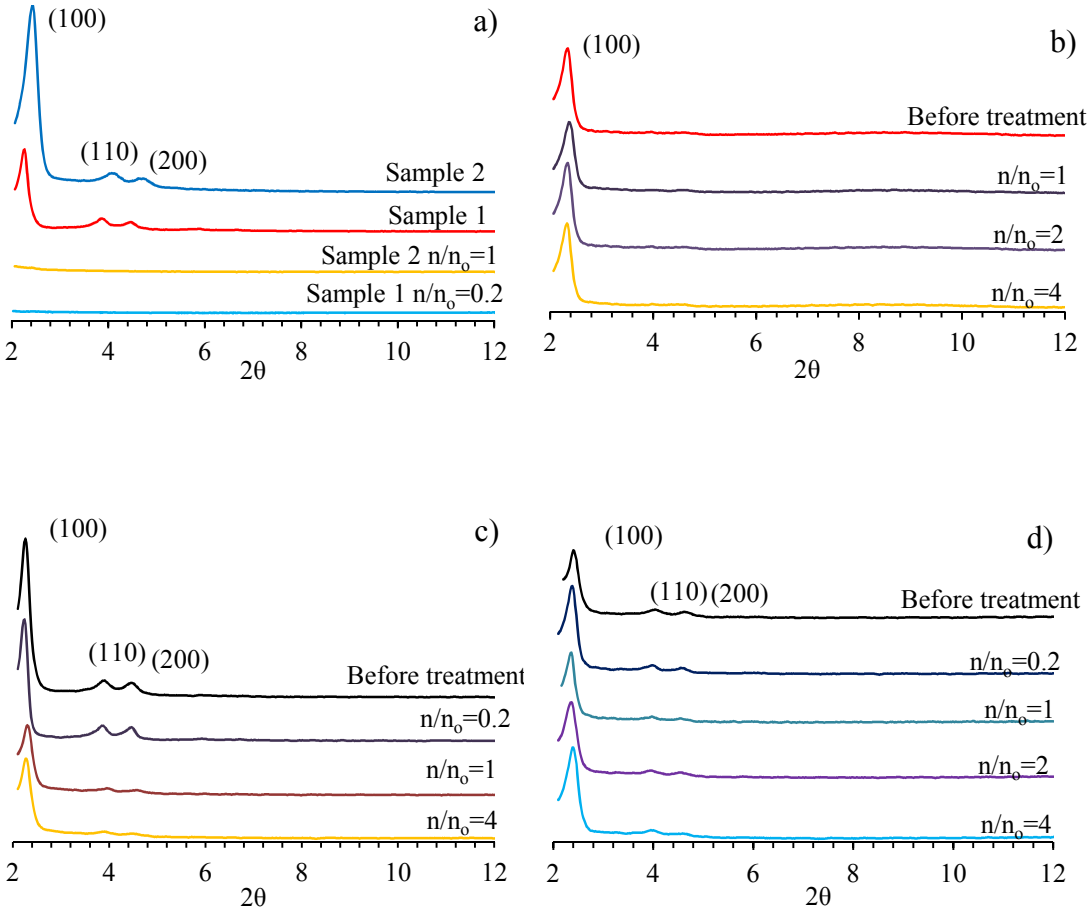

Figure S5. XRD of functionalized MCM-41 after hydrothermal treatment a) MCM-41 (Sample 1) and MCM-41 preheated at 600ºC for 6 h (Sample 2) prior to water treatment; b) MCM41-ETS-HG-6x; c) MCM41-SO_3H-CG; d) MCM41-SO_3H-HG

F. ^{1}H-^{29}Si CPMAS OF HYDROTHERMAL TREATED CATALYSTS

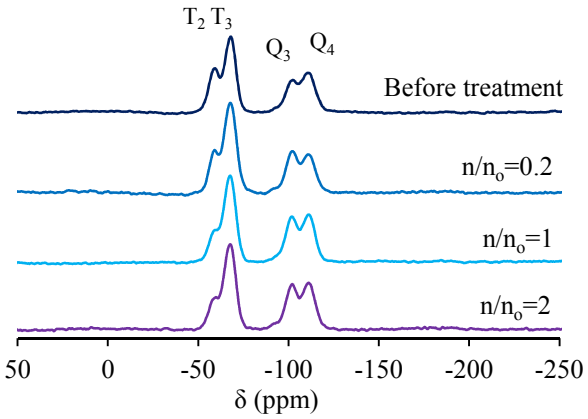

Figure S6. NMR ^{1}H-^{29}Si CPMAS of MCM41-SO_3H-HG treated with different amounts of water

G. ACTIVITY OF FUNCTIONALIZED CATALYSTS AFTER METHANOL WASHSES

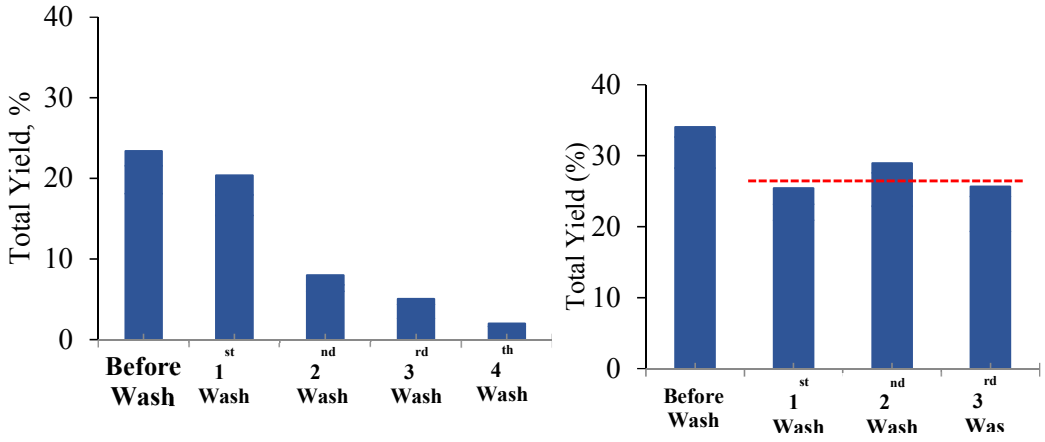

Figure S7. Catalytic activity of the functionalized MCM41 catalysts after multiple sequential washes with methanol at 200°C for 6 h a) MCM41-SO_3H-CG and b) MCM41-SO_3H-HG. The alkylation reaction was carried out at 250°C under 850 Psi of N_2, for 2 h, CPOL/m-cresol feed ratio 0.5M/1.0M in decalin solvent. The total yield is the sum of yields to alkylated products (C-C and C-O)

H. LEACHING TEST OF HYDROPHOBIZED SBA-15 CATALYSTS

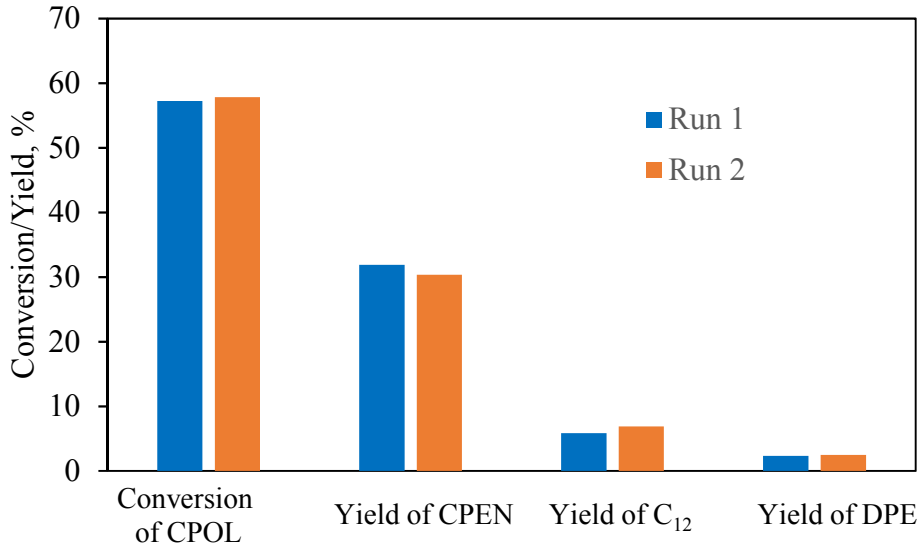

Figure S8. The leaching test result of SBA15-SO_3-CC-HG synthesized by high-temperature grafting with an excess amount of ETS (30.6 mmol ETS precursor per gram of the catalyst). Run 1: 150 mg of SBA15-SO_3-CC-HG; pure CPOL/m-cresol, 250^{o}C, 2 h. Run 2: liquid product (from run 1) at 250^{o}C, 14 h

Table S1. Literature review of the stability of the functionalized mesostructured silica.

Reaction	Catalyst [a]	Solvent	T (°C)	Stability	Reference
Esterification of acetic acid with methanol	SiO_2-SO_3H[b]	Methanol	60	No leaching	[205]
Transesterification/Esterification of mixture of ester, fatty acids and methanol	SBA15-SO_3H[c] SBA15-SO_3H[d] SiO_2 -SO_3H[d]	Methanol	60	No Leaching Leaching	[171]
Etherification of glycerol with isobutene	SBA15-SO_3H[e] SBA15-SO_3H[d]	Glycerol	75	No Leaching	[303]
Aldol condensation of 4-nitrobenzadehyde with acetone	MCM41-SO_3H[c] MCM41-SO_3H[d]	No	50	No Leaching	[304]
Esterification of fatty acids with ethanol	PS–C_8–SiO_2 HNs[c,f]	Ethanol	80	Leaching No Leaching	[206]
Dehydration of fructose	SBA15-SO_3H[c] SBA15-SO_3H[d]	H_2O DMSO[h]	120	Leaching No Leaching	[146]
Hydrolysis of cellobiose	SiO_2-NP-SO_3H[g]	Water	175	Leaching	[199]

[a] Catalysts were synthesized using MPTS as the precursor followed by oxidation to SO_3H
[b] Incipient wetness impregnation of the precursor at room temperature
[c] Catalyst functionalized using CC method
[d] Catalyst functionalized using CG method
[e] Conventional grafting assisted by microwaves
[f] Hybrid mesoporous silica hollow nano spheres (HNs), PS: Polystyrene, PMA: poly(methyl acrylate), C_8: functionalized with OTS
[g] Conventional grafting using different solvents (Ethanol, methanol, acetonitrile, toluene) of silica-coated magnetic nanoparticles of $CoFe_2O_4$
[h] Dimethyl sulfoxide

References

1. Sui, H., et al., *Fractional Condensation of Multicomponent Vapors from Pyrolysis of Cotton Stalk.* Energy & Fuels, 2014. **28**(8): p. 5095-5102.
2. Pollard, A.S., M.R. Rover, and R.C. Brown, *Characterization of bio-oil recovered as stage fractions with unique chemical and physical properties.* Journal of Analytical and Applied Pyrolysis, 2012. **93**(0): p. 129-138.
3. Ciolkosz, D. and R. Wallace, *A review of torrefaction for bioenergy feedstock production.* Biofuels, Bioproducts and Biorefining, 2011. **5**(3): p. 317-329.
4. van der Stelt, M.J.C., et al., *Biomass upgrading by torrefaction for the production of biofuels: A review.* Biomass and Bioenergy, 2011. **35**(9): p. 3748-3762.
5. Prins, M.J., K.J. Ptasinski, and F.J.J.G. Janssen, *More efficient biomass gasification via torrefaction.* Energy, 2006. **31**(15): p. 3458-3470.
6. de Wild, P.J., et al., *Biomass valorisation by staged degasification: A new pyrolysis-based thermochemical conversion option to produce value-added chemicals from lignocellulosic biomass.* Journal of Analytical and Applied Pyrolysis, 2009. **85**(1–2): p. 124-133.
7. Zapata, P., et al., *Condensation/Hydrogenation of Biomass-Derived Oxygenates in Water/Oil Emulsions Stabilized by Nanohybrid Catalysts.* Topics in Catalysis, 2012. **55**(1-2): p. 38-52.
8. Pham, T.N., et al., *Aqueous-phase ketonization of acetic acid over Ru/TiO_2/carbon catalysts.* Journal of Catalysis, 2012. **295**: p. 169-178.
9. González-Borja, M.Á. and D.E. Resasco, *Reaction pathways in the liquid phase alkylation of biomass-derived phenolic compounds.* AIChE Journal, 2015. **61**(2): p. 598-609.
10. West, R.M., et al., *Carbon–carbon bond formation for biomass-derived furfurals and ketones by aldol condensation in a biphasic system.* Journal of Molecular Catalysis A: Chemical, 2008. **296**(1–2): p. 18-27.
11. Barrett, C.J., et al., *Single-reactor process for sequential aldol-condensation and hydrogenation of biomass-derived compounds in water.* Applied Catalysis B: Environmental, 2006. **66**(1–2): p. 111-118.

12. Zheng, H.-Y., et al., *Towards understanding the reaction pathway in vapour phase hydrogenation of furfural to 2-methylfuran.* Journal of Molecular Catalysis A: Chemical, 2006. **246**(1–2): p. 18-23.
13. Karl, J.Z., *Methylfuran*, in *Sugar Series*. 2000, Elsevier. p. 229-230.
14. Shi, S., H. Guo, and G. Yin, *Synthesis of maleic acid from renewable resources: Catalytic oxidation of furfural in liquid media with dioxygen.* Catalysis Communications, 2011. **12**(8): p. 731-733.
15. Choudhary, H., S. Nishimura, and K. Ebitani, *Highly Efficient Aqueous Oxidation of Furfural to Succinic Acid Using Reusable Heterogeneous Acid Catalyst with Hydrogen Peroxide.* Chemistry Letters, 2012. **41**(4): p. 409-411.
16. Corma, A., O. de la Torre, and M. Renz, *Production of high quality diesel from cellulose and hemicellulose by the Sylvan process: catalysts and process variables.* Energy & Environmental Science, 2012. **5**(4): p. 6328-6344.
17. Li, G., et al., *Synthesis of High-Quality Diesel with Furfural and 2-Methylfuran from Hemicellulose.* ChemSusChem, 2012. **5**(10): p. 1958-1966.
18. Williams, C.L., et al., *Cycloaddition of Biomass-Derived Furans for Catalytic Production of Renewable p-Xylene.* ACS Catalysis, 2012. **2**(6): p. 935-939.
19. Bui, T.V., Crossley S., Resasco, D.E. , *C-C coupling for biomass-derived furanics upgrading to chemicals and fuels* in *Chemicals and Fuels from Bio-Based Building Blocks*. 2016, Wiley-VCH. p. 431-494.
20. Hronec, M., et al., *Cyclopentanone: A raw material for production of C15 and C17 fuel precursors.* Biomass and Bioenergy, 2014. **63**(0): p. 291-299.
21. Yang, Y., et al., *Conversion of furfural into cyclopentanone over Ni-Cu bimetallic catalysts.* Green Chemistry, 2013. **15**(7): p. 1932-1940.
22. Sitthisa, S. and D. Resasco, *Hydrodeoxygenation of Furfural Over Supported Metal Catalysts: A Comparative Study of Cu, Pd and Ni.* Catalysis Letters, 2011. **141**(6): p. 784-791.
23. Yan, K., et al., *Production, properties and catalytic hydrogenation of furfural to fuel additives and value-added chemicals*. Renewable and Sustainable Energy Reviews, 2014. **38**(0): p. 663-676.
24. Hronec, M., K. Fulajtarová, and T. Liptaj, *Effect of catalyst and solvent on the furan ring rearrangement to cyclopentanone.* Applied Catalysis A: General, 2012. **437–438**(0): p. 104-111.

25. Zhou, M., et al., *Catalytic Hydroprocessing of Furfural to Cyclopentanol Over Ni/CNTs Catalysts: Model Reaction for Upgrading of Bio-oil.* Catalysis Letters, 2014. **144**(2): p. 235-241.
26. Piutti, C. and F. Quartieri, *The Piancatelli Rearrangement: New Applications for an Intriguing Reaction.* Molecules, 2013. **18**(10): p. 12290-12312.
27. Hronec, M., K. Fulajtárova, and T. Soták, *Highly selective rearrangement of furfuryl alcohol to cyclopentanone.* Applied Catalysis B: Environmental, 2014. **154–155**(0): p. 294-300.
28. Piancatelli, G., et al., *A new synthesis of 3-oxocyclopentenes1.* Tetrahedron, 1978. **34**(18): p. 2775-2778.
29. Scettri, A., et al., *General route and mechanism of the rearrangement of the 4-substituted 5-hydroxy-3-oxocyclopentenes into the 2-substituted analogs.* Tetrahedron, 1979. **35**(1): p. 135-138.
30. Fisher, D., et al., *Efficient synthesis of 4-hydroxycyclopentenones: dysprosium(III) triflate catalyzed Piancatelli rearrangement.* Tetrahedron, 2014. **70**(27–28): p. 4105-4110.
31. Piancatelli, G., A. Scettri, and S. Barbadoro, *A useful preparation of 4-substituted 5-hydroxy-3-oxocyclopentene.* Tetrahedron Letters, 1976. **17**(39): p. 3555-3558.
32. Piancatelli, G. and A. Scettri, *A useful preparation of (±) t-butyl 3-hydroxy-5-oxo-1-cyclopenteneheptanoate ans its 3-deoxy-derivative, important prostaglandin intermediates.* Tetrahedron Letters, 1977. **18**(13): p. 1131-1134.
33. Minai, M., *Process for preparing oxocyclopentene derivatives, US 4970345 A*. 1990.
34. Piancatelli, G., M. D'Auria, and F. D'Onofrio, *Synthesis of 1,4-Dicarbonyl Compounds and Cyclopentenones from Furans.* Synthesis, 1994. **1994**(09): p. 867-889.
35. Veits, G.K., D.R. Wenz, and J. Read de Alaniz, *Versatile Method for the Synthesis of 4-Aminocyclopentenones: Dysprosium(III) Triflate Catalyzed Aza-Piancatelli Rearrangement.* Angewandte Chemie International Edition, 2010. **49**(49): p. 9484-9487.
36. Nieto Faza, O., et al., *Theoretical Study of the Electrocyclic Ring Closure of Hydroxypentadienyl Cations.* Chemistry – A European Journal, 2004. **10**(17): p. 4324-4333.
37. Frontier, A.J. and C. Collison, *The Nazarov cyclization in organic synthesis. Recent advances.* Tetrahedron, 2005. **61**(32): p. 7577-7606.

38. Pellissier, H., *Recent developments in the Nazarov process.* Tetrahedron, 2005. **61**(27): p. 6479-6517.
39. Shimada, N., C. Stewart, and M.A. Tius, *Asymmetric Nazarov Cyclizations.* Tetrahedron, 2011. **67**(33): p. 5851-5870.
40. Tius, M.A., *Some New Nazarov Chemistry.* European Journal of Organic Chemistry, 2005. **2005**(11): p. 2193-2206.
41. Hronec, M. and K. Fulajtarová, *Selective transformation of furfural to cyclopentanone.* Catalysis Communications, 2012. **24**(0): p. 100-104.
42. Ordomsky, V.V., et al., *Biphasic single-reactor process for dehydration of xylose and hydrogenation of produced furfural.* Applied Catalysis A: General, 2013. **451**(0): p. 6-13.
43. Nanni, M., Ta-machi, H., Moriyama-shi., *Japanese Patent Disclosure Bulletin*. 15 April 1982.
44. Curran, T.T., et al., *The preparation of optically active 2-cyclopenten-1,4-diol derivatives from furfuryl alcohol.* Tetrahedron, 1997. **53**(6): p. 1983-2004.
45. Watson, T.J.N., et al., *Development of the Carbocyclic Nucleoside MDL 201449A: A Tumor Necrosis Factor-α Inhibitor.* Organic Process Research & Development, 1998. **2**(6): p. 357-365.
46. Timothy T. Curran, J.C.E., David A. Hay, *Preparation of cis-4-o-protected-2-cyclopentenol derivatives*. Mar. 17, 1998, Hoechst Marion Roussel Inc.
47. Ghorpade, S.R., et al., *Enzymatic kinetic resolution studies of racemic 4-hydroxycyclopent-2-en-1-one using Lipozyme IM®.* Tetrahedron: Asymmetry, 1999. **10**(21): p. 4115-4122.
48. Bandura, A.V. and S.N. Lvov, *The Ionization Constant of Water over Wide Ranges of Temperature and Density.* Journal of Physical and Chemical Reference Data, 2006. **35**(1): p. 15-30.
49. Nakagawa, Y., M. Tamura, and K. Tomishige, *Catalytic Reduction of Biomass-Derived Furanic Compounds with Hydrogen.* ACS Catalysis, 2013. **3**(12): p. 2655-2668.
50. Nakagawa, Y., et al., *Total Hydrogenation of Furfural and 5-Hydroxymethylfurfural over Supported Pd–Ir Alloy Catalyst.* ACS Catalysis, 2014. **4**(8): p. 2718-2726.
51. Sitthisa, S., et al., *Kinetics and mechanism of hydrogenation of furfural on Cu/SiO2 catalysts.* Journal of Catalysis, 2011. **277**(1): p. 1-13.
52. Sexton, B.A., A.E. Hughes, and N.R. Avery, *A spectroscopic study of the adsorption and reactions of methanol, formaldehyde and methyl*

formate on clean and oxygenated Cu(110) surfaces. Surface Science, 1985. **155**(1): p. 366-386.
53. Mavrikakis, M. and M.A. Barteau, *Oxygenate reaction pathways on transition metal surfaces.* Journal of Molecular Catalysis A: Chemical, 1998. **131**(1–3): p. 135-147.
54. Davis, J.L. and M.A. Barteau, *Polymerization and decarbonylation reactions of aldehydes on the Pd(111) surface.* Journal of the American Chemical Society, 1989. **111**(5): p. 1782-1792.
55. Davis, J.L. and M.A. Barteau, *Spectroscopic identification of alkoxide, aldehyde, and acyl intermediates in alcohol decomposition on Pd(111).* Surface Science, 1990. **235**(2–3): p. 235-248.
56. Henderson, M.A., Y. Zhou, and J.M. White, *Polymerization and decomposition of acetaldehyde on rutherium(001).* Journal of the American Chemical Society, 1989. **111**(4): p. 1185-1193.
57. Zhu, H., et al., *Selective hydrogenation of furfural to cyclopentanone over Cu-Ni-Al hydrotalcite-based catalysts.* Korean Journal of Chemical Engineering, 2014. **31**(4): p. 593-597.
58. Guo, J., et al., *Selective Conversion of Furfural to Cyclopentanone with CuZnAl Catalysts.* ACS Sustainable Chemistry & Engineering, 2014. **2**(10): p. 2259-2266.
59. Ohyama, J., et al., *Conversion of 5-hydroxymethylfurfural to a cyclopentanone derivative by ring rearrangement over supported Au nanoparticles.* Chemical Communications, 2014. **50**(42): p. 5633-5636.
60. Pham, T.N., D. Shi, and D.E. Resasco, *Evaluating strategies for catalytic upgrading of pyrolysis oil in liquid phase.* Applied Catalysis B: Environmental, 2014. **145**(0): p. 10-23.
61. Elliott, D.C., *Status of Process Development for Pyrolysis of Biomass for Liquid Fuels and Chemicals Production.* Journal Name: International Sustainable Energy Review, 4(2):56-57; Journal Volume: 4; Journal Issue: 2, 2010: p. Medium: X.
62. Elliott, D.C. and A. Oasmaa, *Catalytic hydrotreating of black liquor oils.* Energy & Fuels, 1991. **5**(1): p. 102-109.
63. Marker, T.L., et al., *Integrated hydropyrolysis and hydroconversion (IH2) for the direct production of gasoline and diesel fuels or blending components from biomass, part 1: Proof of principle testing.* Environmental Progress & Sustainable Energy, 2012. **31**(2): p. 191-199.

64. Domine, M.E., et al., *Coprocessing of Oxygenated Biomass Compounds and Hydrocarbons for the Production of Sustainable Fuel.* ChemSusChem, 2008. **1**(3): p. 179-181.
65. Lappas, A.A., S. Bezergianni, and I.A. Vasalos, *Production of biofuels via co-processing in conventional refining processes.* Catalysis Today, 2009. **145**(1–2): p. 55-62.
66. Li, H.y., Y.j. Yan, and Z.w. Ren, *Online upgrading of organic vapors from the fast pyrolysis of biomass.* Journal of Fuel Chemistry and Technology, 2008. **36**(6): p. 666-671.
67. Gaertner, C.A., et al., *Catalytic coupling of carboxylic acids by ketonization as a processing step in biomass conversion.* Journal of Catalysis, 2009. **266**(1): p. 71-78.
68. Corma, A., O. de la Torre, and M. Renz, *High-Quality Diesel from Hexose- and Pentose-Derived Biomass Platform Molecules.* ChemSusChem, 2011. **4**(11): p. 1574-1577.
69. Corma, A., et al., *Production of High-Quality Diesel from Biomass Waste Products.* Angewandte Chemie International Edition, 2011. **50**(10): p. 2375-2378.
70. Garade, A.C., V.R. Mate, and C.V. Rode, *Montmorillonite for selective hydroxyalkylation of p-cresol.* Applied Clay Science, 2009. **43**(1): p. 113-117.
71. Garade, A.C., et al., *Acidity tuning of montmorillonite K10 by impregnation with dodecatungstophosphoric acid and hydroxyalkylation of phenol.* Applied Clay Science, 2010. **48**(1): p. 164-170.
72. Bolognini, M., et al., *Guaiacol hydroxyalkylation with aqueous formaldehyde: role of surface properties of H-mordenites on catalytic performance.* Applied Catalysis A: General, 2004. **272**(1–2): p. 115-124.
73. Beltrame, P., et al., *Screening of solid acid catalysts for the condensation of acetaldehyde with o-xylene.* Applied Catalysis A: General, 1995. **128**(1): p. 143-154.
74. Climent, M.J., et al., *Acid zeolites as catalysts in organic reactions: condensation of acetophenone with benzene derivatives.* Applied Catalysis A: General, 1995. **130**(1): p. 5-12.
75. Climent, M.J., et al., *Zeolites as catalysts in organic reactions: Condensation of aldehydes with benzene derivatives.* Journal of Catalysis, 1991. **130**(1): p. 138-146.

76. Nowińska, K. and W. Kaleta, *Synthesis of Bisphenol-A over heteropoly compounds encapsulated into mesoporous molecular sieves.* Applied Catalysis A: General, 2000. **203**(1): p. 91-100.
77. Alvaro, M., et al., *Hydroxyalkylation of benzene derivatives by benzaldehyde in the presence of acid zeolites.* Applied Catalysis A: General, 1998. **175**(1–2): p. 105-112.
78. Álvaro, M., et al., *Friedel–Crafts hydroxyalkylation: reaction of anisole with paraformaldehyde catalyzed by zeolites in supercritical CO_2.* Journal of Catalysis, 2003. **219**(2): p. 464-468.
79. Climent, M.J., et al., *Zeolites in organic reactions: Condensation of formaldehyde with benzene in the presence of HY zeolites.* Applied Catalysis, 1989. **51**(1): p. 113-125.
80. Tan, Y., et al., *The hydroxyalkylation of phenol with formaldehyde over mesoporous M(Al, Zr, Al–Zr)-SBA-15 catalysts: The effect on the isomer distribution of bisphenol F.* Catalysis Communications, 2015. **67**: p. 21-25.
81. Garade, A.C., et al., *Structure–activity studies of dodecatungstophosphoric acid impregnated bentonite clay catalyst in hydroxyalkylation of p-cresol.* Catalysis Communications, 2010. **11**(11): p. 942-945.
82. Yang, J., et al., *Synthesis of renewable high-density fuels using cyclopentanone derived from lignocellulose.* Chemical Communications, 2014. **50**(20): p. 2572-2574.
83. Wang, T., et al., *Aviation fuel synthesis by catalytic conversion of biomass hydrolysate in aqueous phase.* Applied Energy, 2014. **136**: p. 775-780.
84. Deng, Q., et al., *Highly controllable and selective hydroxyalkylation/alkylation of 2-methylfuran with cyclohexanone for synthesis of high-density biofuel.* Chemical Engineering Science, 2015. **138**: p. 239-243.
85. Zhang, X., et al., *Hydrophobic mesoporous acidic resin for hydroxyalkylation/alkylation of 2-methylfuran and ketone to high-density biofuel.* AIChE Journal, 2017. **63**(2): p. 680-688.
86. Olah, G.A., *Superelectrophiles.* Angewandte Chemie International Edition in English, 1993. **32**(6): p. 767-788.
87. Pratihar, S., *Triggering the approach of an arene or heteroarene towards an aldehyde via Lewis acid-aldehyde communication.* Organic & Biomolecular Chemistry, 2016. **14**(10): p. 2854-2865.

88. El-Khawaga, A.M., R.M. Roberts, and K.M. Sweeney, *Transacylations between sterically hindered aromatic ketones and various arenes.* The Journal of Organic Chemistry, 1985. **50**(12): p. 2055-2058.
89. Wen, C., et al., *One-step production of long-chain hydrocarbons from waste-biomass-derived chemicals using bi-functional heterogeneous catalysts.* Physical Chemistry Chemical Physics, 2014. **16**(7): p. 3047-3054.
90. C., G.A., et al., *Hydroxyalkylation of p-Cresol to 2,2'-Methylenebis(4-methylphenol) Using Sn/Si-MCM-41 Catalysts.* Chemistry Letters, 2010. **39**(2): p. 126-127.
91. Bui, T.V., T. Sooknoi, and D.E. Resasco, *Simultaneous Upgrading of Furanics and Phenolics through Hydroxyalkylation/Aldol Condensation Reactions.* ChemSusChem, 2017. **10**(7): p. 1631-1639.
92. Wu, X., et al., *Hydroxyalkylation of phenol to bisphenol F over heteropolyacid catalysts: The effect of catalyst acid strength on isomer distribution and kinetics.* Journal of Colloid and Interface Science, 2016. **481**: p. 75-81.
93. Jha, A., et al., *MCM-41 Supported Phosphotungstic Acid for the Hydroxyalkylation of Phenol to Phenolphthalein.* Industrial & Engineering Chemistry Research, 2012. **51**(10): p. 3916-3922.
94. Xia, Q., et al., *Selective One-Pot Production of High-Grade Diesel-Range Alkanes from Furfural and 2-Methylfuran over Pd/$NbOPO_4$.* ChemSusChem, 2017. **10**(4): p. 747-753.
95. Chen, M., et al., *Hydroxyalkylation of Phenol with Formaldehyde to Bisphenol F Catalyzed by Keggin Phosphotungstic Acid Encapsulated in Metal–Organic Frameworks MIL-100(Fe or Cr) and MIL-101(Fe or Cr).* Industrial & Engineering Chemistry Research, 2015. **54**(47): p. 11804-11813.
96. Iovel, I.G. and E. Lukevics, *Hydroxymethylation and alkylation of compounds of the furan, thiophene, and pyrrole series in the presence of H^+ cations (review).* Chemistry of Heterocyclic Compounds, 1998. **34**(1): p. 1-12.
97. Brown, W.H. and H. Sawatzky, *The condensation of furan and sylvan with some carbonyl compounds.* Canadian Journal of Chemistry, 1956. **34**(9): p. 1147-1153.
98. Seppo Pennanen, G.N., *Stydies on the Furan Series, Part I. The Acidic Condensation of Aldeydes with Methyl 2-Furoate.* Acta Chem. Scand., 1972. **26**: p. 1018-1022.

99. Wei, Y., et al., *Short-channeled mesoporous Zr–Al-SBA-15 as a highly efficient catalyst for hydroxyalkylation of phenol with formaldehyde to bisphenol F.* Chemical Engineering Journal, 2016. **298**: p. 271-280.
100. Wang, Q., et al., *The efficient hydroxyalkylation of phenol with formaldehyde to bisphenol F over a thermoregulated phase-separable reaction system containing a water-soluble Brønsted acidic ionic liquid.* RSC Advances, 2014. **4**(63): p. 33466-33473.
101. Garade, A.C., V.S. Kshirsagar, and C.V. Rode, *Selective hydroxyalkylation of phenol to bisphenol F over dodecatungstophosphoric acid (DTP) impregnated on fumed silica.* Applied Catalysis A: General, 2009. **354**(1): p. 176-182.
102. Udayakumar, S., S. Ajaikumar, and A. Pandurangan, *Electrophilic substitution reaction of phenols with aldehydes: Enhance the yield of bisphenols by HPA and supported HPA.* Catalysis Communications, 2007. **8**(3): p. 366-374.
103. Barthel, N., et al., *Hydroxyalkylation of aromatic compounds over protonic zeolites.* Topics in Catalysis, 2000. **13**(3): p. 269-274.
104. Mayr, H., B. Kempf, and A.R. Ofial, *π-Nucleophilicity in Carbon−Carbon Bond-Forming Reactions*. Accounts of Chemical Research, 2003. **36**(1): p. 66-77.
105. Appel, R. and H. Mayr, *Quantification of the Electrophilic Reactivities of Aldehydes, Imines, and Enones.* Journal of the American Chemical Society, 2011. **133**(21): p. 8240-8251.
106. Appel, R., et al., *Electrophilicities of Benzaldehyde-Derived Iminium Ions: Quantification of the Electrophilic Activation of Aldehydes by Iminium Formation.* Journal of the American Chemical Society, 2013. **135**(17): p. 6579-6587.
107. Pratihar, S. and S. Roy, *Reactivity and Selectivity of Organotin Reagents in Allylation and Arylation: Nucleophilicity Parameter as a Guide.* Organometallics, 2011. **30**(12): p. 3257-3269.
108. *Lewis Acids in Organic Synthesis*. 2001, Weinheim, Germany: Wiley-VCH.
109. *Modern Carbonyl Chemistry*. 2000, Weinheim, Germany: Wiley-VCH.
110. Harikrishnan, A., J. Sanjeevi, and C. Ramaraj Ramanathan, *The cooperative effect of Lewis pairs in the Friedel-Crafts hydroxyalkylation reaction: a simple and effective route for the*

synthesis of (+/-)-carbinoxamine. Organic & Biomolecular Chemistry, 2015. **13**(12): p. 3633-3647.
111. Olah, G.A., et al., *Protonated (protosolvated) onium ions (onlum dications)*. Research on Chemical Intermediates, 1989. **12**(2): p. 141-159.
112. Olah, G.A., et al., *Acid-Catalyzed Isomerization of Pivalaldehyde to Methyl Isopropyl Ketone via a Reactive Protosolvated Carboxonium Ion Intermediate.* Journal of the American Chemical Society, 2001. **123**(47): p. 11556-11561.
113. Olah, G.A. and D.A. Klumpp, *Superelectrophilic Solvation.* Accounts of Chemical Research, 2004. **37**(4): p. 211-220.
114. Prakash, G.K.S., et al., *BF_3−H_2O Catalyzed Hydroxyalkylation of Aromatics with Aromatic Aldehydes and Dicarboxaldehydes: Efficient Synthesis of Triarylmethanes, Diarylmethylbenzaldehydes, and Anthracene Derivatives.* The Journal of Organic Chemistry, 2009. **74**(22): p. 8659-8668.
115. Olah, G.A., et al., *Superacid-Catalyzed Condensation of Benzaldehyde with Benzene. Study of Protonated Benzaldehydes and the Role of Superelectrophilic Activation.* Journal of the American Chemical Society, 1995. **117**(45): p. 11211-11214.
116. Saito, S., T. Ohwada, and K. Shudo, *Friedel-Crafts-type reaction of benzaldehyde with benzene. Diprotonated benzaldehyde as the reactive intermediate.* Journal of the American Chemical Society, 1995. **117**(45): p. 11081-11084.
117. Schaarschmidt, A., L. Hermann, and B. Szemzö, *Aldehyde und Äthylen-oxyd bei der Friedel-Craftsschen Synthese.* Berichte der deutschen chemischen Gesellschaft (A and B Series), 1925. **58**(8): p. 1914-1916.
118. Prakash, G.K.S., et al., *N-Halosuccinimide/BF_3−H_2O, Efficient Electrophilic Halogenating Systems for Aromatics.* Journal of the American Chemical Society, 2004. **126**(48): p. 15770-15776.
119. Arnett, E.M. and C.Y. Wu, *Stereoelectronic Effects on Organic Bases. II.1 Base Strengths of the Phenolic Ethers2.* Journal of the American Chemical Society, 1960. **82**(21): p. 5660-5665.
120. Jha, A., et al., *Metal cation-exchanged montmorillonite clay as catalysts for hydroxyalkylation reaction.* Applied Clay Science, 2013. **74**: p. 141-146.
121. Liu, R., et al., *12-Phosphotungstic acid immobilized on activated-bentonite as an efficient heterogeneous catalyst for the*

hydroxyalkylation of phenol. Applied Clay Science, 2015. **105-106**: p. 71-77.
122. Bai, G., et al., *Friedel–Crafts Hydroxyalkylation of Anisole Over Oxalic Acid Modified Hβ Zeolite.* Catalysis Letters, 2010. **138**(3): p. 187-192.
123. Wu, X., et al., *Mesoporous Al-incorporated silica-pillared clay interlayer materials for catalytic hydroxyalkylation of phenol to bisphenol F.* RSC Advances, 2016. **6**(78): p. 74028-74038.
124. Chambon, F., et al., *Cellulose hydrothermal conversion promoted by heterogeneous Brønsted and Lewis acids: Remarkable efficiency of solid Lewis acids to produce lactic acid.* Applied Catalysis B: Environmental, 2011. **105**(1): p. 171-181.
125. Devassy, B.M., F. Lefebvre, and S.B. Halligudi, *Zirconia-supported 12-tungstophosphoric acid as a solid catalyst for the synthesis of linear alkyl benzenes.* Journal of Catalysis, 2005. **231**(1): p. 1-10.
126. Mao, H., et al., *Aluminated mesoporous silica-pillared montmorillonite as acidic catalyst for catalytic cracking.* Applied Clay Science, 2011. **53**(4): p. 676-683.
127. Wu, X., et al., *Hydroxyalkylation of phenol to bisphenol F over Al-pillared clay.* RSC Advances, 2016. **6**(41): p. 34625-34632.
128. Garade, A.C., et al., *Effect of SnO_2/Al_2O_3 ratio of Si-based MFI on its acidity and hydrophobicity: Application in selective hydroxyalkylation of p-cresol.* Catalysis Communications, 2014. **44**: p. 29-34.
129. Deng, Q., et al., *Highly selective self-condensation of cyclic ketones using MOF-encapsulating phosphotungstic acid for renewable high-density fuel.* Green Chemistry, 2015. **17**(8): p. 4473-4481.
130. Resasco, D.E. and S.P. Crossley, *Implementation of concepts derived from model compound studies in the separation and conversion of bio-oil to fuel.* Catalysis Today, 2015. **257**: p. 185-199.
131. Zapata, P.A., et al., *Silylated hydrophobic zeolites with enhanced tolerance to hot liquid water.* Journal of Catalysis, 2013. **308**: p. 82-97.
132. Zapata, P.A., et al., *Hydrophobic Zeolites for Biofuel Upgrading Reactions at the Liquid–Liquid Interface in Water/Oil Emulsions.* Journal of the American Chemical Society, 2012. **134**(20): p. 8570-8578.

133. Resasco, D.E., *Carbon nanohybrids used as catalysts and emulsifiers for reactions in biphasic aqueous/organic systems.* Chinese Journal of Catalysis, 2014. **35**(6): p. 798-806.
134. Masuda, T., et al., *Differential Heat of Adsorption of Ammonia on Hydrothermally Treated Solid Acid Catalysts and Their Catalytic Activity.* Journal of The Japan Petroleum Institute, 1979. **22**(2): p. 67-72.
135. Jae, J., et al., *Investigation into the shape selectivity of zeolite catalysts for biomass conversion.* Journal of Catalysis, 2011. **279**(2): p. 257-268.
136. Siril, P.F., H.E. Cross, and D.R. Brown, *New polystyrene sulfonic acid resin catalysts with enhanced acidic and catalytic properties.* Journal of Molecular Catalysis A: Chemical, 2008. **279**(1): p. 63-68.
137. Tatsuo, M., et al., *Direct Measurement of Interaction Energy between Solids and Gases. II. Microcalorimetric Studies on the Surface Acidity and Acid Strength Distribution of Solid Acid Catalysts*. Bulletin of the Chemical Society of Japan, 1978. **51**(7): p. 1965-1969.
138. Huber, G.W., S. Iborra, and A. Corma, *Synthesis of Transportation Fuels from Biomass: Chemistry, Catalysts, and Engineering.* Chemical Reviews, 2006. **106**(9): p. 4044-4098.
139. Huber, G.W., et al., *Production of Liquid Alkanes by Aqueous-Phase Processing of Biomass-Derived Carbohydrates.* Science, 2005. **308**(5727): p. 1446-1450.
140. Chheda, J.N., G.W. Huber, and J.A. Dumesic, *Liquid-Phase Catalytic Processing of Biomass-Derived Oxygenated Hydrocarbons to Fuels and Chemicals.* Angewandte Chemie International Edition, 2007. **46**(38): p. 7164-7183.
141. Román-Leshkov, Y., et al., *Production of dimethylfuran for liquid fuels from biomass-derived carbohydrates.* Nature, 2007. **447**: p. 982.
142. Alonso, D.M., J.Q. Bond, and J.A. Dumesic, *Catalytic conversion of biomass to biofuels.* Green Chemistry, 2010. **12**(9): p. 1493-1513.
143. Resasco, D.E., *What Should We Demand from the Catalysts Responsible for Upgrading Biomass Pyrolysis Oil?* The Journal of Physical Chemistry Letters, 2011. **2**(18): p. 2294-2295.
144. Norhasyimi Rahmat, A.Z.A.a.A.R.M., *A Review: Mesoporous Santa Barbara Amorphous-15, Types, Synthesis and Its Applications towards Biorefinery Production.* American Journal of Applied Sciences, 2010. **7**(12): p. 1579-1586.

145. Carniato, F., et al., *On the hydrothermal stability of MCM-41 mesoporous silica nanoparticles and the preparation of luminescent materials*. Journal of Materials Chemistry, 2010. **20**(26): p. 5504-5509.
146. van der Graaff, W.N.P., et al., *Stability and catalytic properties of porous acidic (organo)silica materials for conversion of carbohydrates*. Journal of Molecular Catalysis A: Chemical, 2014. **388-389**: p. 81-89.
147. Kim, J.M., et al., *Ion Exchange and Thermal Stability of MCM-41*. The Journal of Physical Chemistry, 1995. **99**(45): p. 16742-16747.
148. Ryoo, R. and S. Jun, *Improvement of Hydrothermal Stability of MCM-41 Using Salt Effects during the Crystallization Process*. The Journal of Physical Chemistry B, 1997. **101**(3): p. 317-320.
149. Tatsumi, T., et al., *Mechanical Stability of Mesoporous Materials, MCM-48 and MCM-41*. Journal of Porous Materials, 1999. **6**(1): p. 13-17.
150. Gusev, V.Y., et al., *Mechanical Stability of Pure Silica Mesoporous MCM-41 by Nitrogen Adsorption and Small-Angle X-ray Diffraction Measurements*. The Journal of Physical Chemistry, 1996. **100**(6): p. 1985-1988.
151. Galacho, C., M.M.L. Ribeiro Carrott, and P.J.M. Carrott, *Evaluation of the thermal and mechanical stability of Si-MCM-41 and Ti-MCM-41 synthesised at room temperature*. Microporous and Mesoporous Materials, 2008. **108**(1): p. 283-293.
152. Sumit, B., et al., *Aminosilanes Grafted to Basic Alumina as CO2 Adsorbents—Role of Grafting Conditions on CO2 Adsorption Properties*. ChemSusChem, 2014. **7**(11): p. 3145-3156.
153. Brunelli, N.A., K. Venkatasubbaiah, and C.W. Jones, *Cooperative Catalysis with Acid–Base Bifunctional Mesoporous Silica: Impact of Grafting and Co-condensation Synthesis Methods on Material Structure and Catalytic Properties*. Chemistry of Materials, 2012. **24**(13): p. 2433-2442.
154. Jones, C.W., K. Tsuji, and M.E. Davis, *Organic-functionalized molecular sieves as shape-selective catalysts*. Nature, 1998. **393**: p. 52.
155. Hoffmann, F., et al., *Silica-Based Mesoporous Organic–Inorganic Hybrid Materials*. Angewandte Chemie International Edition, 2006. **45**(20): p. 3216-3251.

156. Kärger, J. and D. Freude, *Mass Transfer in Micro- and Mesoporous Materials*. Chemical Engineering & Technology, 2002. **25**(8): p. 769-778.
157. Karimi, B., et al., *Sulfonic acid-functionalized periodic mesoporous organosilicas in esterification and selective acylation reactions.* Catalysis Science & Technology, 2015. **5**(7): p. 3624-3631.
158. Dacquin, J.P., et al., *Pore-expanded SBA-15 sulfonic acid silicas for biodiesel synthesis.* Chemical Communications, 2012. **48**(2): p. 212-214.
159. Grieken, R.v., J.A. Melero, and G. Morales, *Fries rearrangement of phenyl acetate over sulfonic modified mesostructured SBA-15 materials*. Applied Catalysis A: General, 2005. **289**(2): p. 143-152.
160. Karaki, M., et al., *Synthesis and characterization of acidic ordered mesoporous organosilica SBA-15: Application to the hydrolysis of cellobiose and insight into the stability of the acidic functions*. Journal of Catalysis, 2013. **305**: p. 204-216.
161. Huang, Y., *Functionalization of Mesoporous Silica Nanoparticles and Their Applications in Organo-, Metallic and Organometallic Catalysis*, in *Chemistry* 2009, Iowa State University: Ames, Iowa
162. García, N., et al., *Functionalization of SBA-15 by an acid-catalyzed approach: A surface characterization study.* Microporous and Mesoporous Materials, 2007. **106**(1–3): p. 129-139.
163. Gholami, M., M.R. Talaie, and S.F. Aghamiri, *CO2 adsorption on amine functionalized MCM-41: Effect of bi-modal porous structure.* Journal of the Taiwan Institute of Chemical Engineers, 2016. **59**: p. 205-209.
164. Huo, Q., D.I. Margolese, and G.D. Stucky, *Surfactant Control of Phases in the Synthesis of Mesoporous Silica-Based Materials.* Chemistry of Materials, 1996. **8**(5): p. 1147-1160.
165. Tucker, M.H., et al., *Acid-Functionalized SBA-15-Type Periodic Mesoporous Organosilicas and Their Use in the Continuous Production of 5-Hydroxymethylfurfural.* ACS Catalysis, 2012. **2**(9): p. 1865-1876.
166. Alba-Rubio, A.C., et al., *Deactivation of organosulfonic acid functionalized silica catalysts during biodiesel synthesis.* Applied Catalysis B: Environmental, 2010. **95**(3): p. 279-287.
167. Petrus, L., E.J. Stamhuis, and G.E.H. Joosten, *Thermal deactivation of strong-acid ion-exchange resins in water.* Industrial & Engineering

Chemistry Product Research and Development, 1981. **20**(2): p. 366-371.
168. Aragon, J.M., J.M.R. Vegas, and L.G. Jodra, *Self-Condensation of Cyclohexanone Catalyzed by Amberlyst-15. Study of Diffusional Resistances and Deactivation of the Catalyst.* Industrial & Engineering Chemistry Research, 1994. **33**(3): p. 592-599.
169. Mo, X., et al., *Activation and deactivation characteristics of sulfonated carbon catalysts.* Journal of Catalysis, 2008. **254**(2): p. 332-338.
170. Suwannakarn, K., et al., *Stability of sulfated zirconia and the nature of the catalytically active species in the transesterification of triglycerides.* Journal of Catalysis, 2008. **255**(2): p. 279-286.
171. Testa, M.L., V. La Parola, and A.M. Venezia, *Transesterification of short chain esters using sulfonic acid-functionalized hybrid silicas: Effect of silica morphology.* Catalysis Today, 2014. **223**: p. 115-121.
172. Canilho, N., et al., *Isocyanate-mediated covalent immobilization of Mucor miehei lipase onto SBA-15 for transesterification reaction.* Colloids and Surfaces B: Biointerfaces, 2013. **112**: p. 139-145.
173. Samolada, M.C., et al., *Selective O-Alkylation of Phenol with Methanol over Sulfates Supported on γ-Al_2O_3.* Journal of Catalysis, 1995. **152**(1): p. 52-62.
174. Chen, S.-Y., et al., *Sulfonic acid-functionalized platelet SBA-15 materials as efficient catalysts for biodiesel synthesis.* Green Chemistry, 2011. **13**(10): p. 2920-2930.
175. Gallo, J.M.R., R. Alamillo, and J.A. Dumesic, *Acid-functionalized mesoporous carbons for the continuous production of 5-hydroxymethylfurfural.* Journal of Molecular Catalysis A: Chemical, 2016. **422**: p. 13-17.
176. Silva, A.R., et al., *Covalent attachment of chiral manganese(III) salen complexes onto functionalised hexagonal mesoporous silica and application to the asymmetric epoxidation of alkenes.* Microporous and Mesoporous Materials, 2006. **91**(1): p. 128-138.
177. Dias, A.S., M. Pillinger, and A.A. Valente, *Dehydration of xylose into furfural over micro-mesoporous sulfonic acid catalysts.* Journal of Catalysis, 2005. **229**(2): p. 414-423.
178. Kamegawa, T., A. Mizuno, and H. Yamashita, *Hydrophobic modification of SO3H-functionalized mesoporous silica and investigations on the enhanced catalytic performance.* Catalysis Today, 2015. **243**: p. 153-157.

179. Laghaei, M., et al., *The effect of various types of post-synthetic modifications on the structure and properties of MCM-41 mesoporous silica.* Progress in Organic Coatings, 2016. **90**: p. 163-170.
180. Matsumoto, A., et al., *Surface Functionalization and Stabilization of Mesoporous Silica Spheres by Silanization and Their Adsorption Characteristics.* Langmuir, 2002. **18**(10): p. 4014-4019.
181. Inumaru, K., J. Kiyoto, and S. Yamanaka, *Molecular selective adsorption of nonylphenol in aqueous solution by organo-functionalized mesoporous silica.* Chemical Communications, 2000(11): p. 903-904.
182. Inumaru, K., et al., *Molecular selective adsorption of dilute alkylphenols and alkylanilines from water by alkyl-grafted MCM-41: tunability of the cooperative organic–inorganic function in the nanostructure.* Physical Chemistry Chemical Physics, 2004. **6**(12): p. 3133-3139.
183. Kimura, T., et al., *Organic Modification of FSM-Type Mesoporous Silicas Derived from Kanemite by Silylation.* Langmuir, 1999. **15**(8): p. 2794-2798.
184. Martin, T., et al., *Great Improvement of Chromatographic Performance Using MCM-41 Spheres as Stationary Phase in HPLC.* Chemistry of Materials, 2004. **16**(9): p. 1725-1731.
185. Yang, H., et al., *Silylation of mesoporous silica MCM-41 with the mixture of $Cl(CH_2)_3SiCl_3$ and CH_3SiCl_3: combination of adjustable grafting density and improved hydrothermal stability.* Microporous and Mesoporous Materials, 2004. **68**(1): p. 119-125.
186. Das, D., J.-F. Lee, and S. Cheng, *Sulfonic acid functionalized mesoporous MCM-41 silica as a convenient catalyst for Bisphenol-A synthesis.* Chemical Communications, 2001(21): p. 2178-2179.
187. Margolese, D., et al., *Direct Syntheses of Ordered SBA-15 Mesoporous Silica Containing Sulfonic Acid Groups.* Chemistry of Materials, 2000. **12**(8): p. 2448-2459.
188. Kresse, G. and J. Furthmuller, *Efficient iterative schemes for ab initio total-energy calculations using a plane-wave basis set.* Physical Review B, 1996. **54**(16): p. 11169-11186.
189. Blochl, P.E., *Projector Augmented-Wave Method.* Physical Review B, 1994. **50**(24): p. 17953-17979.
190. Kresse, G. and D. Joubert, *From ultrasoft pseudopotentials to the projector augmented-wave method.* Physical Review B, 1999. **59**(3): p. 1758-1775.

191. Perdew, J.P., K. Burke, and M. Ernzerhof, *Generalized gradient approximation made simple.* Physical Review Letters, 1996. **77**(18): p. 3865-3868.
192. Grimme, S., et al., *A consistent and accurate ab initio parametrization of density functional dispersion correction (DFT-D) for the 94 elements H-Pu.* Journal of Chemical Physics, 2010. **132**(15): p. 154104.
193. Gierada, M., et al., *Hydration in silica based mesoporous materials: a DFT model.* Physical Chemistry Chemical Physics, 2016. **18**(48): p. 32962-32972.
194. Zhao, X.S. and G.Q. Lu, *Modification of MCM-41 by Surface Silylation with Trimethylchlorosilane and Adsorption Study.* The Journal of Physical Chemistry B, 1998. **102**(9): p. 1556-1561.
195. Kailasam, K. and K. Müller, *Physico-chemical characterization of MCM-41 silica spheres made by the pseudomorphic route and grafted with octadecyl chains.* Journal of Chromatography A, 2008. **1191**(1): p. 125-135.
196. Chen, C.-Y., et al., *Studies on mesoporous materials II. Synthesis mechanism of MCM-41.* Microporous Materials, 1993. **2**(1): p. 27-34.
197. Chen, C.-Y., H.-X. Li, and M.E. Davis, *Studies on mesoporous materials.* Microporous Materials, 1993. **2**(1): p. 17-26.
198. Ortlam, A., et al., *MCM-41 as-synthesized and calcined materials: temporal development of X-ray reflection intensity and pore volume.* Microporous Materials, 1996. **6**(4): p. 171-180.
199. L. Peña, K.L.H., J. Li, X. S. Sun, D. Wang, *Synthesis of Propyl-Sulfonic Acid-Functionalized Nanoparticles as Catalysts for Cellobiose Hydrolysis.* Journal of Biomaterials and Nanobiotechnology, 2014. **5**(4).
200. Zhao, X.S., et al., *Comprehensive Study of Surface Chemistry of MCM-41 Using 29Si CP/MAS NMR, FTIR, Pyridine-TPD, and TGA.* The Journal of Physical Chemistry B, 1997. **101**(33): p. 6525-6531.
201. Zhang, L., et al., *Factors that Determine Zeolite Stability in Hot Liquid Water.* Journal of the American Chemical Society, 2015. **137**(36): p. 11810-11819.
202. Fina, A., et al., *Polypropylene–polyhedral oligomeric silsesquioxanes (POSS) nanocomposites.* Polymer, 2005. **46**(19): p. 7855-7866.
203. Zhang, W., G. Camino, and R. Yang, *Polymer/polyhedral oligomeric silsesquioxane (POSS) nanocomposites: An overview of fire retardance.* Progress in Polymer Science, 2017. **67**: p. 77-125.

204. Bali, S., et al., *Aminosilanes Grafted to Basic Alumina as CO2 Adsorbents—Role of Grafting Conditions on CO2 Adsorption Properties.* ChemSusChem, 2014. **7**(11): p. 3145-3156.
205. Cano-Serrano, E., et al., *Acid-Functionalized Amorphous Silica by Chemical Grafting−Quantitative Oxidation of Thiol Groups.* Langmuir, 2003. **19**(18): p. 7621-7627.
206. Zhang, X., L. Zhang, and Q. Yang, *Designed synthesis of sulfonated polystyrene/mesoporous silica hollow nanospheres as efficient solid acid catalysts.* Journal of Materials Chemistry A, 2014. **2**(20): p. 7546-7554.
207. Koyano, K.A., et al., *Stabilization of Mesoporous Molecular Sieves by Trimethylsilylation.* The Journal of Physical Chemistry B, 1997. **101**(46): p. 9436-9440.
208. Kikhtyanin, O., et al., *Aldol condensation of furfural and acetone on zeolites.* Catalysis Today, 2014. **227**: p. 154-162.
209. Dumitriu, E., et al., *The aldol condensation of lower aldehydes over MFI zeolites with different acidic properties.* Microporous and Mesoporous Materials, 2001. **43**(3): p. 341-359.
210. Dumitriu, E., et al., *Vapor-Phase Condensation of Formaldehyde and Acetaldehyde into Acrolein over Zeolites.* Journal of Catalysis, 1994. **147**(1): p. 133-139.
211. Climent, M.J., et al., *Synthesis of Pseudoionones by Acid and Base Solid Catalysts.* Catalysis Letters, 2002. **79**(1): p. 157-163.
212. Roelofs, J.C.A.A., A.J. van Dillen, and K.P. de Jong, *Base-catalyzed condensation of citral and acetone at low temperature using modified hydrotalcite catalysts.* Catalysis Today, 2000. **60**(3): p. 297-303.
213. Abelló, S., et al., *Aldol Condensations Over Reconstructed Mg–Al Hydrotalcites: Structure–Activity Relationships Related to the Rehydration Method.* Chemistry – A European Journal, 2005. **11**(2): p. 728-739.
214. Tuong V. Bui, N.D., Felipe Anaya, Duong Ngo, Gap Warakunwit, Daniel E. Resasco, *Chemistry of C-C bond formation reactions used in biomass upgrading. Reaction mechanisms, site requirements, and catalytic materials*, in *Chemical Catalysts for Biomass Upgrading*, E.S.-J. Mark Crocker, Editor. 2019, Wiley.
215. Dumitriu, E., et al., *Synthesis, characterization and catalytic activity of SAPO-34 obtained with piperidine as templating agent.* Microporous Materials, 1997. **10**(1): p. 1-12.

216. Dumitriu, E., et al., *Synthesis of acrolein by vapor phase condensation of formaldehyde and acetaldehyde over oxides loaded zeolites.* Journal of Molecular Catalysis, 1993. **79**(1): p. 175-185.
217. Kikhtyanin, O., et al., *Aldol condensation of furfural with acetone over ion-exchanged and impregnated potassium BEA zeolites.* Journal of Molecular Catalysis A: Chemical, 2016. **424**: p. 358-368.
218. Tago, T., et al., *Selective production of isobutylene from acetone over alkali metal ion-exchanged BEA zeolites.* Catalysis Today, 2011. **164**(1): p. 158-162.
219. Tayade, K.N. and M. Mishra, *A study on factors influencing cross and self product selectivity in aldol condensation over propylsulfonic acid functionalized silica.* Catalysis Science & Technology, 2013. **3**(5): p. 1288-1300.
220. Chen, H., et al., *Bifunctional Organic Polymeric Catalysts with a Tunable Acid-Base Distance and Framework Flexibility.* Scientific Reports, 2014. **4**: p. 6475.
221. Jeong, M.S. and H. Frei, *Acetaldehyde as a probe for the chemical properties of aluminophosphate molecular sieves. An in situ FT-IR study.* Journal of Molecular Catalysis A: Chemical, 2000. **156**(1): p. 245-253.
222. Kikhtyanin, O., D. Kubička, and J. Čejka, *Toward understanding of the role of Lewis acidity in aldol condensation of acetone and furfural using MOF and zeolite catalysts.* Catalysis Today, 2015. **243**: p. 158-162.
223. Herrmann, S. and E. Iglesia, *Elementary steps in acetone condensation reactions catalyzed by aluminosilicates with diverse void structures.* Journal of Catalysis, 2017. **346**: p. 134-153.
224. Boekfa, B., et al., *Adsorption and Tautomerization Reaction of Acetone on Acidic Zeolites: The Confinement Effect in Different Types of Zeolites.* The Journal of Physical Chemistry C, 2010. **114**(35): p. 15061-15067.
225. Solans-Monfort, X., et al., *Keto−Enol Isomerization of Acetaldehyde in HZSM5. A Theoretical Study Using the ONIOM2 Method.* The Journal of Physical Chemistry B, 2002. **106**(39): p. 10220-10226.
226. Biaglow, A.I., et al., *A ^{13}C NMR Study of the Condensation Chemistry of Acetone and Acetaldehyde Adsorbed at the Brønsted Acid Sites in H-ZSM-5.* Journal of Catalysis, 1995. **151**(2): p. 373-384.
227. Xu, T., E.J. Munson, and J.F. Haw, *Toward a Systematic Chemistry of Organic Reactions in Zeolites: In situ NMR Studies of Ketones.*

Journal of the American Chemical Society, 1994. **116**(5): p. 1962-1972.
228. Gorte, R.J. and D. White, *Interactions of chemical species with acid sites in zeolites.* Topics in Catalysis, 1997. **4**(1): p. 57-69.
229. Sierra, L.R., E. Kassab, and E.M. Evleth, *Calculation of hydroxymethylation of a zeolite model.* The Journal of Physical Chemistry, 1993. **97**(3): p. 641-646.
230. Šepa, J., et al., *Carbonyl ^{13}C Shielding Tensors and Heats of Adsorption of Acetone Adsorbed in Silicalite and the 1:1 Stoichiometric Complex in H−ZSM-5.* The Journal of Physical Chemistry, 1996. **100**(47): p. 18515-18523.
231. Kikhtyanin, O., et al., *Peculiar behavior of MWW materials in aldol condensation of furfural and acetone.* Dalton Transactions, 2014. **43**(27): p. 10628-10641.
232. Migues, A.N., S. Vaitheeswaran, and S.M. Auerbach, *Density Functional Theory Study of Mixed Aldol Condensation Catalyzed by Acidic Zeolites HZSM-5 and HY.* The Journal of Physical Chemistry C, 2014. **118**(35): p. 20283-20290.
233. Coitino, E.L., J. Tomasi, and O.N. Ventura, *Importance of water in aldol condensation reactions of acetaldehyde.* Journal of the Chemical Society, Faraday Transactions, 1994. **90**(12): p. 1745-1755.
234. Biaglow, A.I., R.J. Gorte, and D. White, *^{13}C NMR Studies of Acetone in Dealuminated Faujasites: A Probe for Nonframework Alumina.* Journal of Catalysis, 1994. **150**(1): p. 221-224.
235. Panov, A.G. and J.J. Fripiat, *Acetone Condensation Reaction on Acid Catalysts.* Journal of Catalysis, 1998. **178**(1): p. 188-197.
236. Venuto, P.B., *Organic catalysis over zeolites: A perspective on reaction paths within micropores.* Microporous Materials, 1994. **2**(5): p. 297-411.
237. Díez, V.K., C.R. Apesteguía, and J.I. Di Cosimo, *Aldol condensation of citral with acetone on MgO and alkali-promoted MgO catalysts.* Journal of Catalysis, 2006. **240**(2): p. 235-244.
238. Noda Pérez, C., et al., *Hydrotalcites as precursors for Mg,Al-mixed oxides used as catalysts on the aldol condensation of citral with acetone.* Applied Catalysis A: General, 2004. **272**(1): p. 229-240.
239. Choudary, B.M., et al., *Knoevenagel and aldol condensations catalysed by a new diamino-functionalised mesoporous material.* Journal of Molecular Catalysis A: Chemical, 1999. **142**(3): p. 361-365.

240. Yu, J.-I., S.Y. Shiau, and A.-N. Ko, *Al-MCM-41 Supported Magnesium Oxide as Catalyst for Synthesis of α-Pentylcinnamaldehyde.* Catalysis Letters, 2001. **77**(1): p. 165-169.
241. Lewis, J.D., S. Van de Vyver, and Y. Román-Leshkov, *Acid–Base Pairs in Lewis Acidic Zeolites Promote Direct Aldol Reactions by Soft Enolization.* Angewandte Chemie International Edition, 2015. **54**(34): p. 9835-9838.
242. Di Cosimo, J.I., V.K. Díez, and C.R. Apesteguía, *Base catalysis for the synthesis of α,β-unsaturated ketones from the vapor-phase aldol condensation of acetone.* Applied Catalysis A: General, 1996. **137**(1): p. 149-166.
243. Ungureanu, A., et al., *Aldol condensation of aldehydes over semicrystalline zeolitic-mesoporous UL-ZSM-5.* Microporous and Mesoporous Materials, 2005. **84**(1): p. 283-296.
244. Wang, S. and E. Iglesia, *Entropy-Driven High Reactivity of Formaldehyde in Nucleophilic Attack by Enolates on Oxide Surfaces.* Journal of the American Chemical Society, 2018. **140**(2): p. 775-782.
245. Swain, C.G., et al., *Use of Hydrogen Isotope Effects to Identify the Attacking Nucleophile in the Enolization of Ketones Catalyzed by Acetic Acid1-3.* Journal of the American Chemical Society, 1958. **80**(21): p. 5885-5893.
246. Swain, C.G., A.J. Di Milo, and J.P. Cordner, *Use of Hydrogen Isotope Effects to Determine the Timing of Proton Transfer Relative to Nucleophilic Attack in the Enolization of Ketones and Reactions of Epoxides Catalyzed by Acetic Acid1-3.* Journal of the American Chemical Society, 1958. **80**(22): p. 5983-5988.
247. Swain, C.G. and A.S. Rosenberg, *Mechanism of Enolization of Ketones in Sulfuric Acid1-3.* Journal of the American Chemical Society, 1961. **83**(9): p. 2154-2158.
248. Lienhard, G.E. and T.-C. Wang, *Mechanism of acid-catalyzed enolization of ketones.* Journal of the American Chemical Society, 1969. **91**(5): p. 1146-1153.
249. Gómez-Bombarelli, R., et al., *Computational Study of the Acid Dissociation of Esters and Lactones. A Case Study of Diketene.* The Journal of Organic Chemistry, 2009. **74**(14): p. 4943-4948.
250. Zhao, Y.H., M.H. Abraham, and A.M. Zissimos, *Fast Calculation of van der Waals Volume as a Sum of Atomic and Bond Contributions and Its Application to Drug Compounds.* The Journal of Organic Chemistry, 2003. **68**(19): p. 7368-7373.

251. Al-Dughaither, A.S. and H. de Lasa, *HZSM-5 Zeolites with Different SiO2/Al2O3 Ratios. Characterization and NH3 Desorption Kinetics.* Industrial & Engineering Chemistry Research, 2014. **53**(40): p. 15303-15316.
252. Kruse, A. and N. Dahmen, *Water – A magic solvent for biomass conversion.* The Journal of Supercritical Fluids, 2015. **96**: p. 36-45.
253. Herron, J.A., et al., *A Systems-Level Roadmap for Biomass Thermal Fractionation and Catalytic Upgrading Strategies.* Energy Technology, 2017. **5**(1): p. 130-150.
254. Zaimes, G.G., et al., *Multistage torrefaction and in situ catalytic upgrading to hydrocarbon biofuels: analysis of life cycle energy use and greenhouse gas emissions.* Energy & Environmental Science, 2017. **10**(5): p. 1034-1050.
255. Gallo, J.M.R., et al., *Production and upgrading of 5-hydroxymethylfurfural using heterogeneous catalysts and biomass-derived solvents.* Green Chemistry, 2013. **15**(1): p. 85-90.
256. Qi, L. and I.T. Horváth, *Catalytic Conversion of Fructose to γ-Valerolactone in γ-Valerolactone.* ACS Catalysis, 2012. **2**(11): p. 2247-2249.
257. Alonso, D.M., et al., *Direct conversion of cellulose to levulinic acid and gamma-valerolactone using solid acid catalysts.* Catalysis Science & Technology, 2013. **3**(4): p. 927-931.
258. Shi, D., et al., *Fischer–Tropsch Synthesis Catalyzed by Solid Nanoparticles at the Water/Oil Interface in an Emulsion System.* Energy & Fuels, 2013. **27**(10): p. 6118-6124.
259. Zapata, P.A., et al., *Condensation/Hydrogenation of Biomass-Derived Oxygenates in Water/Oil Emulsions Stabilized by Nanohybrid Catalysts.* Topics in Catalysis, 2012. **55**(1): p. 38-52.
260. Wang, Q., et al., *Water as an additive to enhance the ring opening of naphthalene.* Green Chemistry, 2012. **14**(4): p. 1152-1158.
261. X. Song, S. and R. A. Kydd, *Activation of sulfated zirconia catalysts Effect of water content on their activity in n-butane isomerization.* Journal of the Chemical Society, Faraday Transactions, 1998. **94**(9): p. 1333-1338.
262. Chen, K., et al., *Zeolite Catalysis: Water Can Dramatically Increase or Suppress Alkane C–H Bond Activation.* ACS Catalysis, 2014. **4**(9): p. 3039-3044.

263. Kostrab, G., et al., *tert-Butylation of toluene with isobutylene over zeolite catalysts: Influence of water.* Applied Catalysis A: General, 2007. **323**: p. 210-218.
264. Hibbitts, D.D., et al., *Mechanistic Role of Water on the Rate and Selectivity of Fischer–Tropsch Synthesis on Ruthenium Catalysts.* Angewandte Chemie, 2013. **125**(47): p. 12499-12504.
265. Krishnamoorthy, S., et al., *An Investigation of the Effects of Water on Rate and Selectivity for the Fischer–Tropsch Synthesis on Cobalt-Based Catalysts.* Journal of Catalysis, 2002. **211**(2): p. 422-433.
266. Iglesia, E., *Design, synthesis, and use of cobalt-based Fischer-Tropsch synthesis catalysts.* Applied Catalysis A: General, 1997. **161**(1): p. 59-78.
267. Faheem, M. and A. Heyden, *Hybrid Quantum Mechanics/Molecular Mechanics Solvation Scheme for Computing Free Energies of Reactions at Metal–Water Interfaces.* Journal of Chemical Theory and Computation, 2014. **10**(8): p. 3354-3368.
268. Shi, D., et al., *Enhanced Activity and Selectivity of Fischer–Tropsch Synthesis Catalysts in Water/Oil Emulsions.* ACS Catalysis, 2014. **4**(6): p. 1944-1952.
269. Rideout, D.C. and R. Breslow, *Hydrophobic acceleration of Diels-Alder reactions.* Journal of the American Chemical Society, 1980. **102**(26): p. 7816-7817.
270. Breslow, R. and U. Maitra, *On the origin of product selectivity in aqueous diels-alder reactions.* Tetrahedron Letters, 1984. **25**(12): p. 1239-1240.
271. Breslow, R., U. Maitra, and D. Rideout, *Selective diels-alder reactions in aqueous solutions and suspensions.* Tetrahedron Letters, 1983. **24**(18): p. 1901-1904.
272. Breslow, R. and T. Guo, *Diels-Alder reactions in nonaqueous polar solvents. Kinetic effects of chaotropic and antichaotropic agents and of .beta.-cyclodextrin.* Journal of the American Chemical Society, 1988. **110**(17): p. 5613-5617.
273. Blokzijl, W., M.J. Blandamer, and J.B.F.N. Engberts, *Diels-Alder reactions in aqueous solutions. Enforced hydrophobic interactions between diene and dienophile.* Journal of the American Chemical Society, 1991. **113**(11): p. 4241-4246.
274. Larsen, S.D. and P.A. Grieco, *Aza Diels-Alder reactions in aqueous solution: cyclocondensation of dienes with simple iminium salts*

generated under Mannich conditions. Journal of the American Chemical Society, 1985. **107**(6): p. 1768-1769.
275. Grieco, P.A., J.J. Nunes, and M.D. Gaul, *Dramatic rate accelerations of Diels-Alder reactions in 5 M lithium perchlorate-diethyl ether: the cantharidin problem reexamined.* Journal of the American Chemical Society, 1990. **112**(11): p. 4595-4596.
276. Lubineau, A. and E. Meyer, *Water-promoted organic reactions. aldol reaction of silyl enol ethers with carbonyl compounds under atmospheric pressure and neutral conditions.* Tetrahedron, 1988. **44**(19): p. 6065-6070.
277. Kizhakevariam, N., X. Jiang, and M.J. Weaver, *Infrared spectroscopy of model electrochemical interfaces in ultrahigh vacuum: The archetypical case of carbon monoxide/water coadsorption on Pt(111).* The Journal of Chemical Physics, 1994. **100**(9): p. 6750-6764.
278. Yuzawa, T., et al., *CO coadsorption-induced recombination of surface hydroxyls to water on Ni(110) surface by IRAS and TPD.* Surface Science, 1995. **325**(3): p. 223-229.
279. Nakamura, M. and M. Ito, *Coadsorption of water monomers with CO on Ru(001) and charge transfer during hydration processes.* Chemical Physics Letters, 2001. **335**(3): p. 170-175.
280. Bertole, C.J., C.A. Mims, and G. Kiss, *The Effect of Water on the Cobalt-Catalyzed Fischer–Tropsch Synthesis.* Journal of Catalysis, 2002. **210**(1): p. 84-96.
281. Schmitz, A.D. and C. Song, *Shape-selective isopropylation of naphthalene over dealuminated mordenites. Increasingβ-substitution selectivity by adding water.* Catalysis Letters, 1996. **40**(1): p. 59-65.
282. Flego, C., G. Pazzuconi, and C. Perego, *Influence of water adsorption on zeolite Beta*, in *Studies in Surface Science and Catalysis*, R. Aiello, G. Giordano, and F. Testa, Editors. 2002, Elsevier. p. 1603-1610.
283. Lefrancois, M. and G. Malbois, *The nature of the acidic sites on mordenite: Characterization of adsorbed pyridine and water by infrared study.* Journal of Catalysis, 1971. **20**(3): p. 350-358.
284. Kunkeler, P.J., et al., *Zeolite Beta: The Relationship between Calcination Procedure, Aluminum Configuration, and Lewis Acidity.* Journal of Catalysis, 1998. **180**(2): p. 234-244.
285. Cannings, F.R., *Acidic sites on mordenite: an infrared study of adsorbed pyridine.* The Journal of Physical Chemistry, 1968. **72**(13): p. 4691-4693.

286. González, M.n.R., et al., *Promotion ofn-Butane Isomerization Activity by Hydration of Sulfated Zirconia.* Journal of Catalysis, 1996. **160**(2): p. 290-298.
287. Kobe, J.M., et al., *Effects of Water on the Performance of Sulfated Zirconia Catalysts for Butane Isomerization.* Journal of Catalysis, 1996. **164**(2): p. 459-466.
288. Gates, B.C., in *Catalytic Chemistry*. 1992, Wiley: New York.
289. Marchese, L., et al., *Formation of hydronium at the Broensted site in SAPO-34 catalysts.* The Journal of Physical Chemistry, 1993. **97**(31): p. 8109-8112.
290. Pelmenschikov, A.G. and R.A. van Santen, *Water adsorption on zeolites: ab-initio interpretation of IR data.* The Journal of Physical Chemistry, 1993. **97**(41): p. 10678-10680.
291. van Santen, R.A. and G.J. Kramer, *Reactivity Theory of Zeolitic Broensted Acidic Sites.* Chemical Reviews, 1995. **95**(3): p. 637-660.
292. Parker, L.M., D.M. Bibby, and G.R. Burns, *An infrared study of H2O and D2O on HZSM-5 and DZSM-5.* Zeolites, 1993. **13**(2): p. 107-112.
293. Smith, L., et al., *On the Nature of Water Bound to a Solid Acid Catalyst.* Science, 1996. **271**(5250): p. 799-802.
294. Haase, F. and J. Sauer, *Interaction of methanol with Broensted acid sites of zeolite catalysts: an ab initio study.* Journal of the American Chemical Society, 1995. **117**(13): p. 3780-3789.
295. Sauer, J., *Probing Catalysts with Water.* Science, 1996. **271**(5250): p. 774-775.
296. Zeets, M., D.E. Resasco, and B. Wang, *Enhanced chemical activity and wettability at adjacent Brønsted acid sites in HZSM-5.* Catalysis Today, 2018. **312**: p. 44-50.
297. Chen, N.Y., *Hydrophobic properties of zeolites.* The Journal of Physical Chemistry, 1976. **80**(1): p. 60-64.
298. Sano, T., et al., *Sorption of water vapor on HZSM-5 type zeolites*, in *Studies in Surface Science and Catalysis*, H. Chon, S.-K. Ihm, and Y.S. Uh, Editors. 1997, Elsevier. p. 1771-1778.
299. Breiter, M.W., et al., *Production of hydronium beta alumina from sodium beta alumina and characterization of conversion products.* Materials Research Bulletin, 1977. **12**(9): p. 895-906.
300. Vjunov, A., et al., *Tracking the Chemical Transformations at the Brønsted Acid Site upon Water-Induced Deprotonation in a Zeolite Pore.* Chemistry of Materials, 2017. **29**(21): p. 9030-9042.

301. Shi, H., et al., *Tailoring nanoscopic confines to maximize catalytic activity of hydronium ions.* Nature Communications, 2017. **8**: p. 15442.
302. Liu, Y., et al., *Enhancing the catalytic activity of hydronium ions through constrained environments.* Nature Communications, 2017. **8**: p. 14113.
303. González, M.D., et al., *Boosted selectivity toward high glycerol tertiary butyl ethers by microwave-assisted sulfonic acid-functionalization of SBA-15 and beta zeolite.* Journal of Catalysis, 2012. **290**: p. 202-209.
304. Zeidan, R.K. and M.E. Davis, *The effect of acid–base pairing on catalysis: An efficient acid–base functionalized catalyst for aldol condensation.* Journal of Catalysis, 2007. **247**(2): p. 379-382.